SYNTHESIS, MODIFICATION AND APPLICATIONS OF LAYERED DOUBLE HYDROXIDES AS PEROXIDASE MIMIC AND DYE ADSORBENT

KITAYANAN PONLAKHET

A THESIS SUBMITTED IN PARTIAL FULFILLMENT OF THE REQUIREMENTS
FOR THE DEGREE OF DOCTOR OF PHILOSOPHY
MAJOR IN CHEMISTRY
FACULTY OF SCIENCE
UBON RATCHATHANI UNIVERSITY
ACADEMIC YEAR 2020

UBON RATCHATHANI UNIVERSITY
THESIS APPROVAL
DOCTOR OF PHILOSOPHY
IN CHEMISTRY FACULTY OF SCIENCE

TITLE SYNTHESIS, MODIFICATION AND APPLICATIONS OF LAYERED DOUBLE HYDROXIDES AS PEROXIDASE MIMIC AND DYE ADSORBENT

AUTHOR MISS KITAYANAN PONLAKHET

EXAMINATION COMMITTEE

ASST. PROF. DR. JAURSUP BOONMAK	CHAIRPERSON
DR. SUPARB TAMUANG	MEMBER
ASSOC. PROF. SAYANT SAENGSUWAN	MEMBER
ASST. PROF. DR. PURIM JARUJAMRUS	MEMBER
ASST. PROF. DR. SANOE CHAIRAM	MEMBER

ADVISOR

Suparb Tamuang
(DR. SUPARB TAMUANG)

Charida Pukahuta
(ASST. PROF. DR. CHARIDA PUKAHUTA)
DEAN, FACULTY OF SCIENCE

A. Pongrat
(ASSOC. PROF. DR. ARIYAPORN PONGRAT)
VICE PRESIDENT FOR ACADEMIC AFFAIRS

ACADEMIC YEAR 2020

ACKNOWLEDGEMENTS

I would like to thank my advisor, Dr. Suparb Tamuang for her constant advice, guidance, insight and for sharing her extensive chemistry knowledge. I'd like to thank Assoc. Prof. Dr.Sayant Saengsuwan, Asst. Prof. Dr. Purim Jarujamrus andAsst. Prof. Dr. Sanoe Chairam for comments and suggestions and Asst. Prof. Dr. Jaursup Boonmak for his advice and criticism as the external examiner.

I also would like to thank the Science Achievement Scholarship of Thailand (SAST) and Ubon Ratchatani University for financial support. My gratitude is extended to Department of Chemistry, Faculty of Science, Ubon Ratchatani University for providing all laboratory facilities.

Above all, my deepest gratitude is given to my beloved parents for their eternal love and care throughout my life.

Kitayanan Ponlakhet
Researcher

บทคัดย่อ

เรื่อง : การสังเคราะห์ ปรับปรุงคุณสมบัติ และการประยุกต์ใช้งานของ
เลเยอร์ดับเบิลไฮดรอกไซด์ เพื่อใช้เป็นเปอร์ออกซิเดสมิมิค และตัวดูดซับสีย้อม
ผู้วิจัย : กฤตยานันท์ พลเขตต์
ชื่อปริญญา : ปรัชญาดุษฎีบัณฑิต
สาขาวิชา : เคมี
อาจารย์ที่ปรึกษา : ดร. สุภาพ ตาเมือง

คำสำคัญ : เลเยอร์ดับเบิลไฮดรอกไซด์, เปอร์ออกซเดสมิมิค, เซนต์เซอร์ตรวจวัดทางสี,
การดูดซับ, สีย้อม

เลเยอร์ดับเบิลไฮดรอกไซด์ (LDHs) เป็นหนึ่งในวัสดุประเภทดินเหนียวที่มีประจุลบ เลเยอร์ดับเบิลไฮดรอกไซด์เป็นวัสดุที่มีความยืดหยุ่นในส่วนขององค์ประกอบของธาตุที่นำมาสังเคราะห์ ซึ่งได้แก่ อัตราส่วนของโลหะประจุ 2+ และ 3+ รวมไปถึงความหลากหลายไอออนประจุลบที่อยู่ระหว่างชั้นโลหะไฮดรอกไซด์ สามารถใช้ได้ทั้งสารอนินทรีย์และสารอินทรีย์ ยิ่งไปกว่านั้น LDHs ได้รับความสนใจอย่างมากเนื่องจากสามารถสังเคราะห์ได้ง่ายในห้องปฏิบัติการ มีความเข้ากันได้ทางชีวภาพที่ดี มีความเป็นพิษต่ำ มีพื้นที่ผิวปริมาณมาก มีความสามารถในการเป็นตัวเร่งปฏิกิริยาที่ดี มีความเสถียรทางเคมี มีความสามารถในการดูดซับที่ดีและการแลกเปลี่ยนไอออนประจุลบ งานวิทยานิพนธ์นี้สนใจที่จะสังเคราะห์ ปรับปรุงคุณสมบัติ และใช้งานวัสดุ LDHs ในการเป็นเปอร์ออกซิเดสมิมิค และการเป็นตัวดูดซับสีย้อม

สำหรับการใช้ LDHs เป็นเปอร์ออกซิเดสมิมิค ได้พัฒนาวิธีการตรวจวัดไฮโดรเจนเปอร์ออกไซด์ทางสีโดยใช้ เฟอร์รัส เฟอร์ริก เลเยอร์ดับเบิลไฮดรอกไซด์นาโนชีท (Fe^{II}Fe^{III} LDHNS) เป็นตัวเร่งปฏิกิริยา วัสดุดังกล่าวถูกสังเคราะห์ขึ้นจากการผสมระหว่าง เฟอร์รัส (Fe^{2+}) และ เฟอร์ริก (Fe^{3+}) ด้วยวิธีการตกตะกอนร่วมในสภาวะเบส จากการทดลองพบว่า เฟอร์รัส เฟอร์ริก เลเยอร์ดับเบิลไฮดรอกไซด์นาโนชีท มีคุณสมบัติและสามารถทำหน้าที่เป็นตัวเร่งปฏิกิริยาได้คล้ายกับเอนไซม์เปอร์ออกซิเดสที่ได้จากธรรมชาติ ดังนั้นวัสดุดังกล่าวจึงถูกใช้เป็นตัวเร่งปฏิกิริยาออกซิเดชันของเปอร์ออกซิเดสซับสเตรทสองชนิด ได้แก่ ทีเอ็มบี (TMB) และ เอบีทีเอส (ABTS) ในสภาวะที่มีไฮโดรเจนเปอร์ออกไซด์ จะทำให้สารละลายเปลี่ยนสีไปเป็นสีฟ้าและสีเขียวตามลำดับ การพัฒนาวิธีการตรวจวัดไฮโดรเจนเปอร์ออกไซด์ทางสีโดยใช้ ทีเอ็มบี และ เอบีทีเอส เป็นเปอร์ออกซิเดสซับสเตรท มีการตอบสนองแบบเป็นเส้นตรงในช่วง 0.1-50 ไมโครโมลาร์ และ 0.2-20 ไมโครโมลาร์ และสอดคล้องกับขีดจำกัดต่ำสุดในการตรวจวัดเท่ากับ 0.05 ไมโครโมลาร์ และ 0.2 ไมโครโมลาร์ ตามลำดับ วิธีการที่พัฒนาขึ้นนี้มีความจำเพาะเจาะจงและความแม่นยำในการตรวจวัดสูง สามารถนำไปใช้ในการตรวจวัดปริมาณไฮโดรเจนเปอร์ออกไซด์ในตัวอย่างนมและน้ำยาล้างแผลได้จริง และ

คาดว่าวิธีที่พัฒนาขึ้นนี้จะมีศักยภาพในการตรวจหาปริมาณไฮโดรเจนเปอร์ออกไซด์ ในงานทางเทคโนโลยีชีวภาพ อุตสาหกรรมอาหาร กระบวนการวินิจฉัยโรคและอุตสาหกรรมอื่น ๆ

นอกจากนี้ยังทำการศึกษาการใช้งาน LDHs ในการเป็นตัวดูดซับสีย้อม โดยได้ทำการสังเคราะห์วัสดุคอมโพสิตที่ประกอบด้วย อนุภาคนาโนของแมกนีไทต์ (Fe_3O_4 NPs) รีดิวซ์กราฟีนออกไซด์ (rGO) และซิงค์อะลูมิเนียมเลเยอร์ดับเบิลไฮดรอกไซด์ (ZnAl-LDHs) เขียนแทนเป็น Fe_3O_4/rGO/ZnAl-LDHs โดยกราฟีนออกไซด์ (GO) ถูกใช้เป็นตัวออกซิไดซ์ ในการออกซิไดซ์เฟอร์รัสให้เกิดเป็นอนุภาคนาโนของแมกนีไทต์ที่เกาะบนพื้นผิวของกราฟีนออกไซด์ (Fe_3O_4/rGO) ส่วนซิงค์อะลูมิเนียมเลเยอร์ดับเบิลไฮดรอกไซด์ ถูกสังเคราะห์ขึ้นด้วยวิธีการตกตะกอนร่วมระหว่างซิงค์ (Zn^{2+}) และ อะลูมิเนียม (Al^{3+}) ในอัตราส่วนโมลเท่ากับ 3:1 ซึ่งเกิดการเกาะติดกับแผ่น Fe_3O_4/rGO ด้วยแรงดึงดูดทางไฟฟ้าและพันธะไฮโดรเจน และได้ผลิตภัณฑ์เป็น Fe_3O_4/rGO/ZnAl-LDHs ซึ่งถูกนำมาใช้เป็นตัวดูดซับและมีคุณสมบัติเป็นแม่เหล็ก ทำให้ ตัวดูดซับดังกล่าวสามารถแยกออกจากสารละลายได้โดยง่ายด้วยการใช้แม่เหล็กดูดออก ตัวดูดซับ Fe_3O_4/rGO/ZnAl-LDHs ที่สังเคราะห์ขึ้นนี้ถูกนำไปใช้ในการดูดซับเพื่อกำจัดสีย้อมชนิดประจุลบ คือ เมทิลออร์เรนจ์ (MO) และสีย้อมชนิดประจุบวก คือ บริลเลียนท์กรีน (BG) ในสารละลาย จากผลการทดลองพบว่า การดูดซับสีย้อมเมทิลออร์เรนจ์และบริลเลียนท์กรีนมีประสิทธิภาพมากที่สุด โดยใช้เวลาที่เหมาะสมที่เวลา 60 และ 360 นาที ตามลำดับ จลนพลศาสตร์และไอโซเทอมของการดูดซับของสีย้อมทั้งสองชนิด สอดคล้องกับปฏิกิริยาอันดับสองเทียม (pseudo-second-order) และ แบบจำลองแลงเมียร์ (Langmuir model) ตามลำดับ ตัวดูดซับที่สังเคราะห์ขึ้นมีความสามารถในการดูดซับสีย้อมเมทิลออร์เรนจ์และ บริลเลียนท์กรีนได้สูงสุดเท่ากับ 1,111 และ 2,000 มิลลิกรัมต่อกรัมของตัวดูดซับ ตามลำดับ เมื่อใช้ความเข้มข้นเริ่มต้นของสีย้อมเท่ากับ 500 มิลลิกรัมต่อลิตร งานวิทยานิพนธ์นี้ได้เสนอวิธีการสังเคราะห์วัสดุดูดซับด้วยวิธีที่ง่าย จึงสามารถนำไปปรับเปลี่ยนชนิดของโลหะที่ในการสังเคราะห์ได้อย่างหลากหลาย เพื่อให้ได้วัสดุชนิดใหม่และสามารถนำไปประยุกต์ใช้งานได้อย่างกว้างขวาง

ABSTRACT

TITLE	:	SYNTHESIS, MODIFICATION AND APPLICATIONS OF LAYERED DOUBLE HYDROXIDES AS PEROXIDASE MIMIC AND DYE ADSORBENT
AUTHOR	:	KITAYANAN PONLAKHET
DEGREE	:	DOCTOR OF PHILOSOPHY
MAJOR	:	CHEMISTRY
ADVISOR	:	SUPARB TAMUANG, Ph.D.
KEYWORDS	:	LAYERED DOUBLE HYDROXIDES, PEROXIDASE MIMICS, COLORIMETRIC SENSORS, ADSORPTION, DYE

Layered double hydroxides (LDHs), are one of anionic clay materials. LDHs are readily synthesized in laboratories and at low cost. They also contain a good biocompatibility, non-toxicity, large surface area, high catalytic activity, chemical stability, good adsorption ability and anion exchange. This work is focused on the application of LDHs as peroxidase enzyme mimic and dye adsorbent.

For the application of LDHs as peroxidase enzyme mimics, the approach for colorimetric detection of H_2O_2 using $Fe^{II}Fe^{III}$ layered double hydroxide nanosheets ($Fe^{II}Fe^{III}$ LDHNS) was reported. The $Fe^{II}Fe^{III}$ LDHNS were constructed from a mixture of divalent and trivalent Fe ions by co-precipitation method. $Fe^{II}Fe^{III}$ LDHNS were found to possess the superior intrinsic peroxidase-like activity. They were used for catalyzing the oxidation of a peroxidase substrate 3,3′,5,5′-tetramethylbenzidine (TMB) and 2,2′-azino-bis(3-ethylbenzo-thiazoline-6-sulfonic acid)-diammonium salt (ABTS) in the presence of H_2O_2 to produce a blue and green solution product, respectively, which provided a colorimetric detection of H_2O_2. The colorimetric assays displayed linearity for H_2O_2 determination by using TMB and ABTS systems in the range of 0.1-50 µM and 0.5-20 µM, and the corresponding limits of detection were found to be 0.05 µM and 0.2 µM, respectively. This selective approach could be applied for H_2O_2 detection in real milk and disinfectant samples. The proposed method is expected to have more potential for a precise detection of H_2O_2 in biotechnology, food industry, clinical diagnosis life process and other industries.

In addition, LDHs was also used as a dye adsorbent. Composite materials consisting of magnetite nanoparticles (Fe_3O_4 NPs), reduced graphene oxide (rGO), and ZnAl layered double hydroxides (ZnAl-LDHs) denoted as Fe_3O_4/rGO/ZnAl-LDHs have been successfully prepared. GO was used as an oxidizing agent to oxidize Fe^{2+} into Fe_3O_4, then Fe_3O_4/rGO was formed *via* the spontaneous *in-situ* deposition of Fe_3O_4 nanoparticles onto the self-reduced GO surface. ZnAl-LDHs were formed by co-precipitation method with molar ratio of Zn^{2+}:Al^{3+} = 3:1 and attached with Fe_3O_4/rGO sheets *via* electrostatic attraction and hydrogen bonding, resulting in Fe_3O_4/rGO/ZnAl-LDHs as magnetic adsorbent. This magnetic adsorbent can easily be separated from aqueous solutions by using external magnet. Fe_3O_4/rGO/ZnAl-LDHs were applied as an adsorbent to remove anionic methyl orange (MO) and cationic brilliant green (BG) from the aqueous solution. The results showed that MO and BG removal reached equilibrium at 60 and 360 minutes, respectively.The adsorption kinetics and isotherm of both organic dyes followed the pseudo-second-order and Langmuir model, respectively. The maximum adsorption capacities were 1111 and 2000 mg g^{-1} (C_0 = 500 mg L^{-1}) for MO and BG, respectively. This thesis suggests a simple synthesis strategy which can be applied for other types of LDHs. Consequently, a variety of applications can be targeted.

CONTENS

CONTENS (CONTINUED)

PAGE

LIST OF TABLE

TABLE **PAGE**

LIST OF TABLE (CONTINUED)

LIST OF FIGURE

LIST OF FIGURE (CONTINUED)

LIST OF FIGURE (CONTINUED)

LIST OF FIGURE (CONTINUED)

FIGURE **PAGE**

LIST OF FIGURE (CONTINUED)

FIGURE **PAGE**

LIST OF ABBREVIATION

ABBREVIATION	DEFINITION
A	Absorbance
ABTS	2,2’-Azino-bis(3-ethylbenzo-thiazoline-6-sulfonic acid) diammonium salt
BG	Brilliant green
cm^{-1}	Reciprocal centimeter (unit of wavenumber)
emu	Electromagnetic unit
Fe_3O_4	Magnetite
g	Gram
h	Hour
HRP	Horseradish peroxidase
KeV	Kiloelectron volts
K_m	Michaelis–Menten constant
LDHs	Layered double hydroxides
LDHNS	Layered double hydroxides nanosheets
LOD	Limit of detection
M	Molar
Min	Minute
m^2	Square meter
mg	Milligram
mL	Milliliter
mM	Millimolar
MO	Methyl orange
mV	Millivolts
nm	Nanometer
NPs	Nanoparticles
Oe	Oersted
R.S.D	Relative standard deviation
S	Second

LIST OF ABBREVIATION (CONTINUED)

SD	Standard deviation
TMB	3,3′,5,5′-Tetramethylbenzidine
V_{max}	Maximal reaction velocity
rGO	Reduce graphene oxide
rpm	Revolutions per minute
μM	Micro molar
μL	Microliter
^{o}C	Degree Celsius
θ	Bragg’s angle

CHAPTER 1

INTRODUCTION

1.1 The important and the source of the research

Layered double hydroxides (LDHs), also known as hydrotalcite-like compounds (HTlcs) or a class of anionic clays possessing sandwich like structure in which negative anions are sandwiched into positively charged metal layers in a repeating manner, have been studied extensively. The general formula of LDHs is $[M^{II}_{1-x}M^{III}_{x}(OH)_2]^{x+}[A^{n-}_{x/n}]\bullet mH_2O$, where M^{II} and M^{III} are metals in the oxidation states +2 and +3, respectively. A fraction of divalent metal ions (such as Mg^{2+}, Fe^{2+}, Co^{2+}, Cu^{2+}, Ni^{2+}, or Zn^{2+}) coordinated octahedrally by hydroxyl groups in the brucite like layers are uniformly replaced by trivalent metals (such as Al^{3+}, Cr^{3+}, Ga^{3+}, Mn^{3+} or Fe^{3+}) with the molar ratio of $M^{II}/(M^{II} + M^{III})$ (the value of x) normally between 0.2 and 0.33. A^{n-} is the interlayer anion of charge n that leads to the electro-neutrality of the LDHs; for example CO_3^{2-}, which is known to have a very high affinity to the LDH layers but can nevertheless be decarbonated and exchanged with other inorganic (such as Cl^-, SO_4^{2-},NO_3^-, etc.) or organic anions (such as acetate, lactate, dodecyl sulfate, etc.) [1-6]. Interestingly, a partial and isostructural M^{II} to M^{III} substitution would induce a positive charge for these layers, balanced with the negatively charged interlayer region containing anions and water molecules. The wonderful feature of layered double hydroxides is the pliancy of interlayer space enabling them to accommodate various anionic species, and high surface area making them efficient in numerous applications such as adsorbents, anion exchange, catalysts, and biological compatible [3-7]. In this study, application of LDHs as catalyst and adsorbent will be focused on.

Hydrogen peroxide (H_2O_2) is a well-documented powerful oxidizing agent and regarded as major reactive oxygen species component of living cells. It is an essential intermediate in pharmaceutical, clinical, industrial and environmental fields. Moreover, it is widely used as equipment and packaging sanitizer in industrial processes such as water treatment, milk production and electrical circuit cleaning to prolong the shelf life of products, and for medical purposes like wound cleaning [7-11]. However, high level of H_2O_2, usually $\geq 50\ \mu M$, is regarded as a cytotoxic agent. High concentrations of H_2O_2 in living organisms could induce some serious diseases such as cardiovascular [12, 13], cancer [14], etc. In addition, H_2O_2 is one of the products from the reaction of glucose and glucose oxidase enzyme, detection of H_2O_2 leads to the determination of glucose in glucose bioassay. Therefore, due to the significance of H_2O_2 in various fields, the development of efficient and accurate methods for H_2O_2 determination is of interest.

There are several analytical techniques which have been developed for monitoring H_2O_2; for instance, fluorescence [15, 16], chromatography [17], chemiluminescence [18, 19], and electrochemical technique [20, 21]. However, each technique has its limitations such as high cost, high complexity, or strict requirement on equipment. Another technique for the detection of H_2O_2 is colorimetric method [22, 23]. Among these techniques, colorimetric method has attracted more attention since it provides a simple and convenient platform for analyte determination. Besides, it is less dependent on equipment, timesaver, inexpensive and easy to operate as well as convenience for practical applications. In addition, the color change of specific substance can also be rapidly observed by the naked eye for qualitative analysis and easily monitored by UV-Vis spectrophotometer for an accurate quantification. Typically, H_2O_2 can be utilized for catalytic oxidation and coloration of chromogenic agent with the aid of horseradish peroxidase (HRP) as a catalyst. Chromogenic agents including 3,3',5,5'-tetramethylbenzidine (TMB), and 2,2'-azino-bis-(3-ethylbenzothiazoline)-6-sulfonic acid (ABTS) react with H_2O_2 immediately in the presence of HRP to produce a blue and green color product, respectively; which serve as a colorimetric output signal [24-26].

HRP is a natural enzyme with a great practical application based on its good selectivity and high sensitivity under mild condition. However, natural enzymes suffered from some serious disadvantages including high cost, inherent instability and easy denaturation under extreme conditions (e.g. in strong acidic and basic condition, high temperature) or digestion by proteases [27], these have often limited their practical applications [28]. Moreover; the preparation, purification and storage of natural enzymes are usually expensive, difficult and time-consuming, which have inevitably restricted their widespread applications [27-29].

Therefore, it is interesting and challenging to develop novel and efficient artificial peroxidase enzyme mimetics that can overcome certain drawbacks of natural enzymes.

Since Gao et al. [24] found that Fe_3O_4 nanoparticles (NPs) possessed an intrinsic enzyme mimetic activity similar to that found in HRP natural enzyme in 2007, Fe_3O_4 nanoparticles were subsequently used as natural enzymes replacement. HRP natural enzyme contains Fe^{2+} or Fe^{3+} in their reaction centers [28], and these metal centers also found in Fe_3O_4 NPs. Thus, the design of nanomaterials with enzyme-like catalytic activity has attracted extensive attention. Nowadays, variety of inorganic nanomaterials including metal particles, metal sulfides, metal oxides, layered structure and carbon-based nanostructures have been explored as efficient enzyme mimics [7, 8]. Amongst these inorganic nanomaterials, layered materials are one of the promising candidates for being used as catalysts for colorimetric assays due to their low cost, environmental friendliness, high conductivity and high redox activity [30].

Several LDHs materials were found to exhibit intrinsic enzyme mimetic activity. In 2012, Zhang et al. [31] reported the CoFe-LDHs as an effective peroxidase mimetic to catalyze the oxidation of TMB in the presence of H_2O_2 to produce a blue solution. Later in the year 2017, NiCo-LDHs microspheres were used to catalyze the oxidation of ABTS in the presence of H_2O_2 to generate green color solution of $ABTS^{\bullet+}$ [32].

$Fe^{II}Fe^{III}$ layered double hydroxides ($Fe^{II}Fe^{III}$ LDHs), as shown in Scheme 1, contain a mixture of cation between Fe^{2+} and Fe^{3+} ions (with the ratio of Fe^{3+}: Fe^{2+} of 0.25–0.33) have been reported [33] but they have never been used in this application. To the best of our knowledge, the present work is the first report of the Fe^{2+} and Fe^{3+} ions in the LDHs that have the same activity as active reaction centers in HRP natural enzyme.

Therefore, this research focused on the developed a new colorimetric method for detection of H_2O_2 by using $Fe^{II}Fe^{III}$ layered double hydroxide nanosheets ($Fe^{II}Fe^{III}$ LDHNS) which act as peroxidase mimetic. The $Fe^{II}Fe^{III}$ LDHNS were constructed from a mixture of divalent and trivalent Fe ions with simple procedures and green solvent (aqueous medium). $Fe^{II}Fe^{III}$ LDHNS were prepared by co-precipitation method and were used as peroxidase mimetic to catalyze the oxidation of TMB and ABTS chromogenic substrates in the presence H_2O_2 to produce a blue and green color product of oxidized TMB and $ABTS^{\bullet+}$, respectively. Furthermore, the developed colorimetric assays could be applied for H_2O_2 detection in real milk and disinfectant samples.

LDHs also used as adsorbent, anionic and cationic dyes are widely used in industries such as paper, printing, plastic, paint, cosmetics, textile and some other industries. They are well known toxic and hazardous pollutants in wastewater. The dye molecules are ordinarily based on the complex aromatic structure, most of these compounds are highly stable, non-biodegradable and resistant to breakdown by chemical, physical, and biological treatments [34, 35]. Moreover, these organic dyes may be degraded to the carcinogen and toxic products under sunlight irradiation; affecting aquatic life, ecosystem and harmful to human health [34-36]. Therefore, effective treatment of wastewater effluents from these industries to remove the organic dyes from wastewater before discharging into the natural water body is extremely important to environmental safety. Over the past years, several techniques for dyes treatment, including biological degradation [37], chemical degradation [38], adsorption, membrane filtration [39], coagulation [40], photo degradation [41, 42], reverse osmosis [43], or the synergic treatment of different methods have been carried out. Among these attempts, adsorption is considered to be one of the most promising alternatives for removing emerging pollutants because of its high efficiency, simplicity, low cost, easy operation and excellent regeneration ability, which makes it an efficient technique for the removal of organic dyes [35-36]. As present, many adsorbent materials such as activated carbon, fly ash, bentonite, zeolites, metal oxides, biopolymer, oxyhalides and clay materials, have been used to remove organic dyes from wastewater [34, 36, 44]. Among them, a class of anionic clays known as layered double hydroxides (LDHs) or hydrotalcite-like compounds with anions sandwiched in between the brucite-like layers has been proved to be effective adsorbents for removal of dye pollutions [45].

This prominent structure feature allows LDHs to have a powerful ability to trap organic dyes in aqueous solutions [46]. Up until now, many pure LDHs materials or LDHs-based composites have been reported due to their high anion exchange and adsorption ability which allows them to be an alternative adsorbent or ion exchanger [44, 45]. ZnAl LDHs have been widely reported to be able to adsorb a wide range of anionic and cationic dyes from aqueous solution such as methyl orange (MO), congo red (CR) and methylene blue (MB) [1, 45, 47]. Despite the high adsorption capacity of organic dyes by ZnAl LDHs, their low separation efficiency and reclaiming adsorbents at the end of the reaction in liquid system still influenced their industrial application scope [47, 48]. Recently, magnetic separation nanotechnology has attracted much attention to solve the challenge for easy separation and recovery of adsorbent materials, which can be applied by external magnetic field [48-50].

Magnetite nanoparticles (Fe_3O_4 NPs), which is a common magnetic iron oxide, have attracted considerable interest due to their superparamagnetic properties. The superparamagnetic properties coupled to an adsorption process has attracted special attention because it is an easy-to-implement, low-cost and environmentally friendly method. Recent studies have presented an improvement in the adsorption process when a magnetic field is applied, which is attributed to different factors and possible modifications that can change properties of the solution and material under magnetic field effect [51]. However, Fe_3O_4 NPs in aqueous suspensions readily aggregates due to a combination of Lifschitz–van der Waals and magnetic forces, resulting in the limitation of their magnetic properties, structural stability and may also affect reactivity due to the loss of the specific activity of an individual nanoparticle [52]. In order to solve the above-mentioned problems, modification of Fe_3O_4 NPs by deposition on solid supports is achieved.

Graphene is an excellent two-dimensional carbon nanomaterial with atomic thickness. It consists of sp^2-hybridized carbon; it has excellent physic physicochemical and mechanical properties, for instance high flexibility, extremely large theoretical specific surface area and mechanical strength [53, 54]. Graphene oxide (GO) and reduced graphene oxide (rGO) are two of the most important derivatives of graphene, containing oxygen functional groups on its basal planes and edges, such as hydroxyl ($-OH$), carboxyl ($-COOH$), carbonyl ($-C=O$) and epoxy ($C-O-C$) groups [53, 55, 56]. These features impart of GO and rGO with excellent sorption capacity for organic dye pollutants [53, 57].

Yuhua Xue et al. (2011) reported that GO could act as strong oxidizing reagents to effectively oxidize Fe^{2+} into Fe_3O_4 NPs, the resultant Fe_3O_4 NPs-decorated reduced graphene oxides (Fe_3O_4/rGO) was formed via the spontaneous in-situ deposition of Fe_3O_4 NPs onto the self-reduced GO surface in one step approach [58]. The Fe_3O_4/rGO shows interesting magnetic and electrochemical behaviors which useful for potential energy storage, biomedical, catalytic and adsorbent applications [51, 58].

Herein, we demonstrate a simple way to synthesize magnetic adsorbent materials consisting of magnetite nanoparticles (Fe_3O_4 NPs), reduced graphene oxide (rGO), and ZnAl layered double hydroxides (ZnAl-LDHs), denoted as Fe_3O_4/rGO/ZnAl-LDHs. Firstly, the simple synthesis of Fe_3O_4/rGO was carried out by using GO which act as oxidizing agent to oxidize Fe^{2+} from $FeCl_2•4H_2O$ into Fe_3O_4, resulting in Fe_3O_4/rGO. The Fe_3O_4/rGO was formed through the spontaneous *in-situ* deposition of Fe_3O_4 NPs onto the self-reduced GO surface in one step with green synthesis method [51, 58]. This method can also prevent the aggregation of Fe_3O_4 NPs and rGO. This synthesis method requires no toxic solvents and simply carried out at room temperature, therefore, it is green and can be easily controlled the process parameters. Next, ZnAl-LDHs were formed by co-precipitation method with molar ratio of Zn^{2+}:Al^{3+} = 3:1 and attached with Fe_3O_4/rGO sheets via electrostatic attraction and hydrogen bonding, resulting in Fe_3O_4/rGO/ZnAl-LDHs. This magnetic adsorbent can easily be separated from aqueous solutions by using external magnet. Fe_3O_4/rGO/ZnAl-LDHs were applied as adsorbent to remove methyl orange (MO); anionic dye and brilliant green (BG); cationic dye from aqueous solution. To our best knowledge, the adsorption properties of MO and BG on Fe_3O_4/rGO/ZnAl-LDHs magnetic adsorbent have not been reported in the published literature.

1.2 Objectives

1.2.1 To prepare the $Fe^{II}Fe^{III}$ layered double hydroxides nanosheets ($Fe^{II}Fe^{III}$ LDHNs) or green rust hydroxysulphate (GR(SO_4^{2-})) by co-precipitation method as an peroxidase mimic enzyme for colorimetric detection of hydrogen peroxide (H_2O_2).

1.2.2 To investigate the catalytic activity of the synthesized $Fe^{II}Fe^{III}$ LDHNs for colorimetric detection of H_2O_2 by using peroxidase substrate; 2,2'-azino-bis(3-ethylbenzo-thiazoline-6-sulfonic acid)-diammonium salt (ABTS) and 3,3′,5,5′-tetramethylbenzidine (TMB)

1.2.3 To study parameters affecting the sensitivity and selectivity of colorimetric H_2O_2 detection by the synthesized $Fe^{II}Fe^{III}$ LDHNs materials.

1.2.4 To applied the developed method for H_2O_2 detection in real milk and disinfectant samples.

1.2.5 To synthesize the magnetite nanoparticles (Fe_3O_4 NPs)-decorated self-reduced graphene sheets (rGO)/ZnAl layered double hydroxides (ZnAl-LDHs), denoted as Fe_3O_4/rGO/ZnAl-LDHs.

1.2.6 To study parameters affecting the adsorption efficiency for MO and BG removal.

1.2.7 To apply Fe_3O_4/rGO/ZnAl-LDHs as adsorbent for methyl orange (MO) removal from aqueous solution.

1.3 Expected outcomes

1.3.1 Preparation of $Fe^{II}Fe^{III}$ LDHNs was successfully by co-precipitation method.

1.3.2 Magnetic adsorbent or Fe_3O_4/rGO/ZnAl-LDHs have been successfully prepared.

1.3.3 Understanding of the properties and morphology of the synthesis $Fe^{II}Fe^{III}$ LDHNs and Fe_3O_4/rGO/ZnAl-LDHs by using XRD, SEM-EDS, XRD, FTIR, UV-visible and BET.

1.3.4 A sensitive and selective for H_2O_2 colorimetric assay was developed by using $Fe^{II}Fe^{III}$ LDHNs. The as prepared $Fe^{II}Fe^{III}$ LDHNs to enhanced peroxidase-like activity for use in H_2O_2 detection by colorimetric assay.

1.3.5 The developed H_2O_2 colorimetric assay based on $Fe^{II}Fe^{III}$ LDHNs as peroxidase mimic enzyme with ABTS and TMB as peroxidase substrate will provide high potential to H_2O_2 quantitation in real milk and disinfectant sample applications.

1.3.6 The modification of ZnAl-LDHs was modified by using Fe_3O_4-decorated rGO has been proposed for the improvement the magnetic properties and adsorption capacity of magnetic adsorbent. The magnetic adsorbent can easily be separated and regenerated from aqueous solutions by using external magnet.

1.3.7 Fe_3O_4/rGO/ZnAl-LDHs were applied as a high efficiency adsorbent to remove anionic methyl orange (MO) and cationic brilliant green (BG) from aqueous solution.

1.4 Scope of Research

In this work, $Fe^{II}Fe^{III}$ LDHNs and Fe_3O_4/rGO/ZnAl were synthesized. Their applications can be divided into two parts:

Part I: Development of H_2O_2 colorimetric assay based on $Fe^{II}Fe^{III}$ LDHNs

Development of a new colorimetric method for detection of H_2O_2 will be carried out by using $Fe^{II}Fe^{III}$ layered double hydroxide nanosheets ($Fe^{II}Fe^{III}$ LDHNS) which act as peroxidase mimetic. The $Fe^{II}Fe^{III}$ LDHNS were constructed from a mixture of divalent and trivalent Fe ions with simple procedures and green solvent (aqueous medium). Preparation of $Fe^{II}Fe^{III}$ LDHNs was successfully by co-precipitation method. The synthesis of $Fe^{II}Fe^{III}$ LDHNs can be proved by various analytical tools including XRD, SEM-EDS, FTIR and XPS. The as-prepared $Fe^{II}Fe^{III}$ LDHNs was used as peroxidase mimetics to catalyze the oxidation of TMB and ABTS chromogenic substrates in the presence H_2O_2 to produce a blue and green color product of oxidized TMB and $ABTS^{\bullet +}$ with a maximum absorption at 652 nm and 418 nm, respectively.

For TMB substrate, H_2O_2 detection was carried out in air-saturated solution referencing literature [7, 8]. In a typical experiment, 50 μL of 0.3 mg mL^{-1} $Fe^{II}Fe^{III}$ LDHNS, 100 μL of different concentrations of H_2O_2, 200 μL of 1 mM TMB (in ethanol) and 400 μL of 0.1 M pH 4.0 acetate buffer solution, were mixed. The mixture was then allowed to react for 30 min at ambient temperature (25 ± 1 °C), then the absorbance was measured by UV-Vis absorption spectrophotometer at 652 nm.

For ABTS substrate, according to a previous report [26], H_2O_2 detection was performed by a facile step in deionized water. The mixed solution, which include 50 μL of 0.3 mg mL^{-1} $Fe^{II}Fe^{III}$ LDHNS, 100 μL of different concentrations of H_2O_2, 100 μL of 20 mM ABTS and 500 μL of deionized water; were mixed together. The solution mixture was kept to react at ambient temperature (25 ± 1 °C) for 30 min prior to monitoring by UV-Vis absorption spectrophotometer at 418 nm.

After that, the proposed method is expected to be more potential for exact detection of H_2O_2 in real milk and disinfectant samples.

Part II: Synthesis of Fe_3O_4/rGO/ZnAl for the removal of methyl orange and brilliant green from aqueous solution

We demonstrate a simple way to synthesize magnetic adsorbent materials consisting of magnetite nanoparticles (Fe_3O_4 NPs), reduced graphene oxide (rGO), and ZnAl layered double hydroxides (ZnAl-LDHs), denoted as Fe_3O_4/rGO/ZnAl-LDHs. Firstly, the simple synthesis of Fe_3O_4/rGO was prepared by using GO which act as oxidizing agent to oxidize Fe^{2+} from $FeCl_2$•$4H_2O$ into Fe_3O_4, resulting to Fe_3O_4/rGO. The Fe_3O_4/rGO was formed through the spontaneous *in-situ* deposition of Fe_3O_4 NPs onto the self-reduced GO surface in one step with green synthesis method. This method can also prevent aggregation of Fe_3O_4 NPs and rGO. Moreover, the synthesis method requires no toxic solvents and simply carried out at room temperature. It is green synthesis method and can easily control the process parameters. Next, ZnAl-LDHs were formed by co-precipitation method and attached with Fe_3O_4/rGO sheets via electrostatic attraction and hydrogen bonding, resulting in Fe_3O_4/rGO/ZnAl-LDHs. This magnetic adsorbent can easily be separated from aqueous solutions by using external magnet. The properties and morphology of magnetic adsorbent were characterized by XRD, SEM-EDS, FTIR, and BET analysis. Fe_3O_4/rGO/ZnAl-LDHs were applied as adsorbent to remove methyl orange (MO, anionic dye) and brilliant green (BG, cationic dye) from aqueous solution.

1.4.1 Synthesis of materials

1.4.1.1 Preparation of $Fe^{II}Fe^{III}$ LDHNs

1.4.1.2 Preparation of graphene oxide

1.4.1.3 Preparation of Fe_3O_4/rGO

1.4.1.4 Preparation of Fe_3O_4/rGO/ZnAl LDHs

1.4.2 Characterization of the $Fe^{II}Fe^{III}$ LDHNs and Fe_3O_4/rGO/ZnAl LDHs

1.4.2.1 X-ray photoelectron spectroscopy (XPS)

1.4.2.2 Scanning Electron Microscopy (SEM)

1.4.2.3 Energy Dispersive X-Ray Spectroscopy (EDS)

1.4.2.4 X-ray Diffraction (XRD) analysis

1.4.2.5 Fourier Transform Infrared Spectroscopy (FTIR)

1.4.2.6 UV-visible spectroscopy (UV-visible)

1.4.2.7 Brunauer-Emmett-Teller (BET) surface area analysis

1.4.2.8 Zeta potential analysis

1.4.2.9 Vibrating Sample Magnetometry (VSM)

1.4.3 Colorimetric method for H_2O_2 detection by using $Fe^{II}Fe^{III}$ LDHNs

1.4.3.1 UV-Visible Absorption spectra of ABTS and TMB reaction

1.4.3.2 Parameters that effect the sensitivity of the H_2O_2 detection

1) Effect of buffer pH (0.2 M acetate buffer)
2) Effect of the reaction time
3) Effect of $Fe^{II}Fe^{III}$ LDHNs concentration
4) Effect of ABTS and TMB substrate concentration

1.4.3.3 The apparent Michaelis-Menten constant (K_m)

1.4.3.4 Linear concentration range of H_2O_2 for ABTS and TMB substrate

1.4.3.5 Application of H_2O_2 determination to milk samples

1.4.4 Adsorption of MO and BG by using Fe_3O_4/rGO/ZnAl LDHs

1.4.4.1 Adsorption behavior of MO and BG from aqueous solution

1) Effect of contact time and initial dyes concentration
2) Effect of pH, adjusted by adding 0.1 M HCl or NaOH solution
3) Effect of adsorbent dosage

1.4.4.2 Adsorption kinetics

1.4.4.3 Adsorption isotherms

1.4.4.4 Adsorption mechanisms

1.4.4.5 Desorption and Regeneration of Fe_3O_4/rGO/ZnAl-LDH

CHAPTER 2
LITERATURE REVIEWS

2.1 Layered double hydroxides (LDHs)

Layered double hydroxides (LDHs) are a group of inorganic lamellar compounds of basic nature. The LDHs are known as hydrotalcite-like compounds (HTlc). The mineral hydrotalcite, which was discovered in Sweden around 1842, is a hydroxycarbonate of magnesium and aluminum and can be considered a prototype of this class of materials [59]. The hydrotalcite $Mg_6A_{l2}(OH)_{16}CO_3 \cdot 4H_2O$ structure results from stacking brucite-like layers $Mg(OH)_2$ containing a positive charge due to a partial substitution of Mg^{2+} by Al^{3+}. The positive charge is compensated by anions located in the interlamellar spaces (Figure 2.1) [59-61]. Although LDHs exist as naturally occurring minerals, they are also relatively simple and economical to synthesize. LDHs have relatively weak interlayer bonding and, as a consequence, exhibit excellent ability to capture organic and inorganic anions. The most interesting properties of LDHs include large surface area, high anion exchange capacity (100-300 $m^2\ g^{-1}$) [62] that is comparable to those of anion exchange resins, and good thermal stability [59-62]. In recent years these materials have received considerable attention due to their specific structure with different potential applications such as catalysts, precursors to mixed metal oxide catalysts, adsorbents, anion exchangers, flame retardants, etc. [63].

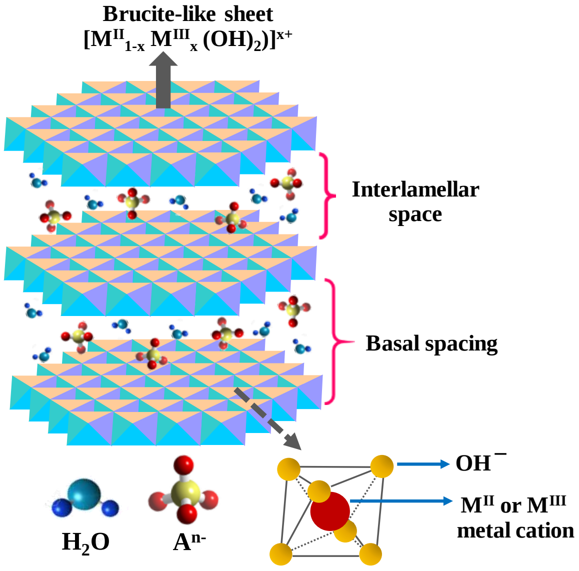

Figure 2.1 Schematic representation of LDHs structure.

2.2 Composition and structure of LDHs

Chemical composition of layered double hydroxides is the exciting feature which defines their use in various applications and imparts phenomenal properties in these compounds. The general formula of LDHs to describe the chemical composition is given as follow[$[M^{II}_{1-x} M^{III}_{x}(OH)_2]^{x+} [A^{n-}_{x/n}]\bullet mH_2O$, where M^{II} and M^{III} can be any divalent and trivalent metal ion whose ionic radius is similar to that of Mg^{2+} such as Mg^{2+}, Ca^{2+}, Fe^{2+}, Co^{2+}, Zn^{2+}, Cu^{2+} and Fe^{3+}, Al^{3+}, Bi^{3+}, In^{3+}, La^{3+}, Ga^{3+}, respectively. A^{n-} can be any compensating anion may be Cl^-, OH^-, CO_3^{2-}, SO_4^{2-}, NO_3^-, organic, inorganic, carboxylate, coordination compound, oxoanion and polyoxometalates [61]. The value of *m* is the amount of water present in the interlamellar region and x is the ratio $M^{III} / (M^{II} + M^{III})$ [59-63]. Additionally, true LDHs phases are often only observed when $0.2 < x < 0.33$ resulting in M^{II} / M^{III} ratios of 2:1- 4:1 being reasonably stable, however, exceptions have been reported in the literature [64, 65]. In the LDHs, the M^{II} and M^{III} cations are linked by OH units coordinated at the octahedral positions forming sheets, which are then stacked on top of each other to give a layered structure similar to that of the mineral brucite ($Mg(OH)_2$), giving positively charged sheet [64]. The net positive charge is compensated by anions in the interlayer region between the brucite-like sheets. Some hydrogen bonded water molecules may occupy the free space in this interlayer region [66-68]. The structure of LDHs and a typical octahedral unit are shown in

Figure 2.1. The basal spacing is the total thickness of the brucite-like sheet and the interlayer region. The octahedral units of M^{II} and M^{III} metal cations (sixfold coordinated to OH^{-}) share edges to form infinite sheets. These sheets are stacked on top of each other and are held together by hydrogen bonding. The anion and the water molecules are randomly located in the interlayer region and are labile, being free to move by breaking bonds to the layers and forming new ones [59-63]. This prominent structure feature allows LDHs to have a powerful ability to trap organic dyes in aqueous solutions [46]. Up until now, many researches have been reported to synthesize pure LDHs materials or LDHs-based on composites due to their have high anion exchange and adsorption ability which allows them to be an alternative adsorbent or ion exchanger [60].

2.3 Properties of LDHs

Anion exchange capacity, colloidal properties, morphological properties, thermal stability, particle size, surface area, crystallinity, porosity and tensile strength are important physical characteristics that influence the applications of LDHs. These properties are dependent on methods of preparation used to synthesize these layered compounds [59].

2.3.1 Anion Exchange Capacity

The Anion Exchange Capacity (AEC) of LDHs depends on the metallic cation ratio (M^{II} / M^{III}), the ability of the involved anion in stabilizing lamellar structure and molecular mass of the cations and anions involved. AEC values might change between 200 and 450 mol kg^{-1}. Values bellow 200 mol kg^{-1} are not possible, once the M^{II} and M^{III} ratio is very low to support LDH structure reported by Leroux and Besse (2004) [69].

2.3.2 Colloidal properties

Particle size is influenced by synthesis condition variables, for example time, temperature, pH and reaction stoichiometry. Small particle size and rough surface is obtained with variable pH, while larger particles are obtained in constant pH method showing sharp peak. SEM and TEM techniques can be used to determine the particle size [70]. The small particle size and low charge density of some LDH are important for systems with colloidal characteristics and/or delamination (stacking structure loss). The large size of the host anion often causes interlayer diffusion problems [69].

2.3.3 Morphological properties

Physical properties such as morphology, surface area, porosity and particle size are extremely important to describe LDH and, of course, can define its applications. Scanning Electron Microscopy (SEM) can be applied to assess the morphology of these materials.

Crystallinity and pore size are important to describe catalytic and adsorptive properties of LDHs. Mass transfer process and regioselectivity are promoted by the uniformity of porous structure. LDHs have high specific surface area of (100 ± 300) m^2 g^{-1}. High surface area facilitates guest host interactions. Larger crystallites synthesized by constant pH method exhibit lower surface area. Surface area of particle can be enhanced after calcination by transforming them into corresponding oxides or oxy hydroxides. Nitrogen adsorption process can be used to analyze porosity of a compound [69, 71].

2.3.4 Thermal stability

Thermal decomposition temperatures are dependent on several factors such as, LDHs crystallinity, nature, cations molar ratio (M^{II} / M^{III}), and the interlayer anion type (organic or inorganic). Thermal characterization of these materials is performed by Thermogravimetric Analysis (TGA) and Differential Scanning Calorimetry (DSC) techniques [69].

2.3.5 Tensile strength

Tensile strength of these compounds decreases by increasing the concentration of LDHs. However, a sharp decrease in elongation at break and steady increase in modulus was observed with increase in concentration of LDHs. It is concluded that change tensile properties with concentration of LDHs is due to the combined effect of compatibilizer and dispersed LDHs particles [72].

2.4 Preparation/Synthesis of LDHs

2.4.1 Co-precipitation method

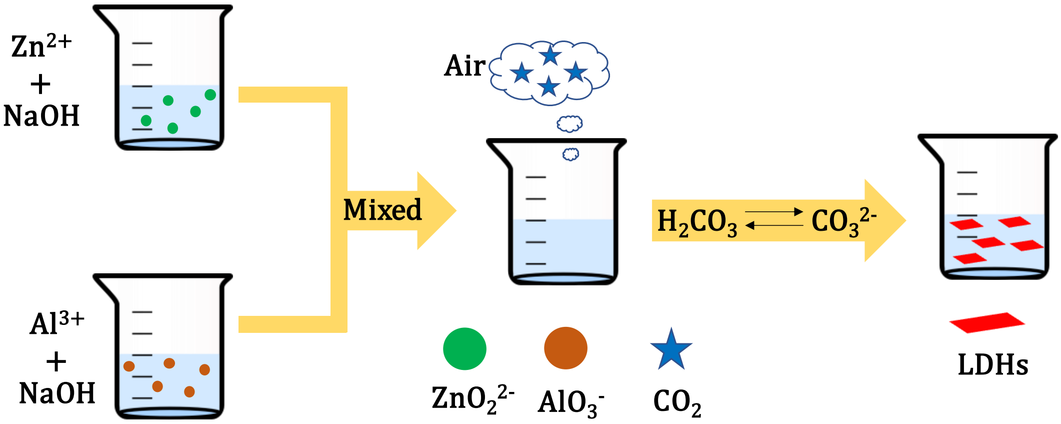

Figure 2.2 Schematic illustrating the preparation process of ZnAl LDHs by co-precipitation method [73].

Co-precipitation method is commonly used procedure for preparing LDHs because it produces large amount of material and is easy to handle at laboratory level. It has been used extensively for the one-pot direct synthesis of LDHs containing a variety of layer cations and interlayer anions [59]. In this procedure aqueous solutions of divalent (M^{2+}) and trivalent metals (M^{3+}) are used as precursors which contain intercalating anions; the M^{2+} and M^{3+} hydroxide layers are nucleated and grown from an aqueous solution containing the anion that is to be incorporated into the LDH. An interesting feature of this method is that there exists diversity in anionic species to intercalate in OH^{-} sheets. The anion that is to be introduced must have a high affinity for the hydroxide layers, otherwise the counter anions of the metal salts may be incorporated, thus contaminating the LDH. For this reason, metal nitrate or chloride salts are commonly utilized because of the low selectivity of LDHs towards these anions [74]. Another interesting feature of this preparative method is that a wide variety of anionic species can be directly intercalated between the hydroxylated sheets. Layered double hydroxides are prepared at low and high supersaturation conditions.

2.4.1.1 Precipitation at low supersaturation

Precipitation at low supersaturation requires slow addition of divalent and trivalent metals salt in the chosen ratio into aqueous solution containing desired anion, and pH is maintained at selected value. A second solution of an alkali is added into the mixture salts solution simultaneously at such a rate as to maintain the pH at a selected value leading to facilitate homogeneous precipitation of the two metallic salts [59, 60, 63, 69]. The anion that is to be introduced should have a high affinity for the LDH layers and be present in excess, otherwise the counter-anions of the metal salts may be incorporated by competing reactions. Consequently, metal nitrate and chloride salts are commonly used because of the low selectivity of LDHs toward these anions. Furthermore, LDHs have a high affinity for carbonate anions and hence, unless this is the target anion, reactions are generally carried out under nitrogen in order to avoid absorption of atmospheric carbon dioxide which would generate carbonate ions in situ [59, 63].

One advantage of this method is that in many cases it allows careful control of the charge density (M^{2+} / M^{3+} ratio) of the hydroxide layers of the resulting LDH by means of precise control of the solution pH. The second advantage is that low supersaturation conditions usually give rise to precipitates with higher crystallinity than those obtained under high supersaturation conditions, because in the former situation the rate of crystal growth is higher than the rate of nucleation [59, 60, 63, 69].

2.4.1.2 Precipitation at high supersaturation

High supersaturation of LDHs precipitation was performed by the instantaneous addition of mixed M^{2+} / M^{3+} salt solution into an alkali solution containing desired interlayer anion. Preparations under conditions of high supersaturation generally give rise to less crystalline materials, because of the high number of crystallization nuclei. Because this method leads to a continuous change in the pH of solution, the formation of impurity $M(OH)_2$ and/or $M(OH)_3$ phases, and consequently an LDH product with an undesired M^{2+} / M^{3+} ratio, often results [59, 60, 63]. Thermal treatment performed following coprecipitation may help increase the crystallinity of amorphous or badly crystallized materials. Hence the synthesis of LDHs at high supersaturation method is less common than low supersaturation for the preparation of LDHs materials [59, 63].

2.4.2 Hydrothermal method

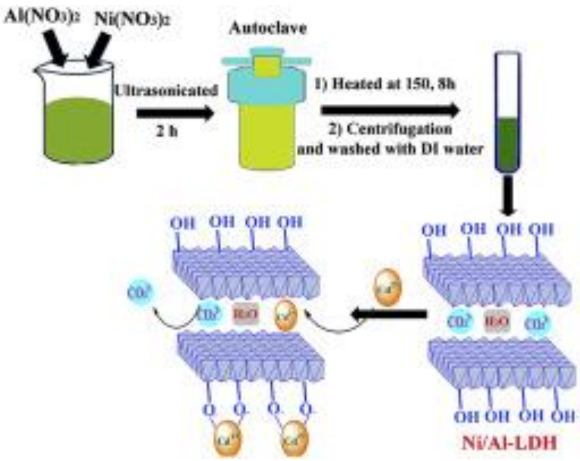

Figure 2.3 Schematic illustrating the preparation process of NiAl LDHs by hydrothermal method [75]**.**

The hydrothermal method is usually used when organic guest species with low affinity for LDHs are required to be intercalated into the interlayers, and when the ion exchange and coprecipitation techniques are ineffective in this case. Hence hydrothermal synthesis has proven efficient because this method ensures no competing anion in the interlayer other than the intended by making insoluble hydroxides as inorganic source. The key features of this method is utilized to control particle size and its distribution [59, 60, 69]. Hydrothermal approach is usually carried out to improve crystallinity and is studied for Mg-Al LDHs. It is found that increase in LDH crystal size results in improved crystallinity of hydrothermally treated samples. One advantage of hydrothermal method, when compared with other co-precipitation ones, is to avoid undesirable waste discard which may be harmful to the environment for instance NO_3^-, OH^-, Cl^-, etc. [60, 69].

2.4.3 Urea hydrolysis method

The urea hydrolysis method is frequently used for synthesis of highly crystalline LDHs to use a urea solution, which gradually hydrolyses to release hydroxide ions and allows an extremely fine control over precipitation. Urea was used as an agent for precipitation from “homogeneous” solution very attractive, and it has long been used in gravimetric analysis to precipitate several metal ions as hydroxides or as insoluble salts when in the presence of a suitable anion [59]. Urea hydrolysis rate can be controlled by the reaction temperature. Hydrolysis of urea proceeds in two steps, the formation of ammonium cyanate (NH_4CNO) as the rate determining step, and the fast hydrolysis of the cyanate to ammonium carbonate [59, 60, 63].

$$CO(NH_2)_2 \rightarrow NH_4CNO \quad (1)$$

$$NH_4CNO + 2H_2O \rightarrow 2NH_4^+ + CO_3^{2-} \quad (2)$$

Hydrolysis rate of urea can be adjusted by controlling the applied temperature during reaction. The hydrolysis of ammonium carbonate gives pH of about 9 which is suitable for precipitating a wide variety of metal hydroxides. Since the working pH for the co precipitation of LDHs is in the range of 9-11, urea is a good candidate for the synthesis of LDHs. On the other hand, the urea method is an ideal way for the preparation of LDHs since during hydrolysis ammonia liberates the hydroxide and carbonate anions which are the main components of LDHs [59, 60, 63]. The compounds prepared using this method display homogeneous sizes and platelet-like primary particles with well-defined hexagonal shapes, crystallinity and specific surface area are observed to increase by using urea, which may be very interesting from the viewpoint of nanotechnology since LDHs offer nano-size two-dimensional spaces for the creation of functional materials [59, 60].

2.4.4 Sol-gel method

In this method, is initially the formation of a sol by hydrolysis and partial condensation of a metallic precursor is then followed by the gel formation. Metallic alkoxides, acetates, or acetylacetonates, as well as many inorganic salts can be used as metallic precursors. The properties of the obtained solid LDHs depend on the hydrolysis and condensation rates of the metallic precursors and can be tuned by controlling different reaction parameters such as pH, nature and concentration of the metallic precursors, solvent and the temperature of synthesis [63, 69].

The sol-gel method has several advantages over traditional methods:

(1) low temperature processing and consolidation is possible

(2) smaller particle size and morphological control in powder synthesis

(3) the homogeneity and structural properties of the resulting solids are controllable at the synthesis level by simply varying the composition of the precursors, temperature, aging time, and removal/addition of reactant species.

The material prepared by sol–gel method has well controlled pore sizes, high specific surface area and high purity [63, 69]. However, currently, it is the less exploited method.

2.4.5 Anion exchange method

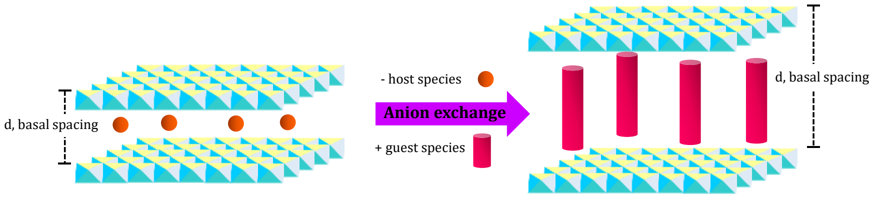

Figure 2.4 Schematic representation of ion-exchange method [59]**.**

Anion exchange method is also a commonly used method for the synthesis of LDHs composites and has been effectively useful for the intercalation of a number of different types of anions. The anion exchange method is useful when the coprecipitation method is inapplicable, in particular when the chosen divalent or trivalent metal cations or the anions involved are unstable in the alkaline solution, or when there is a strong possibility of interaction between the guest species and the metal ion [59, 60]. It is also known as the first LDHs are prepared by co-precipitation method with host anions, most commonly NO_3^-, CO_3^{2-}, and Cl^- as the exchange is easier than multi charged anions. In the later stages, anions present in the interlayer region are exchanged with the preferred anions by stirring the LDH precursor in a solution containing an excess of the anion to be intercalated. To avoid carbonate intercalation the whole process of anion-exchange should be carried out under inert atmosphere [59, 63, 69]. Owing to the fact that the process is reversible, LDHs can be incorporated into polymers after intercalation to improve the chemical and physical properties of the materials, that is, the thermal stability and optical and magnetic properties, and also to change the surface properties of the host from hydrophobic to hydrophilic [63].

The host– guest exchange generally depends on the electrostatic forces between positively charged LDH layers and the exchanging anions. Target anions can be intercalated in two possible ways, as described in the equations [59]:

$$LDH \cdot A^{m-} + X^{n-} \rightarrow LDH \cdot (X^{n-})_{m/n} + A^{m-} \qquad (3)$$

or

$$LDH \cdot A^{m-} + X^{n-} + mH^{+} \rightarrow LDH \cdot (X^{n-})_{m/n} + H_mA \qquad (4)$$

There exists weak electrostatic interaction with layers, and hence these anions can be easily replaced by anions with higher electrostatic interaction with layers [59, 63, 69]. Figure 2.4 shows the schematic representation of ion-exchange method.

There are several factors which determine the extent of ion-exchange in any given case:

(1) Affinity for incoming anion

The exchange efficiency varies depending on the ability of the exchanged anions to stabilize the lamellae and/or to their proportion with respect to the LDHs precursor anion. Generally, the exchange ability of incoming anions increases with increasing charge and decreasing ionic radius. The order of intercalation is as follows: $CO_3^{2-} > HPO_4^{2-} > SO_4^{2-}$ for divalent anions and $OH^- > F^- > Cl^- > Br^- > NO_3^- > I^-$ for monovalent anions. The co-intercalation of a second anion was found to have no effect on the order of ion exchange preference. Because nitrate is exchanged most easily, nitrate pillared LDHs are usually used as the precursors for ion exchange [59, 63, 69].

(2) Exchange medium

The appropriate solvent will favor the anion-exchange process. The interlayer space of LDHs can be expanded to some extent in a suitable solvent medium, which favors the ion exchange process. For example, in aqueous medium favors the exchange by inorganic anions, whilst an organic solvent favors exchange by organic anions [59].

(3) pH value

The working pH should be 4.0 or above 4.0. A low pH value therefore favors liberation of the original anion as the conjugate acid and incorporation of a less basic anion from solution and the hydroxyl layers will break [59].

(4) Chemical composition of the layers

The chemical composition of the LDH sheets influences the charge density of the sheets and the hydration state, thereby affecting the ion exchange process. Some other factors such as temperature also have an impact on the ion exchange process. Anion-exchange process will be more favorable at high temperatures. However, that too high a temperature might have an adverse effect on the structural integrity of the LDHs. Moreover, this method depends on the chemical composition of the brucite type layers [59, 63].

2.4.6 Regeneration/ Rehydration/ Reconstruction method

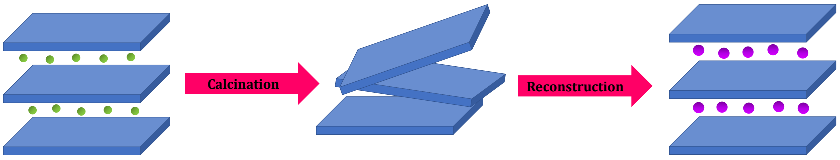

Figure 2.5 Schematic representation of reconstruction method [59]**.**

Regeneration/ Rehydration/ Reconstruction method is based on "memory effect" of some LDH. This method involves calcination of LDHs. Calcination is a process of heating to high temperatures (about 400- 500 °C) in inert atmosphere to remove the interlayer water, interlayer anions, and breakdown partially the hydroxyls from lamellae and convert interlamellar anion into volatile, forming a double oxyhydroxide (or mixed metal oxides). After calcined, a solution containing the anion of interest is added, regenerating the LDHs by hydrolysis and the new intercalated anion. In general, during regeneration process, pH is raised, so it must be corrected to avoid hydroxyl from occupying the interlayer space [59, 60, 69]. This is the method of choice when large anions should be intercalated into LDH or when the chosen anions are not favored for intercalation by ion exchange method. It is also the preferred method for active principle intercalation, because the presence of anions, such as Cl^- or NO_3^-, with possible negative effects into living bodies, is avoided. The incorporation of competing anions is also limited, even if particular care should be paid to the pH value that when raises too much can favor the OH- insertion [59, 69].

2.5 Application of LDHs

The flexibility in composition of LDHs has led to an important class of materials suitable for several existing and future applications in biological, chemical, and environmental processes. LDHs possess high anion exchange capacity, large surface areas, a homogeneous and thermally stable dispersion of the metal ion components. In this work, we have been focused in the research and development of LDHs which enable their use as catalyst precursors or actual catalysts, anion exchangers and adsorbents for diagnosis and environmental applications [60].

2.5.1 Applications in catalysis for colorimetric detection of H_2O_2 and glucose

Flexible composition, synthesis ease (inexpensive or simple), eco-friendliness and high versatility makes LDHs viable candidate in comparison to catalysts used conventionally. LDHs have been largely employed as efficient biosensors, owing to their excellent biocatalytic properties and to the possibility of producing hybrid materials with enzymes. Typically, LDHs employed enzymes were, horseradish peroxidase, and glucose oxidase [76]. Colorimetric method has attracted more attention since it provides a simple and convenient platform for analyte determination. Besides, it is less dependent on equipment, timesaver, inexpensive and easy to operate as well as convenience for practical applications. In addition, the color change of specific substance can also be rapidly observed by the naked eye for qualitative analysis and easily monitored by UV-Vis spectrophotometer for an accurate quantification [31, 77-83]. Initially, glucose oxidase (GOx) catalyzes the oxidation of glucose to generate H_2O_2. Next, horseradish peroxidase (HRP) catalyzes the oxidation of the peroxidase substrate in the presence of newly formed H_2O_2 to produce a colored product, and colorimetric measurement is based on the quantity of this product that is formed. Chromogenic substrates include 3,3',5,5'-tetramethylbenzidine (TMB), and 2, 2'-azino-bis-(3-ethylbenzothiazoline)-6-sulfonic acid (ABTS), which all react immediately and rapidly with H_2O_2 [77-83].

As a natural enzyme, HRP displays a great practical application based on its good selectivity and high sensitivity under mild condition. However, natural enzymes suffered from some serious disadvantages including high cost, inherent instability and easy denaturation under extreme conditions (e.g. in strong acidic and basic condition, high temperature) or digestion by proteases, these have often limited their practical applications. Moreover; the preparation, purification and storage of natural enzymes are usually expensive, difficult and time-consuming, which have inevitably restricted their widespread applications [77-83]. Therefore, it is interesting and challenging to develop novel and efficient artificial peroxidase enzyme mimetics that can overcome certain drawbacks of natural enzymes.

LDHs have been reported as suitable catalysts for many colorimetric reactions, in which they are applied as indicators for many analytical applications [25, 31, 32]. Beginning from the first example of H_2O_2 and glucose colorimetric assay based on the CoFe- LDHs nanoplates. In 2012, Zhang et al. reported the CoFe-LDHs as an effective peroxidase mimetic to catalyze the oxidation of TMB peroxidase substrate in the presence of H_2O_2 to produce a blue solution [31]. Various LDHs materials including CoAl EDLH [77], DNA/CuAl-LDHs [78], C-dot/NiAl-LDHs [79], NiFe-LDHNS [80], Ni-V LDHs/MMO [81] and MXene@NiFe-LDHs [82] have been reported to possess peroxidase-like activity and used for the colorimetric detection of H_2O_2 and glucose by using TMB as peroxidase substrate. In the year 2017, Ni/Co-LDHs microspheres were used to catalyze the oxidation of ABTS in the presence of H_2O_2 to generate green color solution of $ABTS^{\bullet+}$ [32]. LDHs are one of the promising candidates for being used as catalysts for colorimetric assays due to their low cost, environmental friendliness, high conductivity and high redox activity [77-83].

2.5.2 Applications in Adsorbent and Anion-exchange

Fast growing industrial sector has loaded environment with pollutants and toxicants which can cause adverse effects to human health and the surroundings. Recently, environmental pollution is one of the most serious problems in the world due to its deep effect on the future of human beings. Then the investigation for resolving the problem of the environmental pollution in the world began to draw major public attention. Heavy metal ions and organic dye molecules have high toxicity and poor biodegradability for plants and animals at higher concentrations [62]. In recent years, LDHs have been aroused increasing interest as adsorbents by virtue of their properties, which make them attractive materials for adsorbing heavy metal ions and organic dyes. Their abundance in nature, low cost, and good adsorptive properties, a result of their negatively charged layers and high large surface per unit of mass, large porosity, high anion-exchange capacities and flexible interlayer space, etc. i.e. it satisfies all the requisite properties of adsorption of heavy metal ions and organic dye molecules. [62, 69]. The anion-exchange capacity of LDHs is affected by the nature of the interlayer anions initially present and the layer charge density (i.e. the M^{II}/M^{III} molar ratio in the brucite-like sheets). When the layer charge density is very high the exchange reaction may become difficult. LDHs greater affinities for multivalent anions compared with monovalent anions [62].

Adsorption is a surface phenomenon, used for the accumulation of contaminants between two phases such as solid-liquid interface or solid-gas interface. Normally, adsorption mechanism occurs due to intermolecular forces of attraction between adsorbent and adsorbate. When a solution having adsorbate encounters the adsorbent (porous media), surface forces at the interface concentrate the solutes on the surface of the adsorbent [84-87]. LDHs can take up anion species from solution by three different mechanisms: surface adsorption, interlayer anion-exchange and reconstruction of a calcined LDH precursor by the “memory effect” [62].

Removal of dyes from wastewater is of significant consideration because dyes being colored pollutant cause environmental hazards. Up until now, many researches have been reported to synthesize pure LDHs materials or LDHs-based on composites due to their have high anion exchange and adsorption ability which allows them to be an alternative adsorbent or ion exchanger, make these materials favorable to remove contaminants from aqueous systems [44, 45] Moreover, LDHs have been successfully applied in the removal of toxic metals and organic dyes in aqueous solution.

Heavy metal cations and radioactive metals were eliminated by using chelate ligands intercalated LDH because of flexible interlamellar region and specific pH. The adsorption characteristics of metal cations were separately studied and concluded that metal cations were separated due to high bond energy and high sensitivity of OH of LDHs. Various uncalcined and calcined of LDHs have been used to investigate the adsorption of heavy metal cations [88].

ZnAl LDHs have been widely reported to be able to adsorb a wide range anionic and cationic dyes from aqueous solution such as methyl orange (MO), congo red (CR) and methylene blue (MB). Adsorption efficiencies of calcined and uncalcined LDHs were compared and found that better removal efficiency is exhibited by calcined LDHs [1, 45, 47].

2.6 Literature reviews/ Related research

2.6.1 Nanomaterials based on iron (Fe^{2+} and Fe^{3+}) (Magnetite nanoparticles) as peroxidase mimetics and application in H_2O_2 and glucose detection

Fe_3O_4 nanoparticles were subsequently used as natural enzyme replacements. Natural HRP enzyme contains Fe^{2+} or Fe^{3+} in its reaction centers, and these metal centers are also found in Fe_3O_4 NPs. Thus, there has been extensive research performed to design nanomaterials with enzyme-like catalytic activity.

L.Z. Gao et al. (2007) [24] provide the first report that Fe_3O_4 MNPs possess intrinsic peroxidase-like activity comparable to that of an enzyme catalyzed reaction. Peroxidase activity has a wide range of practical applications. The Fenton's reaction is Fe^{2+}/Fe^{3+} ions in solution (Fenton's reagent) are known to catalyst the breakdown of hydrogen peroxide (H_2O_2). Furthermore, a number of peroxidase enzymes (including the haem-containing enzyme HRP) and enzyme mimetics also contain Fe^{2+} or Fe^{3+} in their reaction centres. Moreover, they found that the Fe_3O_4 MNPs catalyzed the reaction of the peroxidase substrate including 3,3,5,5- tetramethylbenzidine (TMB), di-azo-aminobenzene (DAB) and o-phenylenediamine (OPD) in the presence of H_2O_2 to produce a colour reaction. Like enzymatic peroxidase activity, such as observed for the commonly used enzyme HRP. In addition, the catalytic activity of the Fe_3O_4 MNPs is, like HRP, dependent on pH, temperature and H_2O_2 concentration. In this study, they are providing the first report that Fe_3O_4 MNPs possess intrinsic peroxidase-like activity comparable to that of an enzyme catalyzed reaction (HRP). In this work, Fe_3O_4 MNPs catalyzed the reaction of different peroxidase substrates to give the same colour changes as HRP. The fact that Fe_3O_4 MNPs have peroxidase-like activity poses the potential for novel applications and characterized this activity, taking HRP as a comparison. Further, Fe_3O_4 MNPs are highly effective as a catalyst, with a higher binding affinity for the peroxidase substrate than HRP and approximately 40-fold higher level of activity at the same concentration of catalyst. Importantly, Fe_3O_4 MNPs have the additional property of magnetic, which allows them to be recovered for recycling, or to be used as a capture agent when appropriately modified. Taken together, these results demonstrate that Fe_3O_4 MNPs act as a robust and effective peroxidase mimetic, as well as a versatile capture and detection tool.

F.F. Peng et al. (2008) [90] present peroxidase-like catalytic properties of Fe_3O_4 nanoparticles (NPs) with three different sizes, synthesized by chemical co-precipitation and sol-gel methods, were investigated by UV–Vis spectrum analysis. By compare Fe_3O_4 NPs with average diameters of 11, 20, and 150 nm. The Fe_3O_4 NPs with three different sizes can all catalyze the reaction of the typical peroxidase substrate 3,3′,5,5′-tetramethylbenzidine (TMB) in the presence of H_2O_2. The result found that all the three catalysts are active for the substrate, and the activities for the reaction vary substantially in the order 11 nm > 20 nm > 150 nm. It implies that with the reduced particles size, the catalytic activity increases. This phenomenon may be due to the small size particles having more active sites and larger specific surface area, which lead to more efficient contact with the substrate. The data was fitted to the Michaelis–Menten model to obtain the parameter apparent K_m. The result found that the K_m value of Fe_3O_4 NPs with TMB as the substrate was 0.27 mM, which was lower than that of HRP, 0.4 mM. It suggested that Fe_3O_4 NPs have a higher affinity for TMB than HRP and may be used as a hopeful peroxidase mimic. The enzyme mimics, Fe_3O_4 NPs has advantages such as moderate cost, ease of preparation and long-time stability comparing to natural enzymes and show magnetic properties. The peroxidase-like catalytic activity of Fe_3O_4 NPs and its size dependence will extend the application of the materials in biological and chemical field.

H. Wei et al. (2008) [26] present the novel properties of Fe_3O_4 MNPs as peroxidase mimetics reported in 2007 by Yan et al. to detect H_2O_2. The Fe_3O_4 MNPs were prepared via a co-precipitation method. The as-prepared Fe_3O_4 MNPs were then used to catalyze the oxidation of a peroxidase substrate 2,2′-azino-bis(3-ethylbenzo-thiazoline-6-sulfonic acid) diammonium salt (ABTS) by H_2O_2 to the oxidized colored product which provides a colorimetric detection of H_2O_2. Detection of glucose was combination of the catalytic reaction of glucose with glucose oxidase (GOx) and the Fe_3O_4 MNPs catalytic reaction. The developed method exhibited sensitive and selective response toward glucose detection. The colorimetric method showed good response toward H_2O_2 and glucose detection with a linear range from $5x10^{-6}$ to$1x10^{-4}$ mol L^{-1} and $5x10^{-5}$ to $1x10^{-3}$ mol L^{-1} respectively. More importantly, a sensitive and selective analytical platform for glucose detection was fabricated using GOx and the as-prepared Fe_3O_4 MNPs. Thus, the Fe_3O_4 MNPs can rival natural enzymes and obviously that the Fe_3O_4 MNPs possess intrinsic peroxidase-like activity but also showed great potential applications in varieties of easy preparation, simple, robust, cost-effective, stability in rough conditions, and easy-to-make biosensors in the future.

2.6.2 Layered double hydroxides as peroxidase mimetics and application in H_2O_2 and glucose detection

Layered double hydroxides (LDHs), also known as hydrotalcite-like compounds, are a class of anionic clays with two-dimensional (2D) structure. There is great interest in these materials because they are non-toxic, stable, easy to prepare, and also because of their good biocompatibility, large surface area, good adsorption ability, and anion exchange. Several LDH materials were found to exhibit intrinsic enzyme mimetic activity

Y. Zhang et al. (2012) [31] discovered the proof of concept of using CoFe layered double hydroxide (CoFe-LDHs) nanoplates as an effective peroxidase mimetic to catalyze the oxidation of peroxidase substrate 3,3′,5,5′-tetramethylbenzidine (TMB) in the presence of H_2O_2 to produce a blue solution. Based on these findings, a novel CoFe-LDHs nanoplate based colorimetric assay to detect H_2O_2 was developed for the first time. CoFe-LDHs were synthesized by a modified co-precipitation method. They found that, after addition of CoFe-LDHs, the TMB−H_2O_2 solution exhibits three strong adsorption peaks centered at 372, 456, and 652 nm, respectively, which can be attributed to that CoFe-LDHs catalyze the oxidation of TMB by H_2O_2. Additionally, the absorbance at 652 nm increased with increasing H_2O_2 concentration. This peroxidase-like activity is dependent on H_2O_2 concentration, pH, and temperature. The maximum catalytic activity was obtained under the following optimal conditions: pH 4.0, 30 °C. Note that the catalytic activity of the CoFe-LDHs is more stable at higher H_2O_2 concentration than HRP. This behavior was very similar to that observed with other NPs-based peroxidase mimetics and HRP. The linear range and detection limit of H_2O_2 are estimated to be from 1 to 20 mM and 0.4 mM, respectively. The designed method provides a linearity range of glucose from 1 to 10 mM and detection limit about 0.6 mM. As inorganic nanomaterials, CoFe-LDHs are expected to be more stable than natural enzymes. CoFe-LDHs also had good storage stability. When it was stored in water at room temperature for 2 months, no obvious decrease in the response to H_2O_2. Importantly, CoFe-LDHs also had good reusability after repeated cycles of H_2O_2 sensing. In addition, the selectivity of the developed method for glucose determination, they investigated the influence of maltose, lactose and fructose, using the same determination procedure as described for glucose. This develop sensing system exhibits excellent selectivity for glucose detection.

L. Chen et al. (2013) [77] present the novel approach for exfoliation of Co-Al layered double hydroxides (Co-Al LDHs) in aqueous solution of L-asparagine and obtained a stably stored colloidal suspension of 2D nanosheets. Co-Al LDHs were synthesized by salt–acid treatment, and anion exchange methods. L-Asparagine is a water-soluble amino acid whose carbonyl groups would have a strong interaction with the LDH host layers and the amino groups might weaken the interlayer interactions. This simple method did not need reflux at high temperature, overcame the drawback of using organic solvents. Co-Al ELDH could rapidly catalyze oxidation of the peroxidase substrate 3,3′,5,5′-tetramethylbenzidine (TMB) in the presence of H_2O_2, producing a blue color reaction with strong absorption at 652 nm. The 2D nanosheets of Co-Al ELDH had brilliant enhanced peroxidase-like activity compared to unexfoliated LDH and the activity was dependent on pH, temperature, amount of Co-Al ELDH, and H_2O_2 concentration. The optimum conditions were approximately pH 6 at 25 °C for 10 min incubation, which are very similar to the values for HRP natural enzyme. This method provides the linear range is from 0.01 mM to 0.2 mM and the H_2O_2 can be detected as low as 0.01 mM. For glucose detection, the linear range from 0.05 mM to 0.5 mM is realized with the lowest detection of 0.05 mM. On this basis, simple, rapid and selective colorimetric methods for H_2O_2 and glucose detections were developed. The presented means was used for glucose detection in fruit juices and fine results were obtained.

L. Chen et al. (2013) [78] demonstrate that the herring sperm (hs) DNA, which is commonly commercially available, destroys the lamellar structure of LDHs under constant vibration under ambient conditions. The hsDNA molecules consist of negative charge was adsorbed onto positively charged of LDH nanosheets forming

DNA– LDH nanohybrids. They hypothesized that hsDNA molecules impacted and exfoliated the bulk crystal into nanosheets. This effectively increased the specific surface area of the catalyst material. Furthermore, hsDNA adsorbed onto LDH nanosheets via electrostatic forces forming a multicomponent material and led to an enhanced catalytic activity. On the basis of the high catalytic activity of DNA/CuAl–LDH nanosheets, a rapid, sensitive, and convenient approach was developed for colorimetric detection of H2O2 and glucose. The hsDNA-LDH nanohybrids which showed superior catalytic activity compared to pure LDH in the oxidation of 3,3′,5,5′-tetramethylbenzidine (TMB) in the presence of H_2O_2. Considering that the element species of catalysts would be another factor affecting the catalytic activity, three LDHs containing CuAl, CoAl, or NiAl were simultaneously researched. As a result, the DNA/ CuAl– LDH nanosheets expressed better peroxidase- like activity than DNA/CoAl–LDH and DNA/NiAl–LDH nanohybrids. Therefore, DNA/CuAl–LDH nanohybrids could be applied for colorimetric detection of H_2O_2, on the basis of the absorbance of the oxidized TMB product being proportional to the concentration of H_2O_2. The catalytic activity was sensitive to variations in pH, temperature, catalyst amount, and substrate concentration. The suitable conditions for colorimetric detection of H_2O_2 was carried out at pH 4, 35 °C for 15 min incubation. The DNA/CuAl–LDH nanohybrids catalyzed the reaction of H_2O_2 and TMB which showed typical Michaelis–Menton kinetics. The method gave a wide linear range for H_2O_2 and glucose from 2×10^{-5} to 2×10^{-3} M and 4×10^{-5} to 2×10^{-4} M, respectively. The detection limit are 1×10^{-5} M and 8×10^{-6} M for H_2O_2 and glucose, respectively. The lowest visual concentration of glucose by the naked eye is 40 mM. On this basis, colorimetric methods to detect H_2O_2 and glucose were developed. This selective approach could be applied for glucose detection in real serum samples. Due to the low cost, ease of preparation, negligible toxicity, the hsDNA–LDH nanohybrids may be applied in a wide range of fields, such as biocatalysis, environmental monitoring, and medical diagnosis.

Y. Guo et al. (2015) [79] provides a novel carbon dot/NiAl-layered double hydroxide (C-dot/NiAl–LDH) hybrid material is successfully prepared through electrostatic self-assembly of positively charged NiAl–LDH nanoplates (3.74 ± 0.3 mV) and negatively charged C-dots (−5.09 ± 0.5 mV). C-dot/ NiAl–LDH exhibits intrinsic peroxidase-like activity, which shows enhanced catalytic activities compared with

C-dots and NiAl–LDH. The hybrid material facilitates the electron transfer between 3,3′,5,5′- tetramethylbenzidine (TMB) and H_2O_2, which oxidizes TMB to form a blue product with shows maximum adsorption at 652 nm. The catalytic activity is dependent on the pH, temperature, and H_2O_2 concentration. The kinetics analysis indicates that the catalysis is in accordance with typical Michaelis–Menten kinetics and follows a ping–pong mechanism. On the basis of the peroxidase-like activity of C-dot/NiAl–LDH, the hybrid material can employ colorimetric detection of H_2O_2 provide linearity range from 0.2 to 20 μM with a lower detection limit of 0.11 mM. The hybrid material also shows better stability than horseradish peroxidase (HRP) when exposed to solutions with different organic solvents and temperatures. The proposed method is successfully applied for the determination of H_2O_2 in milk samples

T. Zhan et al. (2017) [80] proposed the ultrathin NiFe-layered double hydroxide nanosheets (NiFe-LDHNS) were prepared by exfoliating bulk LDH in l-asparagine aqueous medium. Exfoliation of LDHs by using l-asparagine has become more and more acceptable because of simple procedures and green solvent. The transmission electron microscopy and atomic force microscopy results reveal that NiFe-LDHNS have about 200–300 nm lateral size and less than 2 nm thickness with the broken edges rather than the original hexagon of hydrotalcite. It is believed that exfoliation can endow NiFe-LDHNS with more exposed active sites and more accessible inner surface of host layers. The 2D NiFe-LDHNS can perform the excellent peroxidases-like catalytic activity. In this process, the substrate 3,3′,5,5′-tetramethylbenzidine (TMB) can be efficiently oxidized by NiFe-LDHNS in the presence of H_2O_2 to form a blue dark product (ox-TMB) with an absorption peak at 652 nm. The 2D NiFe-LDHNS exhibited the superior enzyme mimic activity to the bulk NiFe-LDH, which was attributed to the more exposed active sites and more accessible inner surface of single or several layers. Thus NiFe-LDHNS exhibit the much higher peroxidase-like ability than the unexfoliated LDH. Therefore, a simple and sensitive non-enzyme biosensor was developed for colorimetric detection of H_2O_2 and glucose. Based on this, a colorimetric method for H_2O_2 and glucose are developed, which can be applied to glucose detection in real samples.

L. Su et al. (2017) [32] presents a simple strategy development for Ni/Co layered double hydroxides (LDHs) as a substitute for natural peroxidase. The Ni/Co LDHs microspheres were fabricated by a facile one step chemical co-precipitation method. The obtained Ni/Co LDHs exhibited ease of preparation, low-cost, and water-solubility; importantly, this material showed high catalytic activity in neutral pH solutions (phosphate buffer, Tris–HCl buffer, and even water). They found that the Ni/Co exhibit peroxidase-like activity similarly natural enzyme. Ni/Co LDHs, as a peroxidase mimic, exhibits several advantages. Firstly, compared to natural enzymes, Ni/Co LDHs has advantages of ease of preparation, low-cost, and water-solubility. Secondly, Ni/Co LDHs showed high catalytic activity over a broad temperature range, from 10 °1C to 40 °C. Lastly, but most importantly, Ni/Co LDHs had high catalytic activity at neutral pH. Because of the similar optimal conditions (neutral pH, 37 °C) for the catalytic activity of Ni/Co LDHs with glucose oxidase (GOx), choline oxidase (ChOx), acetylcholinesterase (AChE), etc. Moreover, they developed a one-step method for the detection of glucose and ACh in water, which showed shorter reaction times (200 s), simpler steps and ease of operation. Ni/Co LDHs microspheres could rapidly catalyze oxidation of the peroxidase substrate ABTS in the presence of H_2O_2 in ideionized water at 37 °C, producing a green color reaction with strong absorption at 417 nm. Glucose detection was selected as an application model system to evaluate the performance of this method, which showed a linear detection range from 0.5 mM to 100 mM with a detection limit of 0.1 mM. The linear detection range was from 10 mM to 150 mM with the limit of detection as 1.62 mM. The proposed method had ease of operation, simple steps, and was rapid for glucose and AChE detection in real samples. On the basis of these advantages and virtues, Ni/Co LDHs could become attractive nanozymes in biotechnology and bioassays and create a great influence on the next generation of enzyme mimetic systems.

2.6.3 Layered double hydroxides as an adsorbent for removal of cationic and anionic dye from aqueous solution

Up until now, many researches have been reported to synthesize pure LDHs materials or LDHs-based on composites due to their have high anion exchange and adsorption ability which allows them to be an alternative adsorbent or ion exchanger. LDHs have been widely reported to be able to adsorb a wide range anionic and cationic dyes from aqueous solution.

F. Z. Mahjoubi et al (2017) [1] reported the synthesis of Zn–Al layered double hydroxides intercalated with carbonate (CO_3^{2-}), nitrate (NO_3^-), chloride (Cl^-) and sulphate ions (SO_4^{2-}) through a co-precipitation method at a constant solution pH. The presence of the anions in the hydrotalcite structure was confirmed by infrared spectroscopy. The XRD analyses showed that the interlayer spacing followed this order: $Zn\text{-}Al\text{-}SO_4 > Zn\text{-}Al\text{-}Cl > Zn\text{-}Al\text{-}NO_3 > Zn\text{-}Al\text{-}CO_3$. The adsorption affinity correlated with the structural properties, essentially the interlayer spacing, in each LDH. These materials were used as adsorbent for adsorption of methyl orange (MO). The experiments for MO adsorption onto synthesized samples were investigated under various conditions such as contact time, initial dye concentration and solution pH. The effective pH range for the MO removal was found to be 3.5–4.5. The kinetics data can be described accurately by a pseudo-second-order kinetic model instead of a pseudo-first-order model. The equilibrium data were fit well to the Langmuir and Dubinin–Radushkevich isotherm models. The Zn-Al-LDH samples exhibited exceptional Langmuir maximum adsorption capacities of 2758, 2455, 2270 and 1684 mg/g for $Zn\text{-}Al\text{-}SO_4$, Zn-Al-Cl, $Zn\text{-}Al\text{-}NO_3$ and $Zn\text{-}Al\text{-}CO_3$, respectively. The precursors exhibited exceptional adsorption capacities indicating that these materials could be a potentially efficient broad-spectrum adsorbent for dye removal from wastewater. With respect to the selection of sorbents, these results are of practical interest for the optimization of aquatic environment remediation technologies.

N. Kumara et al. (2017) [44] presents the synthesis of microsheets of chlorine interlayer ZnAl layered double hydroxides (Cl-ZnAl LDHs) hexagonal nanoplates by simply varying the molar ratio of salts precursors in the presence of hexamethylenetetramine (HMTA) through a facile and cost-effective, simple chemical route. It was observed that the experimental conditions, especially the varying ratio of salt precursors (aluminium chloride and zinc nitrate), played a pivotal role in the respective morphological transformation and in obtaining the pure phase of Cl-ZnAl LDHs with microsheets like morphology. The Cl-ZnAl LDHs hexagonal nanoplates have been unique structural features and high specific surface area, the adsorption capability of microsheets of Cl-ZnAl LDHs hexagonal nanoplates towards adsorption of Cr(VI) ions and methyl orange (MO) from aqueous solution. The effective pH range for the Cr(VI) ions and MO onto Cl-ZnAl LDHs microsheets were found to be pH 5 and pH 6, respectively. The underlying adsorption kinetics followed the pseudo-second-order model for both Cr(VI) ions and MO pollutants. The adsorption of Cr(VI) ions and MO on the as-synthesised sample was monolayer adsorption which followed well the Langmuir, isotherm model. According to the Langmuir model, the maximum adsorption capacity of Cr(VI) ions and MO onto Cl-ZnAl LDHs microsheets were found to be 172.41- 223.24 mg/g and 284.90–359.71 mg/g respectively in the temperature range 25–35 °C. Further, the XRD, FT-IR and SEM-EDS measurements after adsorption evidenced the entering of Cr(VI) ions into the interlayer and surface adsorption of Cr(VI) ions and MO onto reconstructed LDHs. The excellent adsorption capacity of prepared microsheets of Cl-ZnAl LDHs hexagonal nanoplates is owing to its unique structural morphology, a high specific surface area with high pore volume and different anion uptake mechanisms.

X. Guo et al. (2018) [45] synthesized Hierarchically porous composites constructed by ZnAl-Cl type layered double hydroxides (LDH) nanosheets and amorphous $Al(OH)_3$ nanosheets via a facile sol-gel route for the adsorption of two typical anionic dyes Methyl Orange (MO) and Congo Red (CR) from aqueous solutions. The micro-macrostructure and adsorption properties of hierarchically porous ZnAl-LDH/$Al(OH)_3$ composites before and after calcination were investigated. Calcination at 500 °C allows the transformation from LDH composite to layered double metal oxides (LDO), while the macrostructure is basically maintained with a macropore size of 0.5 μm, a porosity of 53.1% and a BET surface area as high as 122 $m^2 g^{-1}$. Adsorption performances show that hierarchically porous composites exhibit ultrafast adsorption rates and high adsorption capacities in the removal of anionic dyes CR and MO. XRD and FTIR results after the dyes adsorption indicate that the intercalation of MO and CR anions into the LDH structure via ion exchange with the pristine chloride ions group and the attachment on the external $Al(OH)_3$ surface determine the adsorption behavior, thus leading to an expansion of the interlayer space. And the calcined products LDO-based composites can be reversibly transformed back into the LDH structure via reconstruction procedure in the presence of dyes aqueous solution. The maximum adsorption capacities of hierarchically porous LDH- based composites and LDO composites via calcination at 500 °C are 2348. 3 and 1574. 4 mg g^{-1} for CR and 1013. 5 and 1015. 1 mg g^{-1} for MO, respectively. The adsorption kinetics followed the pseudo second-order model, and the adsorption isotherms followed well the Langmuir isotherm model. Ion exchange and hydrogen bond existed in the surface of LDH and amorphous $Al(OH)_3$ were considered as the main adsorption mechanisms for ZnAl-LDH/$Al(OH)_3$, intercalation of dyes anions into the interlayer to reconstruct the structure for ZnAl-LDO, respectively. The adsorption– desorption cycles confirm that the as- prepared ZnAl- LDH/ $Al(OH)_3$ own excellent recyclable properties, which suggest that the adsorbents may be promising for the adsorption of organic dyes from wastewater.

H. Starukh (2019) [47] synthesized ZnAl LDH in carbonate and in calcined forms with Zn:Al ratio 1:2, 1:3 and 1:4. These materials were applied for the study of anionic indigo carmine (IC) and cationic methylene blue (MB) dyes removal from aqueous media in batch mode. The highest adsorption of IC was observed for ZnAl LDH calcined at 600 °C with Zn: Al ratio 2:1. The removal of the dye from aqueous solutions with calcined LDH is accompanied by the reconstruction of their layered structure and formation of ZnAl LDH-carbonate. At small initial concentrations of the dye the adsorption of IC occurs on the external surface of LDH. At higher concentration of IC in solutions the adsorption of IC on the internal surface of LDH takes place. In this case the net increase in the basal spacing from 0.76 nm for ZnAl LDH in carbonate form to 1.92 nm for the IC derivative was determined. The sorption capacity of calcined ZnAl LDH to cationic dye MB was extremely low in single dye solutions. The highly effective removal of MB with calcined ZnAl LDHs was achieved from the solutions that contained MB and IC dyes. The simultaneous adsorption of anionic IC and cationic MB occurred on calcined ZnAl LDH. The complete removal of MB and IC was reached at MB:IC ratio 1:2. IC - modified ZnAl LDH demonstrated high activity for the removal of MB from its solutions. The total removal of both dyes was 930 and 320 mg/g for IC and MB, correspondingly. The effective removal of MB from the solutions was observed also when IC based ZnAl LDH were applied as sorbents. The LDH–dye sludge can be reused as pigment for ink, cosmetics, foods, lacquers, coatings, polymers.

Despite the high adsorption capacity of organic dyes by ZnAl LDHs there are low separation efficiency and reclaiming adsorbents at the end of the reaction in liquid system still influenced their industrial application scope. Recently, magnetic separation nanotechnology has been attracted much attention to solve the challenge for easy separation and recovery of adsorbent materials, which can be applied by external magnetic field [51, 52]. Magnetite nanoparticles (Fe_3O_4 NPs) is a common magnetic iron oxide have attracted considerable interest due to their superparamagnetic properties; a required and important magnetic property in most of separation of adsorbent materials by external magnetic field, their high specific surface area, low-toxicity and hence are biocompatible [48, 53, 57]. However, Fe_3O_4 NPs in aqueous suspensions readily aggregates due to a combination of Lifschitz–van der Waals and magnetic forces, resulting in may limit their magnetic properties, structural stability and may also affect reactivity due to the loss of the specific activity of an individual nanoparticle [57]. In order to solve above problems, introducing modification of Fe_3O_4 NPs with deposits on solid supports. Graphene is an excellent two-dimensional carbon nanomaterial with atomic thickness. It consists of sp^2-hydrized carbon; its excellent physic physicochemical and mechanical properties, for instance high flexibility, extremely large theoretical specific surface area and mechanical strength. Graphene oxide (GO) and reduced graphene oxide (rGO) are one of the most important derivatives of graphene, contains oxygen functional groups on its basal planes and edges, such as hydroxyl (−OH), carboxyl (−COOH), carbonyl (−C=O) and epoxy (C−O−C) groups [53-55]. These features impart of GO and rGO with excellent sorption capacity for organic dye pollutants.

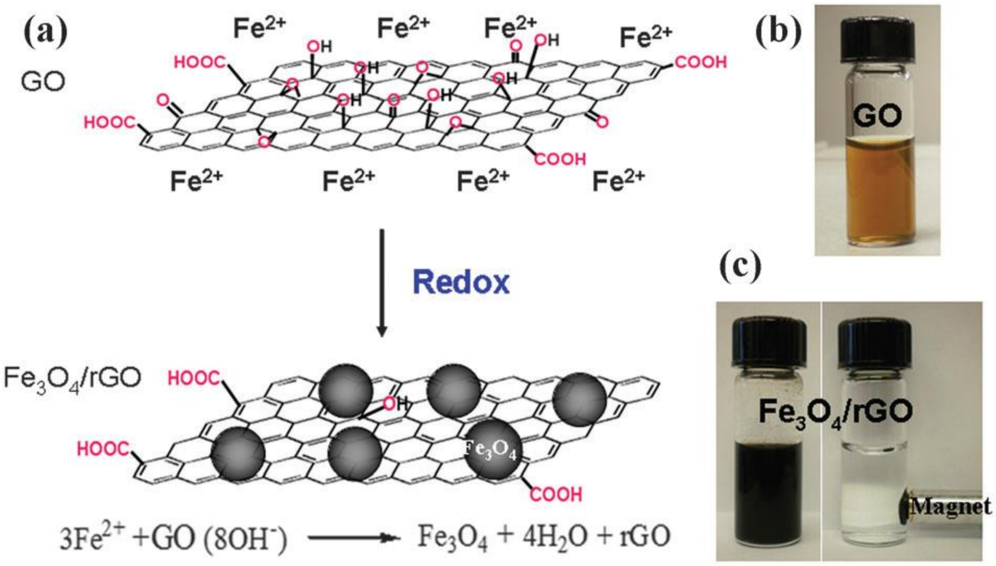

$$3Fe^{2+} + GO\ (8OH^-) \longrightarrow Fe_3O_4 + 4H_2O + rGO$$

Figure 2.6 Scheme of (a) a schematic representation of the preparation route to Fe_3O_4/rGO via redox reaction between GO and Fe^{2+}. Photos showing a water/NH_4OH (pH = 9) solution of Fe_3O_4/rGO (b) before and (c, left panel) after the redox reaction with Fe^{2+}, and (c, right panel) with an applied magnet [58]**.**

Y. Xue (2011) [58] discovered that GOs could act as strong oxidizing reagents to effectively oxidize Fe^{2+} into Fe_3O_4 nanoparticles, which simultaneously deposited on the self-reduced GO surface. The consequence Fe_3O_4-nanoparticle-decorated reduced graphene oxide (Fe_3O_4/rGO) shows interesting magnetic and electrochemical behaviors useful for potential energy storage, catalytic, and even biomedical applications (e.g., supercapacitors, magnetic bioimaging and targeted drug delivery). GO can be used to oxidize many metals and even non-metal ions. Therefore, the methodology developed in this study could be regarded as a facile, but effective and versatile, approach toward the fabrication of reduced graphene sheets decorated with many other metal oxide nanoparticles of practical significance. The simple synthesis of Fe_3O_4/rGO was prepared by using GO which act as oxidizing agent to oxidize Fe^{2+} from $FeCl_2$ or $FeSO_4$ into Fe_3O_4, resulting to Fe_3O_4/rGO. The Fe_3O_4/rGO was formed through the spontaneous *in-situ* deposition of Fe_3O_4 NPs onto the self-reduced GO surface in one step with green synthesis method. The reaction process is described as follows:

$$2\mathrm{Fe}^{2+} + \mathrm{GO} \rightarrow 2\mathrm{Fe}^{3+} + \mathrm{rGO} \tag{5}$$

$$+)\quad \mathrm{Fe}^{2+} + 2\mathrm{Fe}^{3+} + 8\mathrm{OH}^{-} \rightarrow \mathrm{Fe_3O_4} + 4\mathrm{H_2O} \tag{6}$$

$$3\mathrm{Fe}^{2+} + \mathrm{GO}\,(8\mathrm{OH}^{-}) \rightarrow \mathrm{Fe_3O_4} + 4\mathrm{H_2O} + \mathrm{rGO} \tag{7}$$

This method can be also preventing the aggregation of Fe_3O_4 NPs and rGO. Moreover, the synthesis method reported that requires no toxic solvents and simple carry out at room temperature, it is green synthesis method can be easily controlled the process parameters. These Fe_3O_4-nanoparticle-decorated rGO showed strong attraction towards an external magnet, leading to an almost full separation of the Fe_3O_4/rGO out of the solution. This clearly indicates that Fe_3O_4 nanoparticles have imparted useful magnetic properties to the rGO.

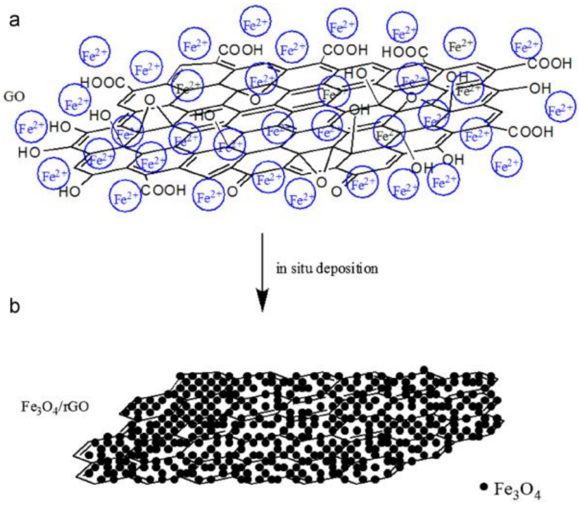

Figure 2.7 Schematic illustration of the formation of Fe_3O_4/rGO nanocomposite via a one-step in situ chemical deposition method [51]**.**

P.S. Teo et al. (2012) [51] propose a simple, cost-effective, efficient, and green approach to synthesize iron oxide/graphene (Fe_3O_4/rGO) nanocomposite using in situ deposition of Fe_3O_4 nanoparticles on reduced graphene oxide (rGO) sheets in analkaline condition. Increasing the weight ratio of Fe^{2+} to GO increases the Fe_3O_4 particle size on the GO sheets and the magnetic strength of the nanocomposites. The

Fe_3O_4/rGO nanocomposites were dispersible in polar solvents for all the prepared weight ratios and were magnetic, and thus they are a promising material for multifunctional applications. The synthesis of the Fe_3O_4/rGO nanocomposite involves the redox reaction between GO and Fe^{2+}. In the redox reaction, the oxidation state of iron (II) is increased to iron (III) while the graphene oxide (GO) is reduced to rGO. The Fe^{2+} ions are first coordinated onto the surface of the GO sheets. The GO acts as an oxidizing agent (Eq. (8)), effectively increasing the oxidation state of the Fe ions from Fe^{2+} to Fe^{3+}. This is followed by the reaction of the Fe^{3+} ions, in an alkaline condition, into Fe_3O_4 nanoparticles (Eq. (9)) on the surface of the rGO. The formation of Fe_3O_4 could also occur using the OH^- groups attached to the GO surface (Eq. (10)). During the redox reaction, the polar oxygenated functional groups on the GO sheets serve as the anchoring sites for the Fe_3O_4 nanoparticles, consequently preventing serious agglomeration of the magnetic nanoparticles.

$$2Fe^{2+} + GO \rightarrow 2Fe^{3+} + rGO \tag{8}$$

$$+)\quad Fe^{2+} + 2Fe^{3+} + 8OH^- \rightarrow Fe_3O_4 + 4H_2O \tag{9}$$

$$3Fe^{2+} + GO\,(8OH^-) \rightarrow Fe_3O_4 + 4H_2O + rGO \tag{10}$$

Separation of the Fe_3O_4/rGO nanocomposite from the solution could be achieved by applying an external magnetic field, thus demonstrating the magnetic properties of the nanocomposite. The Fe_3O_4 particle size, magnetic properties, and dispersibility of the nanocomposite could be altered by adjusting the weight ratio of GO to Fe^{2+} in the starting material.

F. Zhang et al. (2015) [57] synthesized magnetic composites consisting of magnetite (Fe_3O_4), graphene oxide (GO), and Mg_3Al−OH layered double hydroxide (LDH), denoted as MGL composites by a mechano-hydrothermal (MHT). The MHT method provides a simple and environmentally friendly route for synthesizing GO−LDH composite materials. The MGL composites exhibited good water-dispersity and strong magnetic response. The application of the synthesized MGLs used for removing the heavy-metal Pb (II) and the hydrophobic organic pesticide 2,4-dichlorophenoxyacetic acid (2,4-D) from aqueous solutions. More affinity of the MGLs for Pb (II) than for 2,4-D was observed in the competitive sorption. With increasing pH from 4−10 for Pb(II) and 2,4-D. The removal of Pb(II) occurred mainly from the sorption contribution of the LDH component via surface induced precipitation of $Pb_3(CO_3)_2(OH)_2$, whereas that of 2,4-D occurred mainly owing to the sorption contributions of both the LDH and GO components. The sorption of 2,4-D on the LDH component was primarily through the intercalation of 2,4-D anions into the LDH gallery, whereas that on the GO component was attributed to their π−π and hydrophobic interactions. The adsorption isotherms followed well the Langmuir isotherm model. MGL composites are potential sorbents for wastewater treatment. To the best of our knowledge, this is the first report of the magnetic composites of GO and LDHs and their application for the removal of both heavy-metal and hydrophobic organic pollutants. The benefit of MGL composites can be easily separated using a magnetic separation process after being used for the removal of pollutants from aqueous solutions.

B. Zhang et al. (2018) [53] modified the magnetic three-dimensional composites, which contain magnetite (Fe_3O_4) particles, grapheme oxide (GO), and MgAl-layered double hydroxides (MgAl-LDHs) denoted as MGO/MgAl-LDH composites. The synthesis of MGO/MgAl-LDH composites was applied as adsorbents to remove emulsified oils from various oil-in-water (O/W) emulsions. Oil removal study results showed that the maximum removal efficiency for the crude oil was a mass ratio of LDHs/MGO = 1:1, while the maximum removal efficiencies for decane and white oil were a mass ratio of LDHs/MGO = 1:3. Under a suitable mass ratio of LDHs to MGO, 98−99% of emulsified oils could be removed by MGO/MgAl-LDH composites. Experimental data were best fitted to the Langmuir isotherm model. Thermodynamic analysis indicated that the adsorption process was both exothermic and spontaneous. The emulsified oil removal efficiencies were increased with increasing ionic strength. In addition, MGO/MgAl-LDH composites could maintain good oil removal efficiency after reusing over five cycles, indicating their great potential for use in an oily wastewater treatment. The adsorption data were well described by the Langmuir isotherm model. Adsorption thermodynamic results indicated that the adsorption process was both exothermic and spontaneous. The advantage of MGO/MgAl-LDH composites after wrapped with oil droplets were attracted and separated from the solution by an external magnetic field.

CHAPTER 3
EXPERIMENTAL

3.1 Instrumentation

Equipments used in this work were list in table 3.1.

Table 3.1 Instrumentation for characterizations, colorimetric measurements and dyes adsorption.

Instrument	Model	Company
Particle size analyzer	Zetasizer Nano ZS	Malvern Instruments Ltd.
Fourier transform infrared spectrometer (FT-IR)	Spectrum Two	Perkin Elmer, USA
X-ray diffractometer (XRD)	X’PERT MPD	Philip, Finland
Energy dispersive X-Ray spectrometer (EDS)	X-Stream-2	OXFORD instruments, UK
Scanning electron microscope (SEM)	JSM 7610F Plus	JEOL, Japan
X-ray photoelectron spectroscopy (XPS)	AXIS ULTRA^{DLD}	Kratos Analytical, UK
Vibrating sample magnetometry (VSM)	VSM 7403; 79	Lake Shore, USA
Zetasizer analysis	Zetasizer Nano ZS	Malvern Instruments Ltd.
Gas Sorption Surface Area and Pore Size Analyzer	Quadrasorb-EVO	Quantachrome, USA
UV-vis spectrophotometer	UV-2600	Shimadzu, Japan

3.2 Reagents and Chemicals

All chemicals used in this work were summarized in Table 3.2.

Table 3.2 List of reagent, grade and their suppliers.

Chemical and reagent	Grade	Supplier
Ferrous sulfate heptahydrate ($Fe(SO_4)_2$•$7H_2O$)	AR	Acros Organic
Ferric sulfate monohydrate ($Fe_2(SO_4)_3$ •H_2O)	AR	Acros Organic
Sodium hydroxide ($NaOH$)	AR	Carlo Erba
Hydrogen peroxide (H_2O_2) (30%)	AR	Merck
2,2'-Azino-bis(3-ethylbenzo-thiazoline-6-sulfonic acid) diammonium salt (ABTS)	99.99% pure	Sigma-Aldrich
β-D-glucose ($C_6H_{12}O_6$)	AR	Sigma-Aldrich
Maltose ($C_{12}H_{22}O_{11}$)	AR	Sigma-Aldrich
Lactose ($C_{12}H_{22}O_{11}$)	AR	Sigma-Aldrich
Fructose ($C_6H_{12}O_6$)	AR	Sigma-Aldrich
Sodium acetate trihydrate (CH_3COONa•$3H_2O$)	AR	Merck
Ethanol (CH_2OH)	AR	Carlo Erba
Glacial acetic acid (CH_3COOH)	AR	Carlo Erba
3,5,3´5´-tetramethylbenzidine (TMB)	AR	Acros Organics
Methyl orange (MO)	AR	Sigma-Aldrich
Brilliant green (BG)	AR	Sigma-Aldrich
Graphite powder <20 μm	AR	Sigma-Aldrich
Sulfuric acid (H_2SO_4)	AR	Carlo Erba
Sodium nitrate ($NaNO_3$)	AR	Carlo Erba
Potassium permanganate ($KMnO_4$)	AR	Merck
Hydrochloric acid (HCl)	AR	Merck
Ferrous chloride tetrahydrate ($FeCl_2$•$4H_2O$)	AR	Sigma-Aldrich
Ammonium hydroxide (NH_4OH)	AR	Merck
Zinc nitrate hexahydrate ($Zn(NO_3)_2$•$6H_2O$)	AR	Merck
Aluminum nitrate nonahydrate ($Al(NO_3)_3$•$9H_2O$)	AR	Panreac

Table 3.2 **List of reagent, grade and their suppliers (Continued).**

Chemical and reagent	Grade	Supplier
Sodium carbonate (Na_2CO_3)	AR	Univar
Potassium Iodide (KI)	AR	Carlo Erba
Ammonium molybdate [$(NH_4)_6 Mo_7O_{24} \cdot 4H_2O$]	AR	Sigma-Aldrich
Potassium Iodate (KIO_3)	AR	Carlo Erba
Sodium Thiosulfate ($Na_2S_2O_3$)	AR	Merck

3.3 Preparation of $Fe^{II}Fe^{III}$ LDHNS

The synthesis of $Fe^{II}Fe^{III}$ LDHNS was prepared by prescriptive: $[Fe^{2+}]/[Fe^{3+}]$ ratio of 3, total Fe concentration ($[Fe^{2+}] + [Fe^{3+}]$) of 0.2 M and 0.3 M NaOH with a $[OH^-]/([Fe^{2+}] + [Fe^{3+}])$ ratio of 3/2.

3.3.1 Chemical preparation

A mixture solution of Fe^{2+} and Fe^{3+} ions: 0.15 M of Ferrous sulfate heptahydrate ($FeSO_4 \cdot 7H_2O$) and 0.05 M of Ferric sulfate hydrate ($Fe_2(SO_4)_3 \cdot H_2O$).

2.0851±0.0050 g of $FeSO_4 \cdot 7H_2O$ and 0.5223±0.0050 g of $Fe_2(SO_4)_3 \cdot H_2O$ were dissolved and diluted with deionized water to 50 mL by volumetric flask to give a mixture solution of Fe^{2+} and Fe^{3+} ions.

Sodium hydroxide (NaOH) solution (0.3 M)

0.6000±0.0050 g of NaOH was dissolved and diluted with deionized water to 50 mL in beaker to give a 0.3 M NaOH solution.

3.3.2 Synthesis of $Fe^{II}Fe^{III}$ Layered Double Hydroxide (LDHNS)

$Fe^{II}Fe^{III}$ LDHNS were synthesized by co-precipitation method from a mixture of divalent and trivalent Fe ions as described in detail by A. Géhin et al. [33]. In brief, mixed solution of Fe^{2+} and Fe^{3+} ion was prepared by dissolving $FeSO_4 \cdot 7H_2O$ and $Fe_2(SO_4)_3 \cdot H_2O$ in 50 mL of deionized water. The ratio $[Fe^{2+}]/[Fe^{3+}]$ of 3 and total Fe concentration ($[Fe^{2+}] + [Fe^{3+}]$) of 0.2 M were required. Then, 50 mL of 0.3 M NaOH with $[OH^-] / ([Fe^{2+}] + [Fe^{3+}])$ ratio of 3/2 was added to the mixed Fe^{2+}-Fe^{3+} solution. Due to the fact that Fe^{2+} ions can easily be oxidized; the reaction was performed under N_2 gas and magnetic stirring (~500 rpm) was applied to ensure a fast and complete dissolution. The reaction process is as follows [33, 90]:

$$4Fe^{2+}_{aq} + 2Fe^{3+}_{aq} + 12OH^{-} + SO_4^{2-} \rightarrow Fe^{II}_4\, Fe^{III}_2\, (OH)_{12}SO_4 \qquad (11)$$

A black-brown precipitate appeared immediately. After complete addition, the pH was maintained at approximately 6.9. Then, the precipitate was aged for 24 hours under N_2 gas at room temperature. Finally, the solid product was separated from the solution by centrifugation and washed three times with deionized water; the green-brown powder was obtained. The expected final product was $Fe^{II}Fe^{III}$ LDHNS of formula $[Fe^{II}_4Fe^{III}_2\,(OH)_{12})]^{2+}\bullet[SO_4\cdot mH_2O]^{2-}$ [33, 90].

3.4 Characterizations of $Fe^{II}Fe^{III}$ LDHNS

3.4.1 X-ray Diffraction (XRD) analysis

X-ray diffraction (XRD) used for characterized the crystalline nature of as prepared nanosheets was done using X-ray diffractometer model X’PERT MPD, Philip in Finland as shown in Figure 3.7. The XRD analysis of $Fe^{II}Fe^{III}$ LDHNS was carried out by using Cu_{α} radiation wavelength 0.154 nm in 2θ values were taken from 10^o to 80^o (θ value is 1.5416 Å). The results are present in Section 4.1.1.

3.4.2 Scanning Electron Microscopy (SEM)

Scanning Electron Microscopy (SEM) model JSM 7610FPlus, JEOL in Japan as shown in Figure 3.8 was used to examine the morphology of as prepared materials. The morphologies of the $Fe^{II}Fe^{III}$ LDHNS was studied with scanning electron microscope under these following parameters. Nanosheets was attached on SEM stubs coated with platinum (20 mA, 60 s) before measurement for characterized by SEM. The SEM was operated at 15 kV and magnification at 10,000X in the vacuum atmosphere. The results are present in Section 4.1.2.

3.4.3 Energy Dispersive X-Ray Spectroscopy (EDS)

Energy Dispersive X-Ray Spectroscopy (EDS or EDX) model x-stream-2, OXFORD instruments from United Kingdom as shown in Figure 3.8 used in conjunction with scanning electron microscopy (SEM) was used to investigate the elemental composition. $Fe^{II}Fe^{III}$ LDHNS was attached on SEM stubs for studied the elemental composition by using EDS. The results are present in Section 4.1.3.

3.4.4 X-ray photoelectron spectroscopy (XPS)

X-ray photoelectron spectroscopy (XPS) model AXIS ULTRADLD, Kratos Analytical, Manchester from United Kingdom as shown in Figure 3.9. XPS was also used to verify the valence of Fe in the synthesized materials. The samples were excited with Al K_α radiation. The results are present in Section 4.1.4.

3.5 Colorimetric method for H_2O_2 detection

3.5.1 Chemical preparation

2,2'-Azino-bis (3-ethylbenzothiazoline-6-sulphonic acid) diammonium salt or ABTS solution (20 mM)

0.0329±0.0010 g of ABTS was dissolved in deionized water to 5 mL volumetric flask to give a 20 mM ABTS solution.

3, 3', 5, 5'-tetramethylbenzidine or TMB stock solution (8 mM)

0.0192±0.0010 g of TMB was dissolved in ethanol to 10 mL volumetric flask to give a 8 mM TMB stock solution.

Hydrogen peroxide (H_2O_2) stock solution (100 mM)

Stock solution of H_2O_2 was prepared by pipette 255 μL from 30% H_2O_2 solution then diluted with deionized water to 25 mL volumetric flask.

Acetic acid (CH_3COOH) solution (0.1 M)

0.1 M CH_3COOH was prepared by transferring 1.45 mL from 99.5% CH_3COOH solution. The solution was diluted with deionized water to 250 mL in beaker.

Sodium acetate trihydrate ($NaCH_3COO.3H_2O$) solution (0.1 M)

1.3608±0.0050 g of $NaCH_3COO.3H_2O$ was dissolved and diluted with deionized water to 100 mL in volumetric flask to give a 0.1 M $NaCH_3COO•3H_2O$ solution.

Acetate buffer solution (0.2 M) pH 4.0

0.1 M acetate buffer solution pH 4.0 was prepared by mixing 0.1 M of CH_3COOH and 0.1 M of $NaCH_3COO•3H_2O$ then mixture was adjusted to pH 4.0.

$Fe^{II}Fe^{III}$ LDHNS stock solution (3 mg mL^{-1})

0.0900±0.0010 g of $Fe^{II}Fe^{III}$ LDHNS was dispersed in 3 mL of deionized water to give a 30 mg mL^{-1} $Fe^{II}Fe^{III}$ LDHNS solution. 0.3 mg mL^{-1} of $Fe^{II}Fe^{III}$ LDHNS solution was prepared by pipette 300 µL from 3 mg mL^{-1} $Fe^{II}Fe^{III}$ LDHNS solution and diluted with 2,700 µL of deionized water. Finally, the solution was sonicated in an ultrasonic bath for 10 min.

3.5.2 H_2O_2 detection using $Fe^{II}Fe^{III}$ LDHNS as peroxidase mimetics

To investigate the peroxidase-like catalytic activity of $Fe^{II}Fe^{III}$ LDHNS, the as-synthesized $Fe^{II}Fe^{III}$ LDHNS were directly employed to catalyze the oxidation of chromogenic substrate, ABTS and TMB, in the presence of H_2O_2 by a facile step at ambient temperature. Therefore, colorimetric detection of H_2O_2 can be achieved.

For TMB substrate, H_2O_2 detection was carried out in air-saturated solution referencing literature [77-80]. In a typical experiment, 50 µL of 0.3 mg mL^{-1} $Fe^{II}Fe^{III}$ LDHNS, 100 µL of different concentrations of H_2O_2, 200 µL of 1 mM TMB (in ethanol) and 400 µL of 0.1 M pH 4.0 acetate buffer solution, were mixed. The mixture was then allowed to react for 30 min at ambient temperature (25 ± 1 °C), then the absorbance was measured by UV-Vis absorption spectrophotometer at 652 nm.

For ABTS substrate, according to a previous report [32], H_2O_2 detection was performed by a facile step in deionized water. The mixed solution, which include 50 µL of 0.3 mg mL^{-1} $Fe^{II}Fe^{III}$ LDHNS, 100 µL of different concentrations of H_2O_2, 100 µL of 20 mM ABTS and 500 µL of deionized water; were mixed together. The solution mixture was kept to react at ambient temperature (25 ± 1 °C) for 30 min prior to monitoring by UV-Vis absorption spectrophotometer at 418 nm.

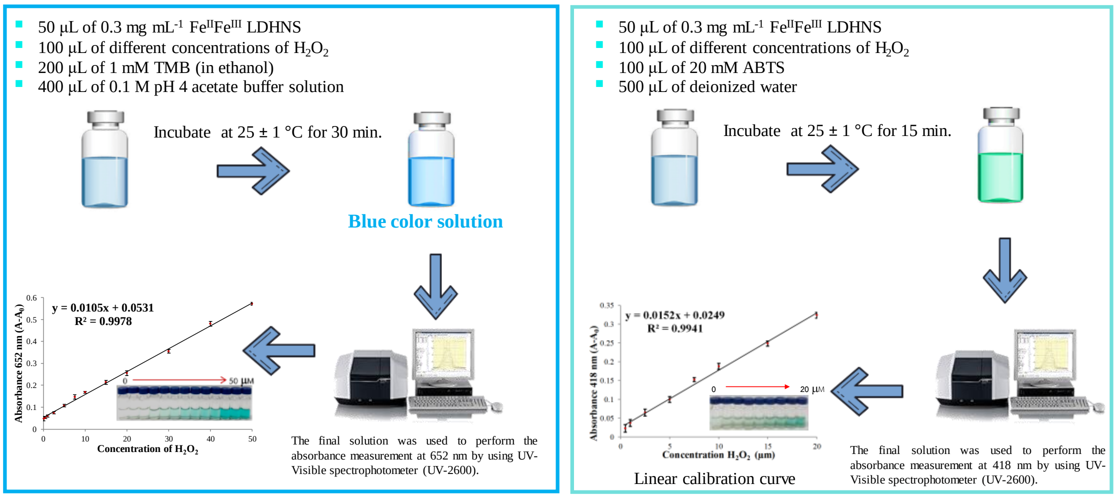

Figure 3.1 Schematic diagram of colorimetric method for H_2O_2 detection by using $Fe^{II}Fe^{III}$ LDHNS with ABTS and TMB substrate.

3.5.3 Studies of parameters that effect the sensitivity of the H_2O_2 detection

3.5.3.1 Effect of buffer pH (0.1 M acetate buffer solution)

The effect of buffer pH on oxidation reaction of TMB peroxidase substrate by using the peroxidase-like activity of $Fe^{II}Fe^{III}$ LDHNS was investigated over the range 3.0-7.5 using 0.1 M acetate buffer solution. UV-visible absorption spectra of H_2O_2 were recorded using 0.1 M acetate buffer solution of varying pH. The results are present in Section 4.2.2.1.

3.5.3.2 Effect of the reaction time

The effect of the reaction time on catalytic activity using the peroxidase-like activity of $Fe^{II}Fe^{III}$ LDHNS was investigated over the range 2.5 to 30 min. The results are present in Section 4.2.2.2.

3.5.3.3 Effect of $Fe^{II}Fe^{III}$ LDHNS concentration

The effect of the $Fe^{II}Fe^{III}$ LDHNS loading in the reaction was investigated over the range 0.1 to 2.0 mg mL^{-1}. The amount of $Fe^{II}Fe^{III}$ LDHNS was prepared by dispersing 0.0, 0.1, 0.3, 0.5, 0.8, 1.0, 1.5 and 2.0 mg of $Fe^{II}Fe^{III}$ LDHNS in 1 mL of deionized water. 50 µL of the various concentration of $Fe^{II}Fe^{III}$ LDHNS was examined to find the most condition for H_2O_2 detection. The results are present in Section 4.2.2.3.

3.5.4 Kinetic analysis

The experiments for kinetics study were also performed at ambient temperature (25 ± 1 °C) by using 0.3 mg mL^{-1} of $Fe^{II}Fe^{III}$ LDHNS with ABTS and TMB substrate in the presence of H_2O_2 under optimal condition. The apparent steady-state kinetics was performed by varying concentration of ABTS or TMB at a fixed concentration of H_2O_2 or varying H_2O_2 concentration while fixing ABTS or TMB concentration. The Michaelis–Menten equation in equation (12) describes the kinetic properties of isolated enzymes [77, 80]. It is also used in modeling the dynamics of enzyme systems and displayed oscillatory behavior. If low oscillatory reaction is shown, many biochemical processes catalyzed by enzymes take place. Michaelis-Menten constant (K_m) can be calculated by the Lineweaver-Burk equation, which is shown in equation (13):

$$v = V_{\max} \frac{[S]}{[S] + K_m} \tag{12}$$

$$\frac{1}{v} = \left(\frac{K_m}{V_{\max}}\right)\left(\frac{1}{[S]}\right) + \frac{1}{V_{\max}} \tag{13}$$

where; v is the initial velocity, V_{max} is the maximal reaction velocity, and [S] represents substrate concentration [77, 80].

3.5.5 Linear concentration range of H_2O_2

Calibration standard of H_2O_2 was examined to the experiment in section 3.5.2 by using H_2O_2 solution. Standard solution of H_2O_2 were prepared by diluting the appropriate amount of H_2O_2 with deionize water to give working solution in the range of 0.1 μM–1.0 mM for TMB substrate and 0.5–100 μM for ABTS substrate, with the three triplicate measurements. The reaction solution to produce a blue and green color reaction, absorbance responses of H_2O_2 concentration were recorded by UV-visible spectrophotometer at 652 nm and 418 nm, respectively. The results were shown in Section 4.2.3.

3.5.6 Studies the effect of interference

In this study, the selectivity of the developed method for H_2O_2 was assessed. The considered interferences in this study were glucose, maltose, lactose, fructose, ascorbic acid (AA), Na^+, Zn^{2+} and Mg^{2+}; which are the components in milk samples. The concentrations of interferences (100 µM) were five-fold higher than that of the standard H_2O_2 (20 µM) with the three triplicate measurements. The experiments were performed under the optimized conditions for TMB and ABTS substrate. Interfere was defined as the concentration of the foreign ion that caused a signal alteration between ±5% of glucose signals. The results are presented in Section 4.2.5.

3.5.7 Real sample application

Two disinfectant samples bought from local pharmacy were used for H_2O_2 colorimetric detection to validate the method. H_2O_2 concentrations designated on the package are 3% and 6% (w/v). These disinfectants were diluted appropriately with deionized water before measurement. In addition, nine brands of milk samples manufactured with sterilization process purchased from local supermarkets were used. Before detection, the milk samples were firstly treated by using 20% (w/w) trichloroacetic acid (TCA) to precipitate protein from solution [79]. The mixed solution was vigorously stirred at 500 rpm for 40 min to ensure the completion of protein precipitation. After that, the solution was filtrated through 0.45 micron syringe ultra-filter membrane. The final solution was split into 2 portions, one for direct detection and another for method validation by spiking H_2O_2 standard solution.

Figure 3.2 Samples of energy and sport drinks used for glucose determination.

3.5.8 Hydrogen Peroxide Quantification via Iodometric Titration

3.5.8.1 Principle of iodometric titration

Iodometric titration was used to measure the presence of H_2O_2 through two major steps[91, 92]. This method is designed for the determination of low levels of hydrogen peroxide (0.1% to 5%) in aqueous solutions. In the first step, H_2O_2 in the sample reacts with excess potassium iodide under acidic conditions in the presence of an ammonium molybdate catalyst. H_2O_2 oxidizes iodide to iodine per the following reaction [91, 92]:

$$H_2O_2 + 2\ KI + H_2SO_4 \rightarrow I_2 + K_2SO_4 + 2\ H_2O \tag{14}$$

The iodine formed (related to the initial amount of Peroxide by 1:1 stochiometry) is then titrated with a thiosulfate solution of known concentration.

$$I_2 + 2\ Na_2S_2O_3 \rightarrow Na_2S_4O_6 + 2\ NaI \tag{15}$$

Early in the titration, the presence of iodine is indicated by a characteristic yellow-brown color of the solution. In the final stages of the titration (after the solution has reached a pale, yellow color), starch is added as an indicator to determine the final end point. This is because starch forms a deep, dark blue complex with minute amounts of triiodide ions that are formed only in the presence of both iodine and Iodide in solution. Hence, the blue color will disappear once all the Iodine is reduced to iodide [91, 92].

3.5.8.2 Reagents

1) 10% Potassium Iodide (KI)

2) Acid Mixture: Ammonium molybdate [$(NH_4)_6\ Mo_7O_{24}$•$4H_20$] in 750 mL of water. While stirring, slowly add 300 mL of H_2SO_4 (conc.).

3) 0.1 N Potassium Iodate Solution (KIO_3)

4) Starch Solution (10 g/L)

5) 0.1 N Sodium Thiosulfate Solution ($Na_2S_2O_3$)

3.5.8.3 Standardization of Sodium Thiosulfate (0.1N)

1) Pipette 20.0 mL of KIO_3 (0.1N) into a 500 mL Erlenmeyer flask containing 100 mL of H_2O. Add about 20 mL of KI (10%) and mix well.

2) Add 25 mL of acid mixture, stopper the flask, and wait five minutes. Using a 50 mL burette, titrate with the $Na_2S_2O_3$ (0.1 N) until the brown triiodide color is nearly dispersed to a pale straw color. Add about 1 mL of the starch solution and titrate until the solution changes sharply from blue to colorless.

3) Record the titration volume and calculate the normality of the $Na_2S_2O_3$ (0.1 N) as shown below. Restandardize every few days, or as often as the solution is needed.

4) Repeat procedure two additional times (3 total) and take the average of the three values as the standardized normality.

$$\text{Normality of } Na_2S_2O_3 = \frac{(\text{g } KIO_3)(\text{mL } KIO_3)}{(\text{mL } Na_2S_2O_3)(35.67 \text{ g.L/eq})} \tag{16}$$

3.5.8.4 Procedure determination of H_2O_2 by iodometric titration

1) Weigh 3 g of sample into a 500 mL Erlenmeyer flask.

2) Add 200 mL of water, 20 mL of KI, and 25 mL of the acid mixture.

3) Mix well, stopper, and let stand five minutes.

4) Using a 50 mL burette, titrate with $Na_2S_2O_3$ (0.1 N) until the brown triiodide color has been reduced to a light straw color.

5) Add a 2 mL of the starch solution (10 g/L) and continue titrating until the color of the solution changes sharply from blue to colorless and record the volume of $Na_2S_2O_3$ to calculate H_2O_2 concentration follow equation (7).

$$\text{mol } H_2O_2 = \frac{1}{2} \text{ mol } Na_2S_2O_3 \tag{17}$$

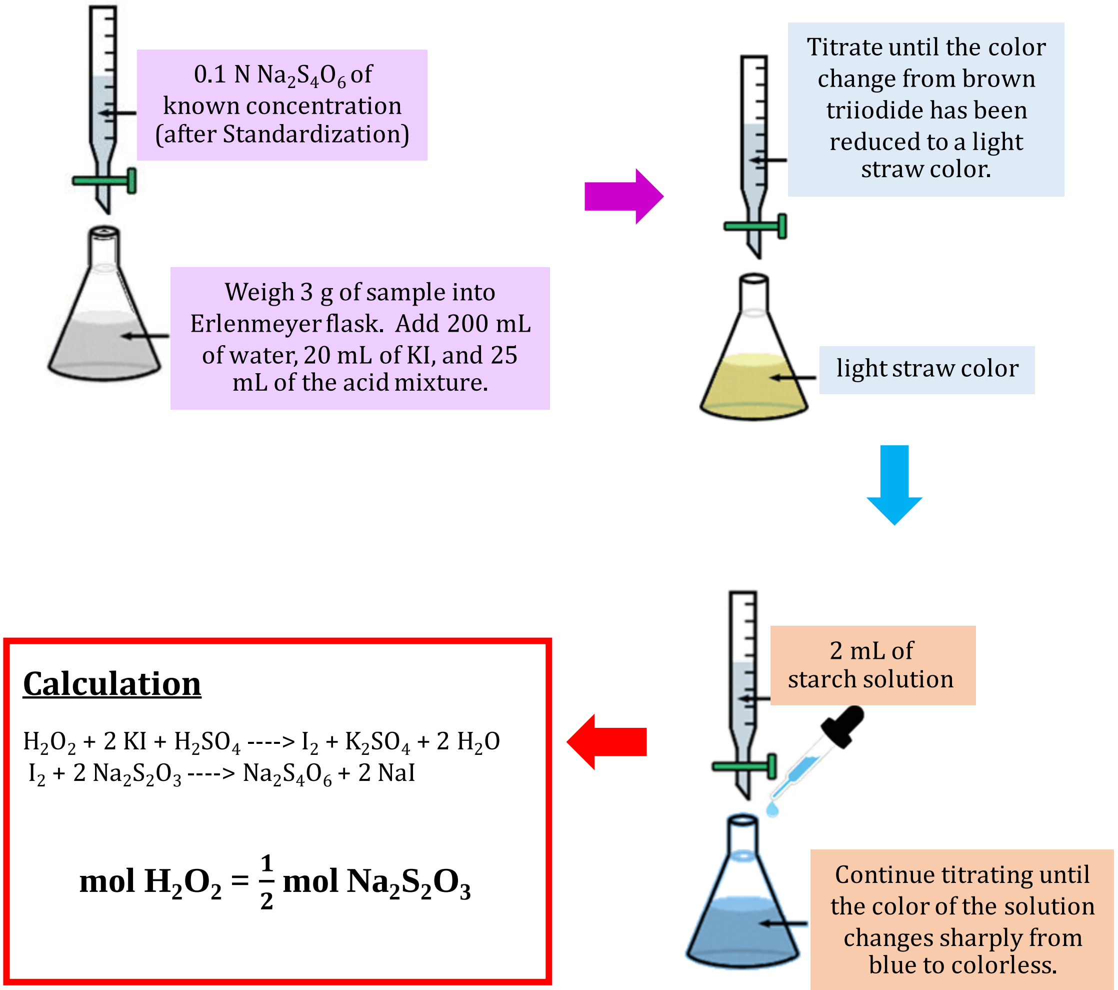

Figure 3.3 Schematic of determination of H_2O_2 by iodometric titration method.

3.6 Preparation of Fe_3O_4/rGO/ZnAl-LDHs composites

3.6.1 Preparation of graphene oxide (GO)

In typical procedure, GO was synthesized by acid oxidation of graphite powder using modified Hummer's method [93-95]. In detail, 3 g of graphite powders was added to 70 ml concentrated H_2SO_4 under magnetic stirring in a 500 ml glass beaker. 1.5 g of $NaNO_3$ was then added into above mixture solution at room temperature. The mixture was then cooled down to 0 °C and transferred to a water bath. Therefore, $KMnO_4$ (9 g) was slowly added to this solution under vigorously stirring below 20 ºC and the mixture solution was again stirred for 30 min at about 35 ºC in a water bath. Upon completion of the reaction, 100 ml of de-ionized water and 15 ml of H_2O_2 (30%) was dropped slowly into this solution to stop the reaction and kept stirring for 30 min at 90 °C. The exothermic reaction occurred and let it to cool down. The dark suspended solution was collected by using centrifuge at 10,000 rpm for 10 min. The resulting solution was washed with 10% HCl solution and de-ionized water until neutral pH using centrifuge at 10,000 rpm. Finally, the product was dried at 60 °C for 24 h and a black product of GO was obtained.

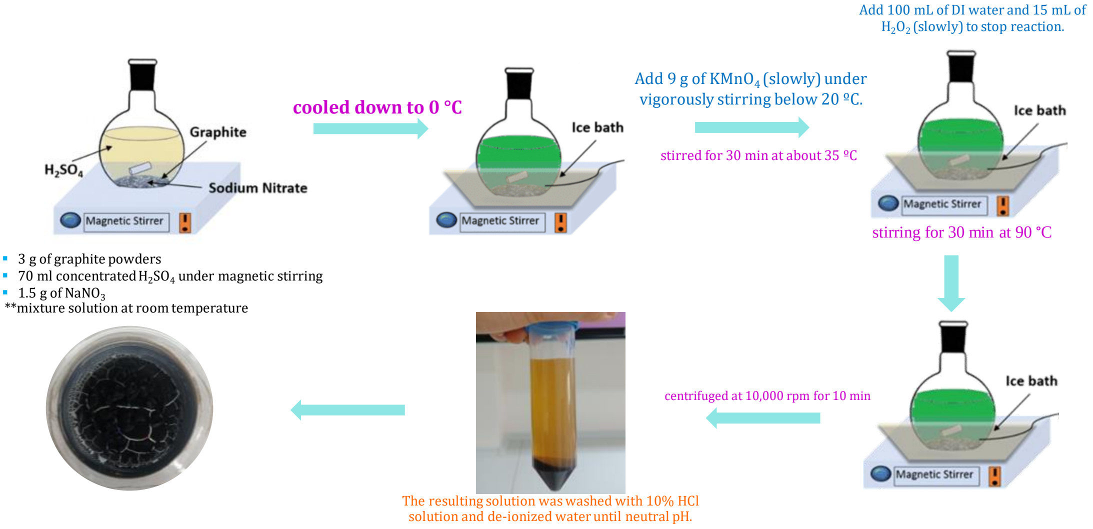

Figure 3.4 Schematic diagram of preparation of graphene oxide (GO).

3.6.2 Preparation of Fe_3O_4 nanoparticles onto the self-reduced graphene oxide (rGO) sheets (Fe_3O_4/rGO)

The Fe_3O_4/rGO was synthesized by redox reaction between GO and Fe^{2+} [58]. The GO was used as an efficient oxidizing reagent to oxidize Fe^{2+} from $FeCl_2$•$4H_2O$ to form Fe_3O_4/rGO *via* the spontaneous *in-situ* deposition of Fe_3O_4 nanoparticles onto the self-reduced GO surface. Briefly, GO was dispersed in NH_4OH solution at pH 9, the suspension solution was sonicated for 15 min to form a homogeneous dispersion. Then, the $FeCl_2$ was added into GO dispersion solution with weight ratio of $FeCl_2$•$4H_2O$ to GO as 10 : 1. The solution color changed from yellow to dark was evident that the redox reaction was occurred. The formed black of Fe_3O_4/rGO showed strong attraction was separated out of solution by using an external magnetic field, washed with water three times by magnetic decantation, and then dried in a desiccator. This evidently reveal that Fe_3O_4 nanoparticles could be decorated rGO and facilitate for separation of this material from aqueous solution with magnetic properties.

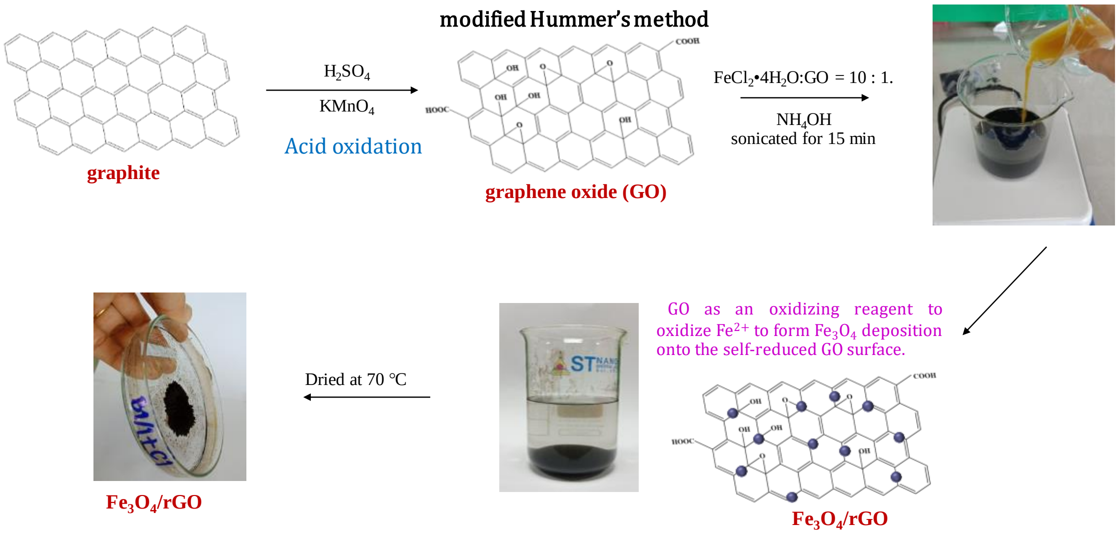

Figure 3.5 Schematic diagram of preparation of Fe_3O_4/rGO.

3.6.3 Preparation of Fe_3O_4/rGO/ZnAl-LDHs composites

The synthesis of Fe_3O_4/rGO/ZnAl-LDHs composites was prepared via co-precipitation method [96, 97]. Typically, 500 mg of Fe_3O_4/rGO was dispersed in de-ionized water (50 ml). Subsequently $Zn(NO_3)_2•6H_2O$ (7.44 g) and $Al(NO_3)_3•9H_2O$ (3.13 g) salt mixture (molar ratio of Zn/Al = 3) was added. The mixture was magnetically stirred for 30 min in order to firm a colloidal dispersion. Afterward, 50 mL alkaline solution of NaOH (3.30 g) and Na_2CO_3 (2.50 g) was added to above solution under vigorous magnetic stirring at 65 °C. After complete addition of solution (pH 10), the precipitate was aged at this temperature for 8 h. Finally, the products were separated by a magnet, washed with de-ionized water five times and dried at 70 °C overnight.

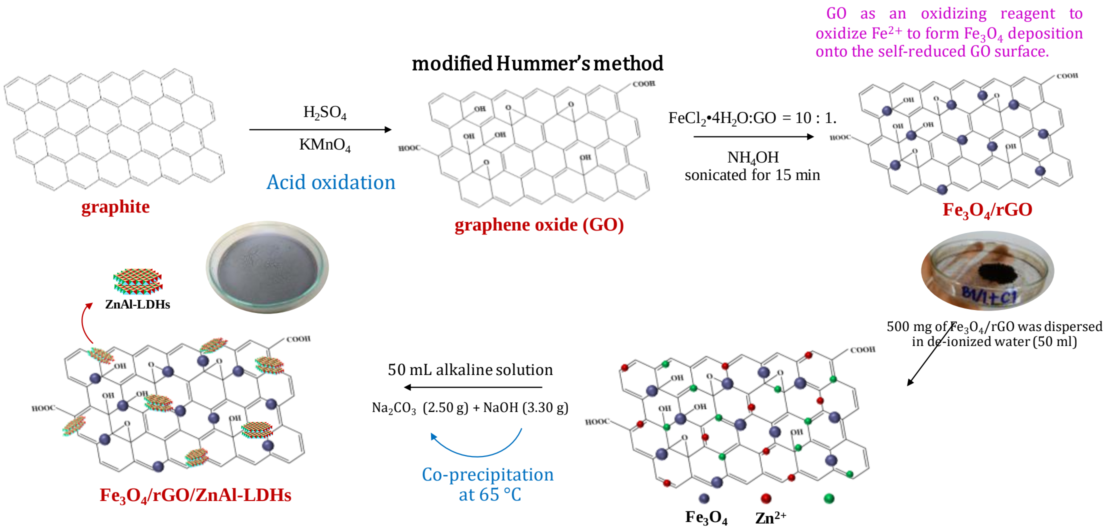

Figure 3.6 Schematic diagram of preparation of Fe_3O_4/rGO/ZnAl-LDHs.

3.7 Characterization of Fe_3O_4/rGO/ZnAl-LDHs composites

3.7.1 X-ray Diffraction (XRD) analysis

X-ray diffraction (XRD) is a powerful nondestructive technique for characterizing crystalline nature of as prepared nanosheets was done using X-ray diffractometer model X'PERT MPD, Philip in Finland as shown in Figure 3.7. The XRD patterns of graphite, GO, Fe_3O_4/rGO and Fe_3O_4/rGO/ZnAl LDHs were carried out by using Cu_{α} radiation wavelength 0.154 nm in 2θ values were taken from 5° to 70°. The results are present in Section 4.3.1.

3.7.2 Scanning Electron Microscopy (SEM)

Scanning Electron Microscopy (SEM) model JSM 7610FPlus, JEOL in Japan as shown in Figure 3.8 was used to examine the morphology of as prepared materials. The morphologies of the graphite, GO, Fe_3O_4/rGO and Fe_3O_4/rGO/ZnAl LDHs were studied with scanning electron microscope under these following parameters. The SEM was operated at 15 kV in the vacuum atmosphere. The results are present in Section 4.3.2.

3.7.3 Energy Dispersive X-Ray Spectroscopy (EDS)

Energy Dispersive X-Ray Spectroscopy (EDS or EDX) model x-stream-2, OXFORD instruments from United Kingdom as shown in Figure 3.8 used in conjunction with scanning electron microscope (SEM) was used to investigate the elemental composition. Graphite, GO, Fe_3O_4/rGO and Fe_3O_4/rGO/ZnAl LDHs were attached on SEM stubs for studied the elemental composition by using EDS. The results are present in Section 4.3.3.

3.7.4 Fourier Transform Infrared Spectroscopy (FT-IR)

Fourier transform infrared spectroscopy (FT-IR) is an important technique in the functional groups identification in materials. Graphite, GO, Fe_3O_4/rGO, ZnAl LDHs and Fe_3O_4/rGO/ZnAl LDHs were characterized by FT-IR spectrophotometer, model: Spectrum RX I from Perkin Elmer as shown in Figure 4.21. FT-IR data were collected by ATR mode from wavenumber of 500 to 4,000 cm^{-1} with a resolution of 9 cm^{-1}. The results are present in Section 4.3.4.

3.7.5 Surface area and pore analysis (N_2 adsorption-desorption isotherm)

Surface area and pore analysis provides precise specific surface area evaluation of GO, Fe_3O_4/rGO, ZnAl LDHs and Fe_3O_4/rGO/ZnAl LDHs by nitrogen multilayer adsorption measured as a function of relative pressure using a fully automated analyzer. Nitrogen adsorption-desorption isotherms were measured at 77 K (temperature of liquid nitrogen), using an automated instrument (Gas sorption surface area and pore size analyzer, Quadrasorb-EVO) shown in Figure 3.12. The volumetric technique is based on pressure measurements in an enclosed volume and provides more information, since many adsorption and/or desorption points are measured providing a full isotherm with information on BET surface area and pore volume. The results are present in Section 4.3.5.

3.7.6 Zeta potential analysis

Zeta potential is an important indicator to determine the surface charge of the materials and to characterize the stability of dispersions of GO, Fe_3O_4/rGO and Fe_3O_4/rGO/ZnAl LDHs. The preparation of these nanoparticles were dispersed in deionized water (0.1 mg mL^{-1}). Then, these solutions were diluted 50-fold and measured at 25 °C in backscattering mode at an angle of 173° by zetasizer nano ZS, Malvern from United Kingdom as shown in Figure 3.13. In water treatment, monitoring dosage using zeta potential measurements can reduce the cost of chemical additives by optimizing the dosage control. The results are present in Section 4.3.6.

3.7.7 Vibrating sample magnetometry (VSM)

The magnetic properties of the Fe_3O_4/rGO and Fe_3O_4/rGO/ZnAl LDHs were measured using a vibrating sample magnetometer of model VSM 7403; 79 Lake Shore as shown in Figure 3.14. These specimens were finely pulverized and dried at 80 °C. Then, 20 mg of sample was contained to sample holder for VSM analysis. The measured magnetic properties were carried out by using applied magnetic field ±10000 Oe at temperature of 300 K. The results are present in Section 4.3.7.

3.8 Dyes adsorption experimental

3.8.1 Standard curve of methyl orange (MO) and brilliant green (BG)

A calibration curve of MO and BG was prepared by measuring absorbance of different predetermined concentrations of MO and BG at λ_{max} at 465 and 624 nm, respectively. Concentration of dyes in the experimental solution were calculated from the calibration curve. Stock solution of 100 mg L^{-1} of MO and BG were prepared by dissolving approximately 0.0250±0.0010 g with deionized water in volumetric flask 250 mL. Different concentrations of the MO dye with 0.1, 1, 5, 7.5, 10, 15 mg L^{-1} and 0.1, 0.5, 1, 2.5, 5, 7.5 mg L^{-1} for BG in deionized water were made and measured.

3.8.2 Batch Adsorption experiments

All the batch experiments were conducted with Fe_3O_4/rGO/ZnAl-LDHs composites for the adsorption of ionic dyes from aqueous solution in bottles. The effects of adsorbent dosage, contact time, solution pH, and initial dye concentration were investigated. In typical experiment, 10 - 60 mg adsorbents were added to 50 mL of freshly prepared dye solution at different initial concentrations from 5 to 200 mg L^{-1} for brilliant green (BG) and methyl orange (MO). Then the bottles were shaken with 160 rpm at room temperature (25±1 °C) for 24h. After adsorption had occurred, the suspension was quickly separated from the sample solution by using magnet and the residual dye concentration in the clear supernatant solution was determined by the UV-vis spectrophotometer at 624 nm (BG) and 465 nm (MO) using a calibration curve. The study about the effect of initials pH on the adsorption was performed at 50 mg L^{-1} for BG and MO solution in different pH (2.0–12.0), adjusted by adding 0.1 M HCl or NaOH solution.

The removal efficiency, adsorption capacity at equilibrium (q_e, mg g^{-1}) and adsorption capacity (q_t, mg g^{-1}) at certain time of BG and MO from solutions were calculated according to the formula [98-100]:

$$\text{Removal efficiency (\%)} = \left(\frac{C_0 - C_e}{C_0}\right) \times 100 \tag{18}$$

$$q_e\ (mg\ g^{-1}) = \left(\frac{C_0 - C_e}{m}\right) \times V \tag{19}$$

$$q_t(mg\ g^{-1}) = \left(\frac{C_0 - C_t}{m}\right) \times V \tag{20}$$

where C_0 (mg L^{-1}) is the initial concentration, C_e and C_t (mg L^{-1}) are the concentrations of BG and MO at equilibrium and time t (min), respectively. V (L) is the volume of the aqueous solution, m (g) is the mass of adsorbents.

3.8.3 Adsorption kinetics

The adsorption kinetics is important due to it can be described the adsorption rate and provide valuable data for understanding the mechanism of sorption reactions. The adsorption kinetics of MO and BG on of Fe_3O_4/rGO/ZnAl-LDHs were analyzed by the pseudo-first order, pseudo-second order kinetic models and Weber-Morris intra-particle mass diffusion model, which are the most common models for the prediction of sorption kinetics [99-102].

3.8.3.1 Pseudo-first order model

The pseudo-first order model suggests a proportional relation for the rate of adsorption, described by the following equations [99-102]:

$$ln(q_e - q_t) = \ln q_e - \left(\frac{k_1}{2.303}\right)t \qquad (21)$$

where, q_t (mg g^{-1}) and q_e (mg g^{-1}) represent the amount of MO or BG adsorbed at time t and at equilibrium time, respectively. k_1 (min^{-1}) represents the adsorption rate constant which is calculated from the plot of $ln(q_e-q_t)$ against t.

3.8.3.2 Pseudo-second order model

The pseudo-second order model suggests a quadratic relation for the rate of adsorption. This model defines the kinetic of adsorption as [99-102]:

$$\frac{t}{q_t} = \frac{1}{k_2 q_e^2} + \frac{t}{q_e} \qquad (22)$$

where, k_2 (g (mg min)$^{-1}$) is the pseudo second-order rate constant of sorption, the q_e and k_2 can be obtained by linear plot of t/qt versus t.

3.8.3.3 Weber-Morris intra-particle mass diffusion model

The Weber-Morris intra-particle mass diffusion model describes the process during adsorption internal diffusion determines the adsorption rate in most of the liquid systems. Intra-particle mass diffusion model as the following equation [101-103]:

$$q_t = k_d t^{1/2} + C \qquad (23)$$

where k_d is the intra-particle diffusion rate constant (mg $g^{-1}\cdot min^{1/2}$) and C is the intercept which represents the thickness of the boundary layer ((mg g^{-1}). The values of k_{id} and C can be calculated from the slope and the intercept of the linear plot of q_t versus $t^{1/2}$. The value of the intercept C provides information about the thickness of the boundary layer, and the larger the intercept, the greater the boundary layer effect [99-101]. If the intra-particle diffusion is involved in the adsorption process, the plot of qt versus $t^{1/2}$ will be linear; and if this line passes through the origin, the rate-limiting process is only due to the intra-particle diffusion.

3.8.4 Adsorption isotherms

The adsorption isotherm usually describes the distribution of the adsorbate between the aqueous and solid phase of adsorbent at equilibrium state during the adsorption process. On the basis of the shape of the isotherm, the nature of the studied process can be determined [99]. The adsorption capacity of the adsorbent for the adsorbate can be determined from the equilibrium adsorption isotherm [48].

3.8.4.1 Langmuir isotherm

The Langmuir isotherm is applicable to homogeneous sorption occured on specific homogeneous adsorbent sites where the sorption of each sorbate molecule onto the surface has equal sorption activation energy. Therefore, the Langmuir isotherm assumption that sorption comes from the monolayer coverage of the adsorbate over a homogeneous adsorbent surface [1, 108]. The Langmuir isotherm can be presented in the form [99-106]:

$$q_e = \frac{q_m K_L C_e}{1 + K_L C_e} \tag{24}$$

Linear form of the Langmuir model can be described by the following equation [99-106]:

$$\frac{C_e}{q_e} = \frac{1}{q_m K_L} + \frac{C_e}{q_m} \tag{25}$$

where C_e is the equilibrium concentration of dye aqueous solution (mg L^{-1}); q_e is the amount of dye adsorbed by elementary mass of adsorbent (mg g^{-1}); q_m is the maximum adsorption capacity (mg g^{-1}); and K_L is the Langmuir adsorption constant. A plot of C_e/q_e versus C_e gives a straight line with the slope of $1/q_m$ and the intercept C_e/q_m, as shown in Figure 4.30; the calculated isotherm parameters are shown in Table 4.11.

A dimensionless parameter R_L from the Langmuir model is commonly used to predict the feasibility of the adsorption process. R_L can be represented by Eq. (26):

$$R_L = \frac{1}{1 + K_L C_0} \tag{26}$$

where R_L value indicates the shape and feasibility of isotherm, the isotherm can be unfavourable ($R_L > 1$), linear ($R_L = 1$), favourable ($0 < R_L < 1$) or irreversible ($R_L = 0$) [102-106].

3.8.4.2 Freundlich isotherm

The Freundlich isotherm is an empirical model based on the assumption that the adsorption process occurs on heterogenous surface of the adsorbent with a non-uniform distribution of heat sorption and means of multilayer adsorption characterized by the heterogeneity factor 1/n. The values of 1/n in the range of 0-1 show favorable adsorption while 1/n above 1 is an indicative of cooperative adsorption [99]. The Freundlich model is described by [99-106]:

$$q_e = K_F C_e^{1/n} \tag{27}$$

The linear form of the Freundlich isotherm models is represented as follows [99-106]:

$$\ln q_e = \ln K_F + \frac{1}{n} \ln C_e \tag{28}$$

where K_F is the Freundlich isotherm constant; q_e and C_e has the same meaning as that in Eq. (28); 1/n is the influence coefficient of solution concentration to the equilibrium adsorbed amount.

3.8.5 Desorption and Reusability studies

Desorption and reusability studies were conducted in batch mode to recover the adsorbed BG and MO to generate the used samples for further dyes removal. The adsorbent was separated from the dye solution by external magnetic. Initially, 10 mg of adsorbent used sample was treatment with ethanol and followed by 0.01 M of NaOH (shake at 160 rpm for 1h). Subsequently, the adsorbent washed again with de-ionized water for three time and dried at 60 °C for 24h and reused. The obtained samples of Fe_3O_4/rGO/ZnAl-LDHs composites with regenerated active sites were again used for adsorption of BG and MO for next adsorption-desorption cycles.

Figure 3.7 X-ray diffractometer: XRD (X’PERT MPD, Philip).

Figure 3.8 Scanning Electron Microscopy (JSM 7610F Plus, JEOL) combined with Energy Dispersive X-Ray Spectroscopy (X-Stream-2, OXFORD).

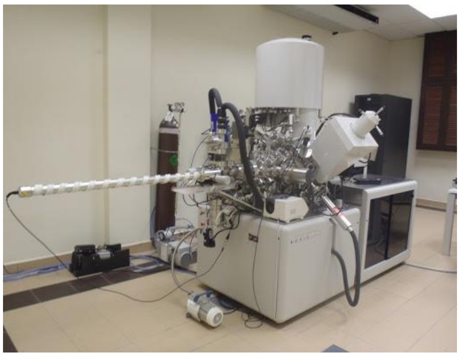

Figure 3.9 X-ray photoelectron spectroscopy (XPS; AXIS ULTRA^{DLD}).

Figure 3.10 UV-visible spectrophotometer (UV-2600, Shimadzu).

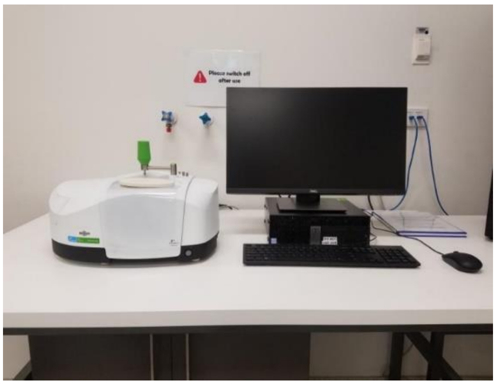

Figure 3.11 Fourier transform infrared spectrometer: FT-IR (Spectrum Two, Perkin Elmer).

Figure 3.12 Gas sorption surface area and pore size analyzer (Quadrasorb-EVO).

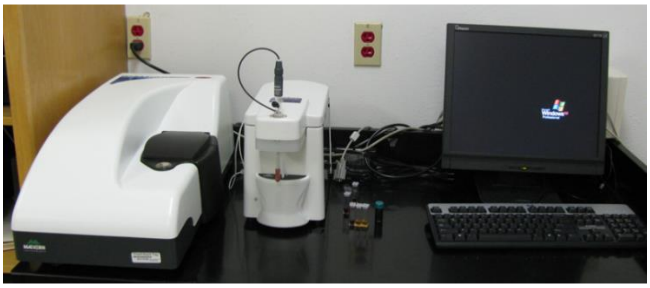

Figure 3.13 Particle size analyzer (Zetasizer Nano ZS, Malvern).

Figure 3.14 Vibrating Sample Magnetometer (VSM 7403; 79).

CHAPTER 4

RESULTS AND DISCUSSION

4.1 Characterization $Fe^{II}Fe^{II}$ Layered Double Hydroxides Nanosheets (LDHNS)

4.1.1 X-ray Diffraction (XRD)

The XRD pattern of $Fe^{II}Fe^{III}$ LDHNS recorded from 2θ of 15° to 80° shows as Figure 4.1 reveals the main diffraction peaks for $Fe^{II}Fe^{III}$ LDHNS at 2θ angles of 21.03°, 26.63°, 32.93°, 36.39°, 40.69°, 53.03°, 62.55°, 68.31° and 70.73°, which were assigned to a series of planes (002), (003), (004), (101), (102), (104), (105), (110) and (111) according to that proposed by Bernal et al [112]. Various small lines (*) would indicate that some ordering of sulphate ions occurs inside the interlayers of the structure [33, 108]. Thus, all main lines found in the XRD pattern are correlated with crystalline structures of $Fe^{II}Fe^{III}$ LDHNS.

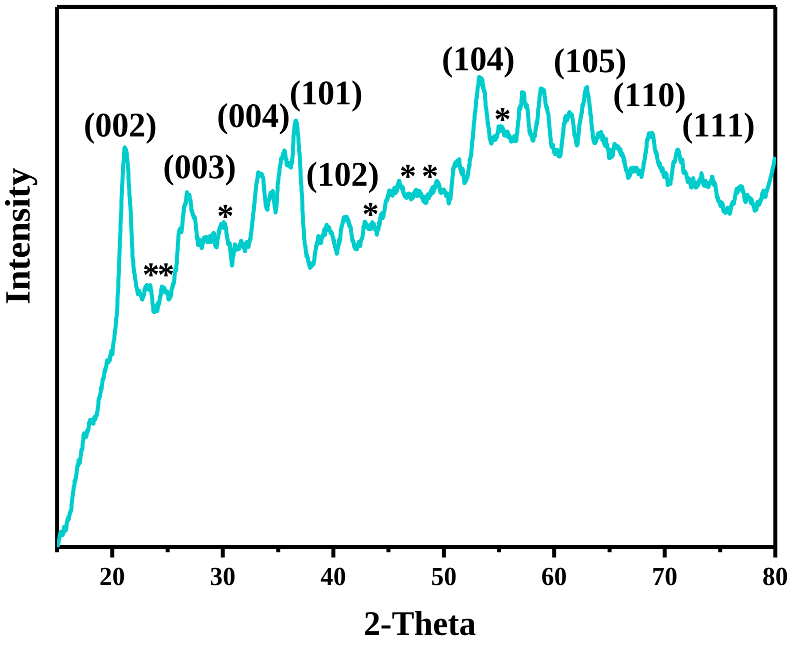

Figure 4.1 X-ray diffraction pattern of $Fe^{II}Fe^{II}$ LDHNS.

4.1.2 Scanning Electron Microscopy (SEM)

Scanning electron microscopy (SEM) was employed to investigate the morphologies of $Fe^{II}Fe^{III}$ LDHNS. Figure 4.2 illustrates the SEM image of $Fe^{II}Fe^{III}$ LDHNS; the figure reveals that the product exhibits a plate-like morphology, which is a stereotype of the LDHs [109-111]. In addition, it is clearly seen that the plate-like form in this product appears in the irregular shape with the length and width of approximately 397.64 nm and 217.53 nm, respectively.

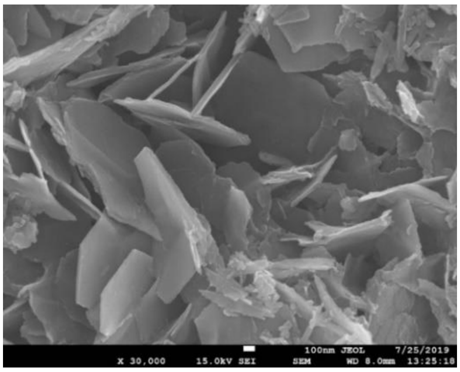

Figure 4.2 SEM image of $Fe^{II}Fe^{III}$ LDHNS.

4.1.3 Energy Dispersive X-Ray Spectroscopy (EDS)

Energy dispersive spectroscopy (EDS) analysis connected with scanning electron microscopy were performed for the morphology and composition analysis of the as prepared materials. The EDS spectrum shows in Figure 4.3 reveals that the $Fe^{II}Fe^{III}$ LDHNS mainly contains the Fe, O, S and C elements. In the $Fe^{II}Fe^{III}$ LDHNS EDS spectrum, the peaks at approximately 0.7 ($L_{\alpha1}$), 6.4 ($K_{\alpha1}$) and 7.0 ($K_{\beta1}$) keV which associated with the binding energies of iron (Fe) were observed. The signal of binding energies of oxygen (O) and sulfur (S) at around 0.5 and 2.3 keV, respectively, were also observed as sulfate is charge balancing ion in the product interlayer [111]. Moreover, the peak around 0.3 keV which relates with the binding energies of carbon (C) is influenced by carbon film on the SEM stub holder. The percentage of element Fe, O, S and C are summarized in Table 4.1. Additionally, the distribution of these elements was investigated with the elemental mapping using SEM-EDS as displayed in Figure 4.4(a-d). The elements C, O, S and Fe appear to be uniformly distributed and these also confirm the presence of Fe, S and O in the nanosheets product.

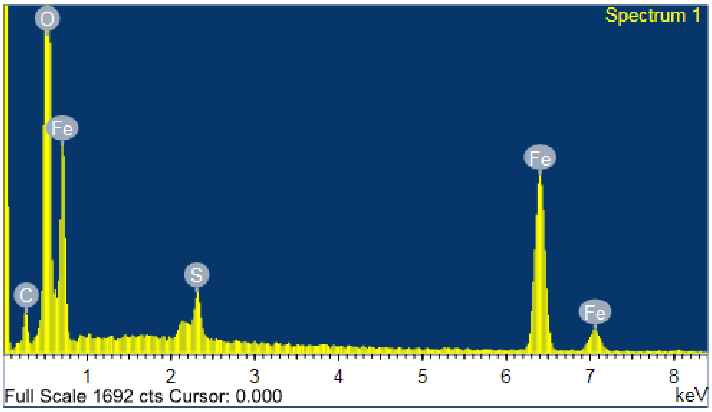

Figure 4.3 EDS spectra of $Fe^{II}Fe^{III}$ LDHNS.

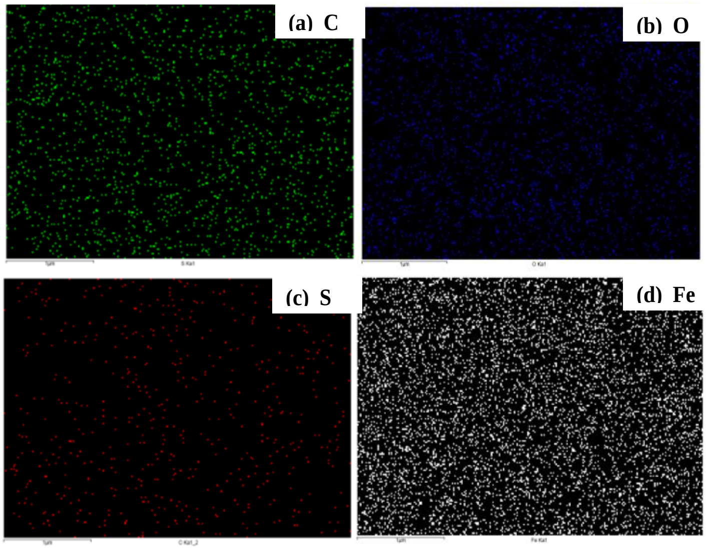

Figure 4.4 SEM-EDS elemental mapping images of $Fe^{II}Fe^{III}$ LDHNS.

Table 4.1 The elemental quantity of the elements normalized for $Fe^{II}Fe^{III}$ LDHNS.

Sample	Elememnt	Weight (%)	Atomic (%)
$Fe^{II}Fe^{III}$ LDHNS $[Fe_4^{2+}Fe_2^{3+}(OH^-)_{12}]^{2+}$• $[SO_4^{2-}$•$2H_2O]^{2-}$	C	6.22	12.03
	O	46.72	67.89
	S	1.58	1.15
	Fe	45.47	18.93
	Total	100	100

4.1.4 X-ray Photoelectron Spectroscopy (XPS)

X-ray Photoelectron Spectroscopy (XPS) was also used to verify the valence of Fe in the synthesized materials. The XPS data in Figure 4.5(a) indicate the presence of Fe (2p), O (1s), and S (2p). The binding energy of iron observed at 725.4 and 711.5 eV. Figure 4.5(b), corresponds to the characteristics of Fe(II) and Fe(III), respectively [140, 141]. Three peaks of O (1s) at 530.2, 531.6, and 532.5 eV (Figure 4.5(c)) were assigned to O–Fe, O–H, and adsorbed water, respectively [140]. Note that the S (2p) at 168.8 and 170.0 eV (Figure 4.5(d)), indicates the presence of SO_4^{2-} in the interlayers of the sample [140, 141].

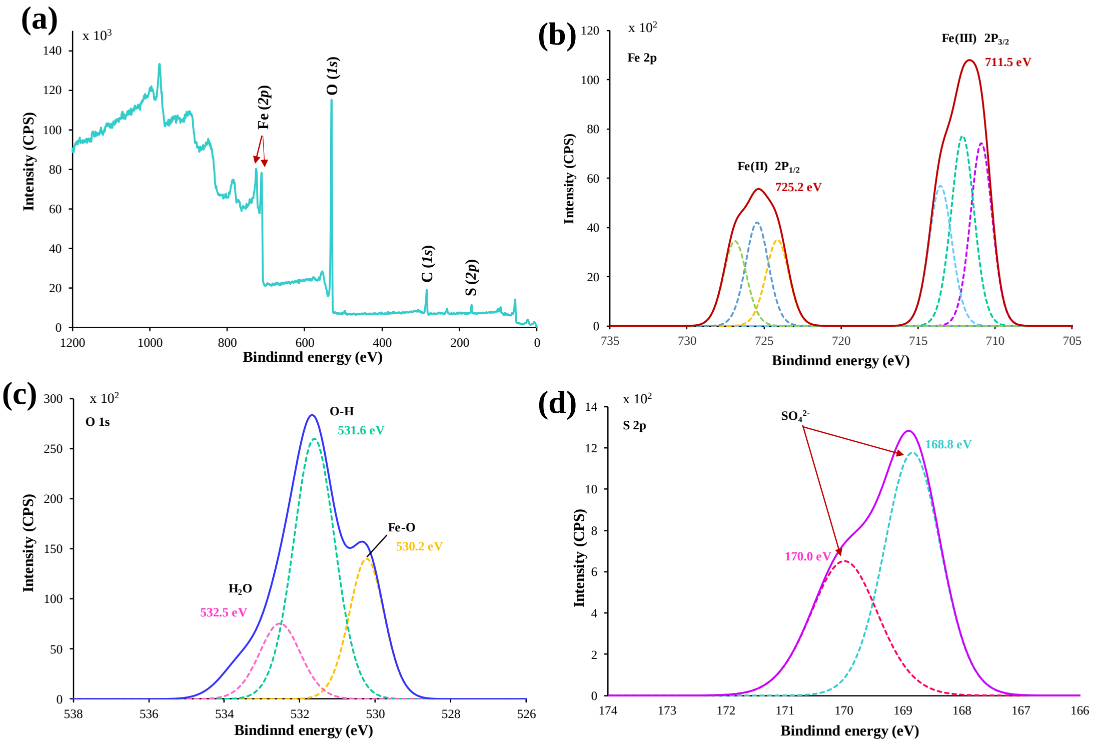

Figure 4.5 **(a) X-ray photoelectron spectroscopy (XPS) survey spectra of $Fe^{II}Fe^{III}$ LDHNS. The high resolution XPS spectra of (b) Fe (2p), (c) O (1s) and (d) S (2p) for $Fe^{II}Fe^{III}$ LDHNS.**

4.2 Colorimetric method for H_2O_2 detection

4.2.1 The peroxidase-like catalytic activity of $Fe^{II}Fe^{III}$- LDHNS

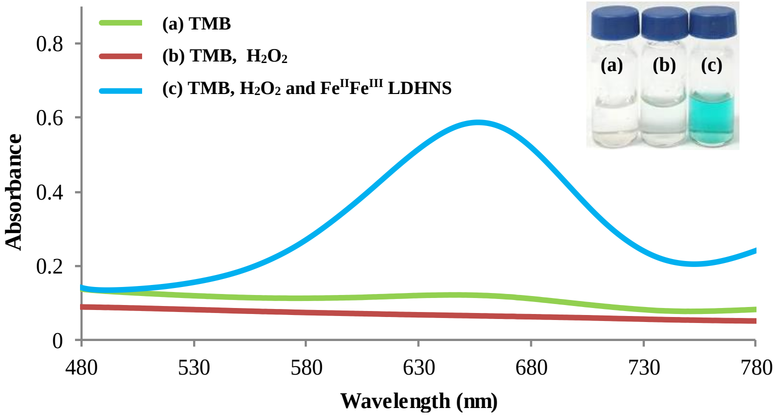

Figure 4.6 UV-vis absorption spectra of TMB solution (1 mM in ethanol) in 0.1 M acetate buffer solution pH 4. The reactions were incubated at 25 ± 1 °C for 30 min in different reaction systems: (a) TMB, (b) TMB and H_2O_2, (c) TMB, H_2O_2 and $Fe^{II}Fe^{III}$ LDHNS. The H_2O_2 concentration was 50.0 µM.

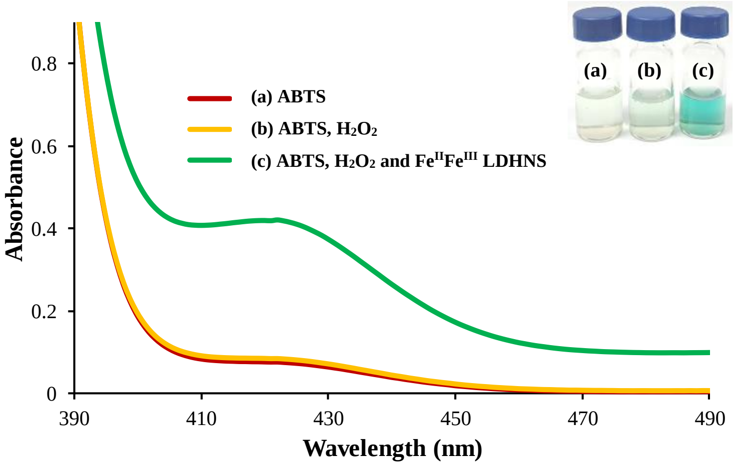

Figure 4.7 UV-vis absorption spectra of ABTS solution (20 mM) in DI water. The reactions were incubated at 25 ± 1 °C for 30 min in different reaction systems: (a) ABTS, (b) ABTS and H_2O_2, (c) ABTS, H_2O_2 and $Fe^{II}Fe^{III}$ LDHNS. The H_2O_2 concentration was 20.0 µM.

To investigate the catalytic activity of $Fe^{II}Fe^{III}$ LDHNS; ABTS and TMB substrate were chosen, these chromogenic substrates were normally used to study the peroxidase-like activity of enzymes [25, 32]. Only system that included H_2O_2, $Fe^{II}Fe^{III}$ LDHNS and chromogenic substrate (Figure 4.6 (c) for TMB and Figure 4.7 (c) for ABTS) could produce the colored product and can easily be observed by the naked eyes (inset image). The results indicated that the $Fe^{II}Fe^{III}$ LDHNS possess the peroxidase like activity and can catalyze the oxidation reaction of TMB and ABTS in the presence of H_2O_2 [25, 83, 112]. These reactions proceed via the Fenton's mechanism as shown in the following equations:

$$H_2O_2 \xrightarrow{Fe^{II}Fe^{III}\text{ LDHNS}} HO^{-} + HO^{\bullet} \qquad (29)$$

$$HO^{\bullet} + TMB \xrightarrow{Fe^{II}Fe^{III}\text{ LDHNS}} H_2O + TMB(ox) \qquad (30)$$

$$HO^{\bullet} + ABTS \xrightarrow{Fe^{II}Fe^{III}\text{ LDHNS}} 2H_2O + ABTS^{\bullet+} \qquad (31)$$

The $Fe^{II}Fe^{III}$ LDHNS catalyze H_2O_2 decomposition to produce $HO^{\bullet}$ as shown in Eq. (1) [112-114]. Then, the produced $HO^{\bullet}$ oxidizes TMB to provide blue color solution of the oxidized products of TMB in Eq (2). This system displays the characteristic absorbance at 652 nm (Figure 4.6: blue line (c)) originating from its distinctive charge-transfer of diamine/diimine complex [115]. The H_2O_2 concentration corresponds to the color change and absorbance signal at 652 nm. Similarly; in the case of ABTS substrate, the $HO^{\bullet}$ oxidizes ABTS to produce the green colored product of $ABTS^{\bullet+}$ in Eq. (3), exhibiting the maximum absorbance at 418 nm (Figure 4.7: green line (c)) [116]. The results reveal that $Fe^{II}Fe^{III}$ LDHNS can catalyze the oxidation of the TMB and ABTS in the presence of H_2O_2. The principle of the detection system is described in Figure 4.8. Color change and the corresponding reaction mechanisms for oxidation of TMB and ABTS are in accordance with the previous reports [25, 83, 112]. These results strongly suggest that $Fe^{II}Fe^{III}$ LDHNS possess an intrinsic peroxidase-like activity, which derived from electron transfer between pairs of different oxidation states of metal cations (e.g. Fe^{2+} and Fe^{3+}) on the brucite-like layer [112].

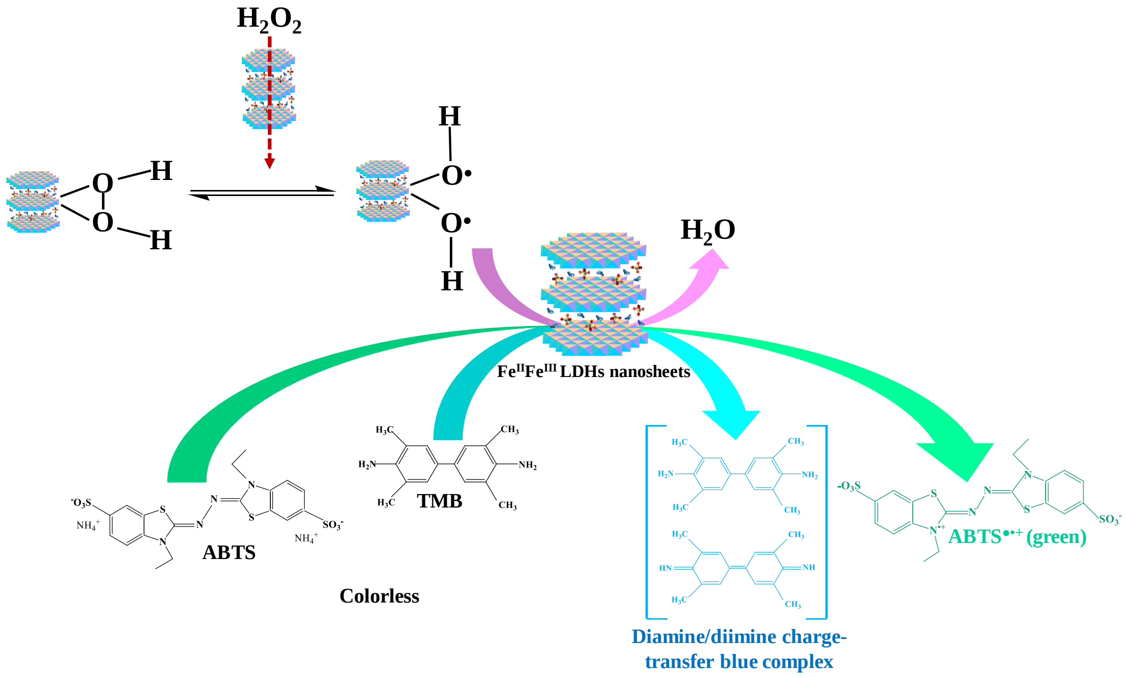

Figure 4.8 The principle of the colorimetric detection of H_2O_2 by using Fe^{II}Fe^{III} LDHNS enzyme mimic [115, 116].

4.2.2 Studies of parameters that effect the sensitivity of the H_2O_2 detection

Similar to HRP and other nanomaterial-based peroxidase mimics, the catalytic activity is dependent on the pH, temperature, concentration of H_2O_2 and reaction time. Influences of reaction time and other experimental conditions on the catalytic activity of Fe^{II}Fe^{III} LDHNS with chromogenic peroxidase substrate, TMB and ABTS, were studied. Effect of pH was only investigated for TMB, since reaction of ABTS was carried out in DI water.

4.2.2.1 Effect of the pH (0.1 M acetate buffer)

The peroxidase-like activity of Fe^{II}Fe^{III} LDHNS is strongly dependent on the physical reaction conditions. An optimum pH range is vital to the sensitivity of H_2O_2 detection and influence on catalytic behavior of nanoplates. To study effect of pH for TMB and ABTS systems, experiments were performed by varying pH in the range from 3 to 7.5 using 0.1 M acetate buffer, the results were shown in Figure 4.9. The absorbance at 652 nm as shows in Figure 4.9 (a), which originated from the oxidized TMB product revealed that Fe^{II}Fe^{III} LDHNS exhibited greater activity in acidic solution than that of neutral pH. The results indicated maximum catalytic efficiency of

$Fe^{II}Fe^{III}$ LDHNS at pH 3.0. Additionally, Figure 4.9 (b) shows the effects of pH on the $Fe^{II}Fe^{III}$ LDHNS catalytic activity for ABTS system was investigated using acetate buffer solution (pH 3 to 7.5) and deionized water approximately pH 5.6. The result showed that in acidic solution the nanocatalyst performed more effective than it is at neutral pH. The absorption band at 418 nm, which originates from the ABTS oxidation product and shows the greatest absorption at pH 3 then remained unalterable at pH 4 to 5.6 (deionized condition). However, according to the previous report, $Fe^{II}Fe^{III}$ LDHNS was unstable at pH $\leq$ 3.0. As a consequence, at low pH, the Fe^{2+} ions in the nanosheets might leach into the reaction solution and subsequently play a catalytic role [26, 83]. The absorbance dropped to nearly zero at pH > 5 for TMB system and pH > 6 for ABTS system; as in neutral or basic solutions, H_2O_2 tends to decompose into H_2O and O_2 rather than producing reactive oxygen species to react with peroxidase substrate. It was also proven that alkaline condition could inhibit the combination and dissociation rates between peroxidase substrate and the nanosheets [117]. Therefore, the suitable pH condition of $Fe^{II}Fe^{III}$ LDHNS for TMB system was at about an acetate buffer solution of pH 4 to ensure that the observed catalytic activity originated from the nanosheets not from leached Fe^{2+} ions. Notably, the optimal pH solution for $Fe^{II}Fe^{III}$ LDHNS was similar to those for HRP natural enzyme [26]. Given all this result of ABTS system, deionized water was selected as the optimal reaction medium for the catalysis reaction by $Fe^{II}Fe^{III}$ LDHNS, which showed reduce the chemicals and ease of operation condition.

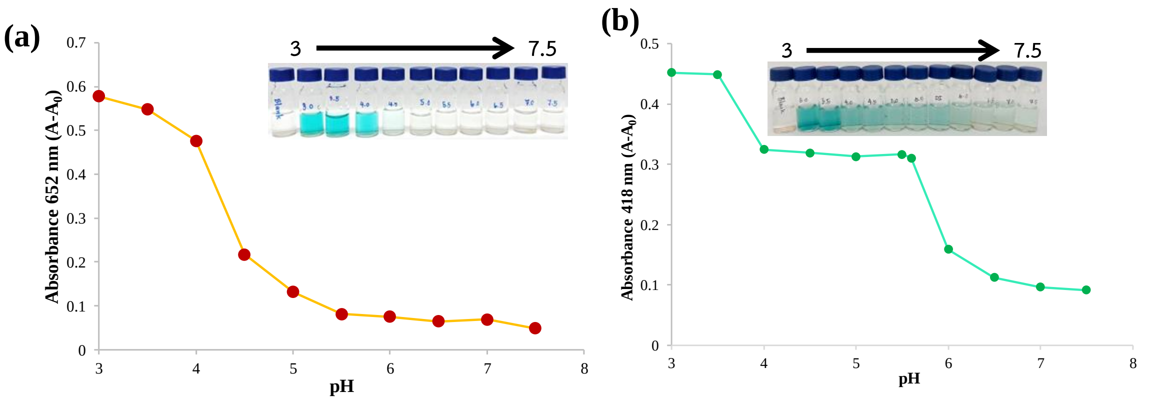

Figure 4.9 Effect of pH for TMB (a) and ABTS (b) on the catalytic activity of $Fe^{II}Fe^{III}$ LDHNS.

4.2.2.2 Effect of reaction time

The influences of reaction times were studied because it is a critical parameter for determination of H_2O_2 with colorimetric method. In this study, optimization of the reaction time was investigated. Effect of the reaction time on the catalytic activity was studied in the time period of 2-30 min for both TMB and ABTS substrate; the results are shown in Figure 4.10 (a-b). Figure 4.10 (a), for TMB substrate, the absorbance was significantly increased when increasing the reaction time from 20 to 30 min. The reaction time of 30 min was chosen as optimal to maximize sensitivity of H_2O_2 colorimetric detection with TMB substrate. Figure 4.10 (b), for ABTS substrate, absorption increased dramatically when reaction time increased from 2 to 10 min, and this tended to be rising slowly from 15 to 30 min. Therefore, 15 min was chosen as the optimum reaction time to maximize the sensitivity towards H_2O_2 detection while minimizing the time required for analysis. Moreover, experiments of both peroxidase substrates were carried out by incubating at room temperature contributing reduction of the experimental process and facilities required.

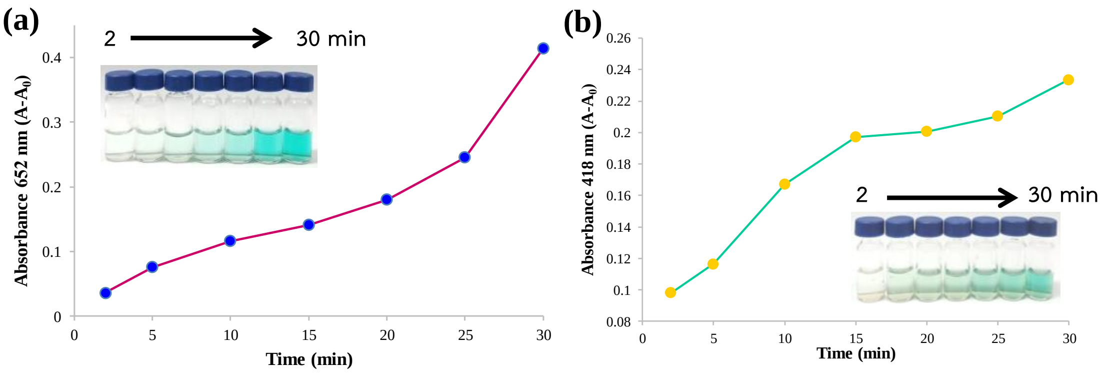

Figure 4.10 Effect of reaction time for TMB (a) and ABTS (b) on the catalytic activity of $Fe^{II}Fe^{III}$ LDHNS.

4.2.2.3 Effect of $Fe^{II}Fe^{III}$ LDHNS concentration

The concentration of $Fe^{II}Fe^{III}$ LDHNS is a key factor in this development colorimetric method and vital to sensitivity of H_2O_2 detection. In this study, optimization of the catalyst concentration was investigated. The effect of $Fe^{II}Fe^{III}$ LDHNS concentration for TMB and ABTS systems on catalytic activity was studied over the range of 0 to 2.0 mg mL^{-1}. Figure 4.11 (a) and Figure 4.11 (b) showed UV-vis absorption spectra on effects of Fe^{II}Fe^{III} LDHNS concentration on the catalytic oxidation of TMB and ABTS in the absent and presence with various amount of Fe^{II}Fe^{III} LDHNS. It was observed that absorbance at 652 nm and 418 nm increases with increasing Fe^{II}Fe^{III} LDHNS concentration from 0.1 to 2.0 mg mL^{-1} for TMB and ABTS system. However, the baseline of signal was increased with increasing Fe^{II}Fe^{III} LDHNS concentration from 0.1 to 2.0 mg mL^{-1} for both systems. Clearly seen that the baseline of signal at 0.3 mg mL^{-1} of Fe^{II}Fe^{III} LDHNS concentration and without Fe^{II}Fe^{III} LDHNS was resemble, which indicated that the absorbance at 652 nm and 418 nm obtained from the catalytic activity of Fe^{II}Fe^{III} LDHNS. Therefore, 0.3 mg mL^{-1} of Fe^{II}Fe^{III} LDHNS concentration was selected as the optimal reaction for both systems to get the highest sensitivity for H_2O_2 detection without to noise from baseline signal.

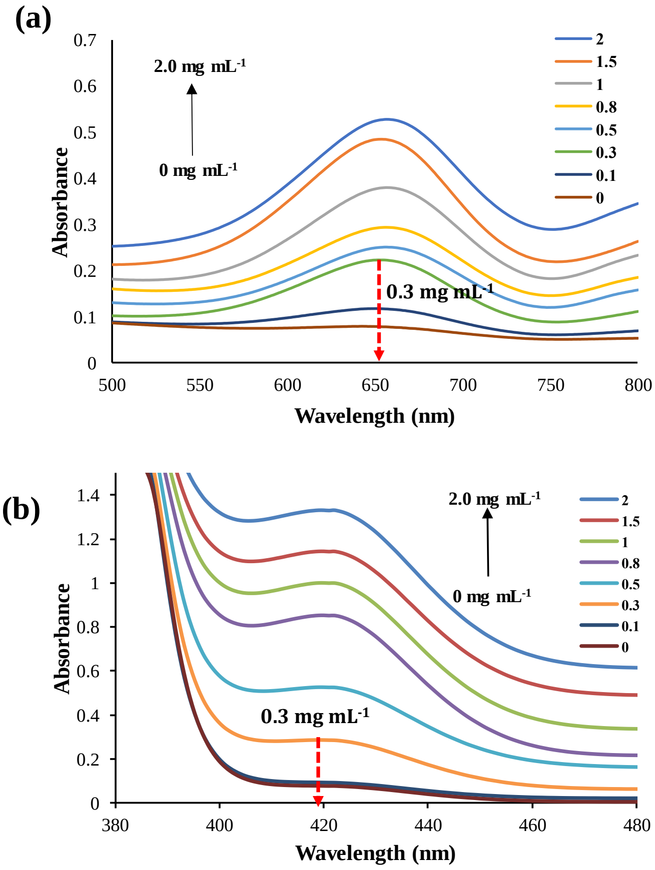

Figure 4.11 Absorption spectra on effects of Fe^{II}Fe^{III} LDHNS concentration on the catalytic oxidation of TMB (a) and ABTS (b) in the absent and presence with various amount of Fe^{II}Fe^{III} LDHNS.

4.2.3 The apparent Michaelis-Menten constant (K_m)

The peroxidase-like activity of $Fe^{II}Fe^{III}$ LDHNS was further studied based on a steady-state kinetics analysis using TMB, ABTS and H_2O_2 as substrate under optimal reaction condition. Kinetic data were obtained by fixing one substrate concentration while varying another substrate concentration; i.e. fixing H_2O_2 concentration while varying concentration of TMB or ABTS, on the other hand, fixing TMB or ABTS while varying H_2O_2 concentration. Series of experiments were carried out and the absorbance data were used to calculate the concentration of oxidized form of both peroxidase substrates based on a molar absorption coefficient of 39,000 and 36,000 M^{-1} cm^{-1} for TMB and ABTS derived oxidation product, respectively [27, 118]. The concentration was calculated from absorbance data by using the Beer Lambert's law following equation (32) [27, 118]:

$$A = \varepsilon bc \tag{32}$$

where A is the measured absorbance, ε is molar absorptivity coefficient (M^{-1} cm^{-1}), b is the path length (cm), and c is the analyte concentration (M). Michaelis-Menten constant (K_m) and maximal reaction velocity (V_{max}) of the $Fe^{II}Fe^{III}$ LDHNS enzyme mimic can be calculated by the Lineweaver-Burk equation, which is shown in equation (33):

$$\frac{1}{v} = \left(\frac{K_m}{V_{\max}}\right)\left(\frac{1}{[S]}\right) + \frac{1}{V_{\max}} \tag{33}$$

where; v is the initial velocity, V_{max} is the maximal reaction velocity, and [S] represents substrate concentration [78-80]. The V_{max} and K_m was obtained from the intercept and slope, respectively.

Figure 4.12 shows the TMB-H_2O_2 (a-b) and ABTS-H_2O_2 (c-d) dependent reaction rates, respectively. K_m value is an indicator of the enzyme affinity towards its substrate, a lower K_m value indicates a stronger affinity between enzyme and its substrate. The kinetics parameters for TMB and ABTS were calculated and summarized in Table 4.2-4.5.

For TMB-H_2O_2 system, the K_m values for $Fe^{II}Fe^{III}$ LDHNS when TMB and H_2O_2 were used as substrate are 0.23 and 3.07 mM, which is lower than that of HRP (0.434 and 3.7 mM) [26]. These results indicated the strong affinity of $Fe^{II}Fe^{III}$ LDHNS towards TMB and H_2O_2 and are comparable to HRP. For ABTS-H_2O_2 system, the K_m value for $Fe^{II}Fe^{III}$ LDHNS with ABTS as a substrate is 0.68 mM, this value was found to be lower than that of HRP (1.56 mM) [62]. This result indicated that the higher affinity of $Fe^{II}Fe^{III}$ LDHNS than HRP towards ABTS was achieved. This can be understood since a HPR molecule contains only one iron ion which decomposes H_2O_2 to generate $OH^{\bullet}$, while the surface of nanosheets is decorated with a lot of iron ions. On the other hand, the K_m value of $Fe^{II}Fe^{III}$ LDHNS with H_2O_2 as a substrate in ABTS-H_2O_2 system is 2.26 mM, which is higher than that for HRP (0.24 mM) [62], suggesting that the affinity of $Fe^{II}Fe^{III}$ LDHNS towards H_2O_2 is lower than that of HRP. From these results, it is clearly seen that $Fe^{II}Fe^{III}$ LDHNS can act as peroxidase enzyme mimic and show the improved catalytic activity for colorimetric detection of H_2O_2 by using TMB and ABTS peroxidase substrate. Thus, we conclude that $Fe^{II}Fe^{III}$ LDHNS are the promising materials for applications requiring high-sensitivity H_2O_2 detection and analysis.

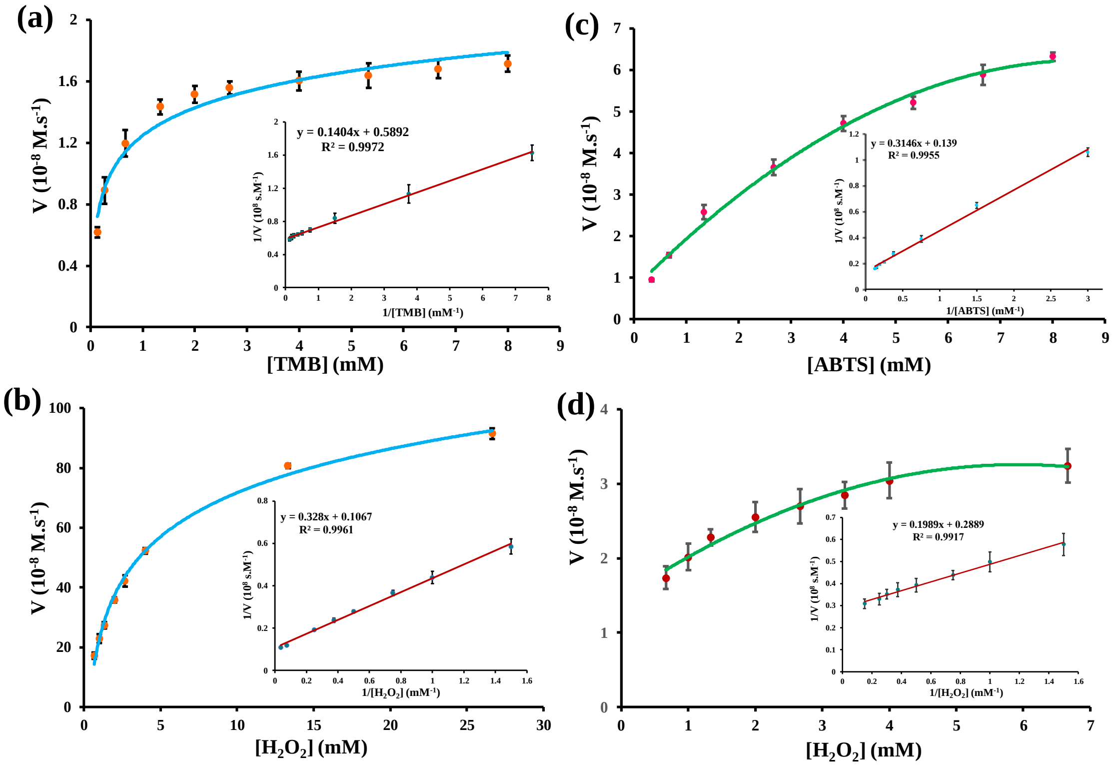

Figure 4.12 Michaelis Menten model and Lineweaver Burk model (inset curve): (a) and (c) fixed concentration of H_2O_2 (1.0 µM) with varied concentration of peroxidase substrate from 0.1 – 8.0 µM and 0.3 – 8.0 µM for TMB and ABTS, respectively. (b) fixed concentration of TMB (100 µM) with varied concentration of H_2O_2 from 0.5 – 200 µM. (d) fixed concentration of ABTS (10 mM) with varied concentration of H_2O_2 from 0.5 – 100 µM. The error bars represent the standard deviation of three measurements.

Table 4.2 Comparison of the Michaelis–Menten constant (K_m) obtained from $Fe^{II}Fe^{III}$ LDHNS for TMB substrate.

Catalyst[a]	K_m (mM)		Reference
	TMB	H_2O_2	
HRP	0.434	3.7	[24]
Fe_3O_4 NPs	0.098	154	[24]
Co–Al ELDH	0.37	22.13	[92]
DNA/CuAl-LDHs	1.78	10.24	[79]
NiFe-LDHNS	0.5	2.4	[81]
C-dot/NiAl-LDHs	0.34	4.72	[80]
$Fe^{II}Fe^{III}$ LDHNS	0.23	3.07	This work

[a] Catalyst: HPR (horseradish peroxidase), NPs (nanoparticles), ELDHs (exfoliated layered double hydroxides), LDHs (layered double hydroxides), LDHNS (layered double hydroxide nanosheets).

Table 4.3 Comparison of the Michaelis–Menten constant (K_m) obtained from $Fe^{II}Fe^{III}$ LDHNS for ABTS substrate.

Catalyst[a]	**K_m (mM)**		**Reference**
	ABTS	**H_2O_2**	
HRP	1.56	0.24	[124]
Fe_3O_4-NH_2-SH	0.25	5.7	[125]
$NiFe_2O_4$	0.46	2.60	[25]
Prussian blue NPs	157.45	0.028	[26]
NiCo-LDHs	3.43	13.2	[32]
Fe_3O_4@Au–Cys–FA NPs	0.44	0.36	[84]
$Fe^{II}Fe^{III}$ LDHNS	0.68	2.26	This work

[a] Catalyst: HPR (horseradish peroxidase), NPs (nanoparticles), ELDHs (exfoliated layered double hydroxides), LDHs (layered double hydroxides), LDHNS (layered double hydroxide nanosheets).

Table 4.4 Comparison of maximum reaction rate (V_{max}) obtained from $Fe^{II}Fe^{III}$ LDHNS for TMB substrate.

Catalyst[a]	V_{max} (10^{-8} M s^{-1})		Reference
	TMB	H_2O_2	
HRP[a]	10.0	8.71	[24]
Fe_3O_4 NPs	3.44	9.78	[24]
Co–Al ELDH	-	-	[92]
DNA/CuAl-LDHs	4.09	2.30	[79]
NiFe-LDHNS	-	-	[81]
C-dot/NiAl-LDHs	5.52	7.89	[80]
$Fe^{II}Fe^{III}$ LDHNS	1.70	9.37	This work

[a] Catalyst: HPR (horseradish peroxidase), NPs (nanoparticles), ELDHs (exfoliated layered double hydroxides), LDHs (layered double hydroxides), LDHNS (layered double hydroxide nanosheets).

Table 4.5 Comparison of maximum reaction rate (V_{max}) obtained from $Fe^{II}Fe^{III}$ LDHNS for ABTS substrate.

Catalyst[a]	**V_{max} (10^{-8} M s^{-1})**		**Reference**
	ABTS	**H_2O_2**	
HRP	-	-	[124]
Fe_3O_4-NH_2-SH	60.0	51.0	[125]
NiCo-LDHs	3.29	3.24	[25]
Fe_3O_4@Au–Cys–FA NPs	10.95	2.03	[26]
Prussian blue NPs	-	-	[32]
$NiFe_2O_4$	17.48	14.11	[84]
$Fe^{II}Fe^{III}$ LDHNS	3.46	7.19	This work

[a] Catalyst: HPR (horseradish peroxidase), NPs (nanoparticles), ELDHs (exfoliated layered double hydroxides), LDHs (layered double hydroxides), LDHNS (layered double hydroxide nanosheets).

4.2.4 Linear concentration range of H_2O_2

H_2O_2 is an important enzymatic intermediate that is produced by many enzyme-substrate reactions and substances that are used in many areas including food safety, pharmaceutical assay, bio-analysis, and clinical diagnostics. Analytes commonly used for clinical diagnosis such as lactase, uric acid, cholesterol, and glucose may be quantitatively analyzed based on oxidase enzyme reactions that produce H_2O_2. Therefore, it is of practical significance to develop methods for H_2O_2 detection. Analytical performance of the developed colorimetric method to detect H_2O_2 by using UV-Vis spectrophotometer was investigated. Figure 4.13 displays the UV-Vis spectra of TMB (a) and ABTS (b) obtained from solutions in the presence of different H_2O_2 concentration. The absorbance increased upon increasing the concentration of H_2O_2, corresponding to the solution color that gradually change from colorless to blue (inset image a) and green (inset image b), respectively. As shown in Figure 4.13 (c-d), the linearity range of the analytical system was studied by using different concentrations of standard H_2O_2 in both TMB and ABTS substrate system. For TMB substrate, signals of different H_2O_2 concentrations as well as linear calibration curve are shown in Figure 4.13 (c). The linear calibration curve of H_2O_2 ranges from 0.1-50 µM.

Figure 4.13 (d) shows the linear calibration curve for ABTS substrate which is in a range from 0.5-20 µM. The outstanding features of the proposed method for ABTS substrate is not only lower limit of detection; but this method also provides simple reaction conditions (in DI water), convenient process, less chemical used and environmental friendly. Furthermore, a catalyst separation procedure for both proposed methods is not required as very small amount of $Fe^{II}Fe^{III}$ LDHNS (0.3 mg mL^{-1}) were used, and they do not interfere the absorbance measured by UV-vis spectrophotometer. The analytical performances of the $Fe^{II}Fe^{III}$ LDHNS systems are comparable to that of other reported nanomaterial-based colorimetric assays reported in Table 4.6.

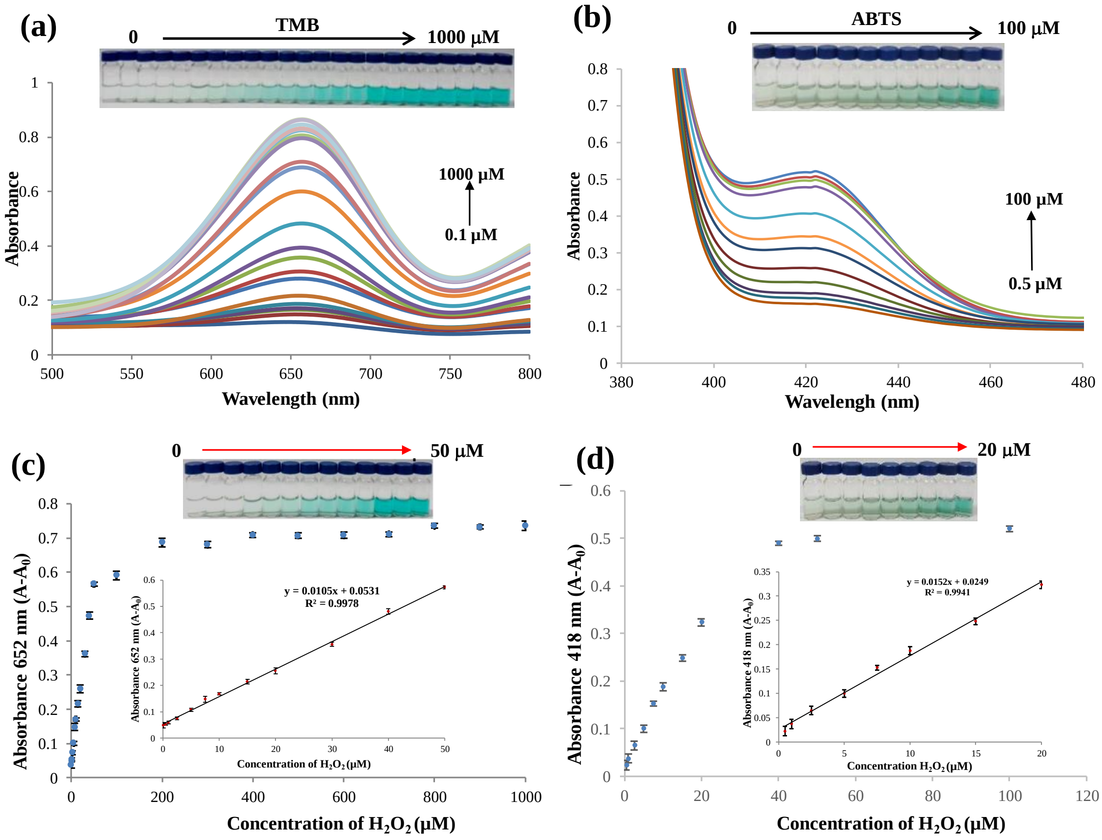

Figure 4.13 A dose-response curve for H_2O_2 detection using $Fe^{II}Fe^{III}$ LDHNS with TMB and ABTS substrate (a-b), respectively. The linear calibration plot for H_2O_2 in the range of 0.1- 50 µM and 0.5-20 µM for TMB and ABTS substrate (c-d), respectively. The upper insets show the corresponding photographs of different solutions. Error bars represent the standard deviation based on three repeated measurements.

4.2.5 Limit of detection of H_2O_2

In this study, detection of limit (LOD) of H_2O_2 detection was investigated by measurement of blank solution with ten replicates. The detection limit was calculated as three times of standard deviation of the blank signal of H_2O_2 divided by the slope of calibration curve (3S.D.$_{blank}$/slope). The calculated LOD was 0.05 µM and 0.2 µM for TMB and ABTS substrate, respectively. The LOD of the $Fe^{II}Fe^{III}$ LDHNS systems are comparable to that of other reported nanomaterial-based colorimetric assays reported in Table 4.6.

Table 4.6 Colorimetric detection of H_2O_2 with nanomaterials as peroxidase mimics.

Nanomaterials[a]	Peroxidase substrate	H_2O_2 (µM)		Reference
		Linear range	LOD	
CoFe-LDHs	TMB	1-20	0.4	[31]
CoAl-ELDHs	TMB	10-200	10	[92]
DNA/CuAl-LDHs	TMB	20-2000	10	[74]
NiFe-LDHNS	TMB	10-500	4.4	[81]
C-dot/NiAl-LDHs	TMB	0.2-20	0.11	[80]
Fe_3O_4@Au–Cys–FA NPs	ABTS	5-10000	2.9	[84]
Fe_3O_4 NPs	ABTS	5-100	3	[84]
Prussian blue NPs	ABTS	0.05-50	0.031	[27]
$Fe^{II}Fe^{III}$ LDHNS	TMB	0.1-50	0.05	This work
$Fe^{II}Fe^{III}$ LDHNS	ABTS	0.5-20	0.2	This work

[a]Nanomaterials: LDHs (layered double hydroxides), ELDHs (exfoliated layered double hydroxides), LDHNS (layered double hydroxide nanosheets), NPs (nanoparticles), LDHNS (layered double hydroxide nanosheets).

4.2.6 Studies the effect of interferences

The selectivity is very important in real sample application as there probably are other substances in the sample that might affect the measurement. The considered interferences in this study were glucose, maltose, lactose, fructose, ascorbic acid (AA), Na^+, Zn^{2+} and Mg^{2+}; which are the components in milk samples. The concentrations of interferences (100 µM) were five-fold higher than that of the standard H_2O_2 (20 µM). The experiments were performed under the optimized conditions for TMB and ABTS substrate. It can be obviously seen that the absorbance obtained from these ions are relatively weak compared to H_2O_2 and can be neglected; because no colored products were formed (inset image) for both TMB (Figure 4.14 (a)) and ABTS (Figure 4.14 (b)). These results clearly indicated that the $H_2O_2/Fe^{II}Fe^{III}$ LDHNS/TMB and $H_2O_2/Fe^{II}Fe^{III}$ LDHNS/ABTS systems exhibited high selectivity towards H_2O_2 detection.

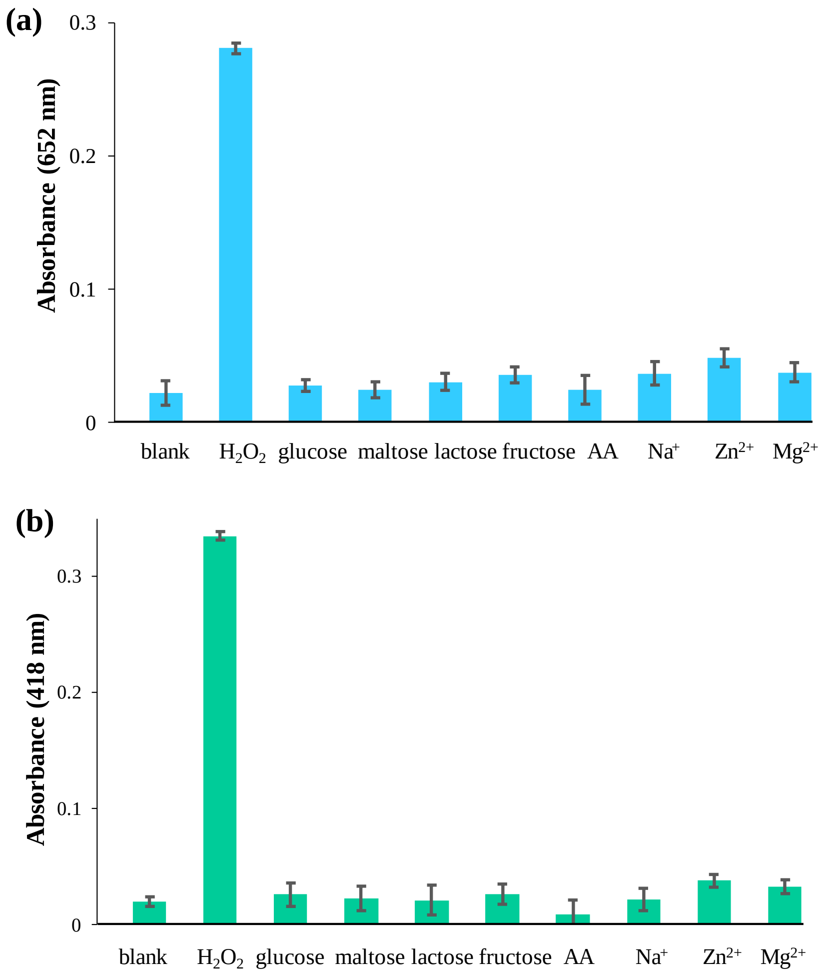

Figure 4.14 Selectivity of the colorimetric method of (a) the H_2O_2/Fe^{II}Fe^{III} LDHNS/TMB and (b) H_2O_2/Fe^{II}Fe^{III} LDHNS/ABTS systems for H_2O_2 detection by measuring absorbance at 418 nm and 652 nm, respectively. Error bars represent the standard deviation for three measurements. Inset: photographs of different interference solutions.

4.2.7 Stability of Fe^{II}Fe^{III} LDHNS

The long-term stability of Fe^{II}Fe^{III} LDHNS is significant for continuous and reliable monitoring of H_2O_2. To evaluate the stability of the developed methods, the Fe^{II}Fe^{III} LDHNS were dispersed in deionized water (0.3 mg mL^{-1}) and stored at 4 °C. They were used to measure the absorbance response for 20 µM of H_2O_2 every three days for 21 days. As shown in Figure 4.15 (a), the absorbance for H_2O_2/Fe^{II}Fe^{III}

LDHNS/TMB system slightly decreased over time; however it retained 90% of original response until week 3. Upon further storage to 21 days, 80% of its original response still retained. For the H_2O_2/Fe^{II}Fe^{III} LDHNS/ABTS system, the absorbance also slightly declined over storage time. Its absorbance response retained approximately 92% of the original value over a storage period of 9 days (Figure 4.15 (b)). These results indicated that the Fe^{II}Fe^{III} LDHNS exhibited better long-term stability towards H_2O_2 detection for TMB than that for ABTS system. Nevertheless; both systems demonstrate good stability, more than 90 % of the original absorbance retained for the storage period of longer than a week.

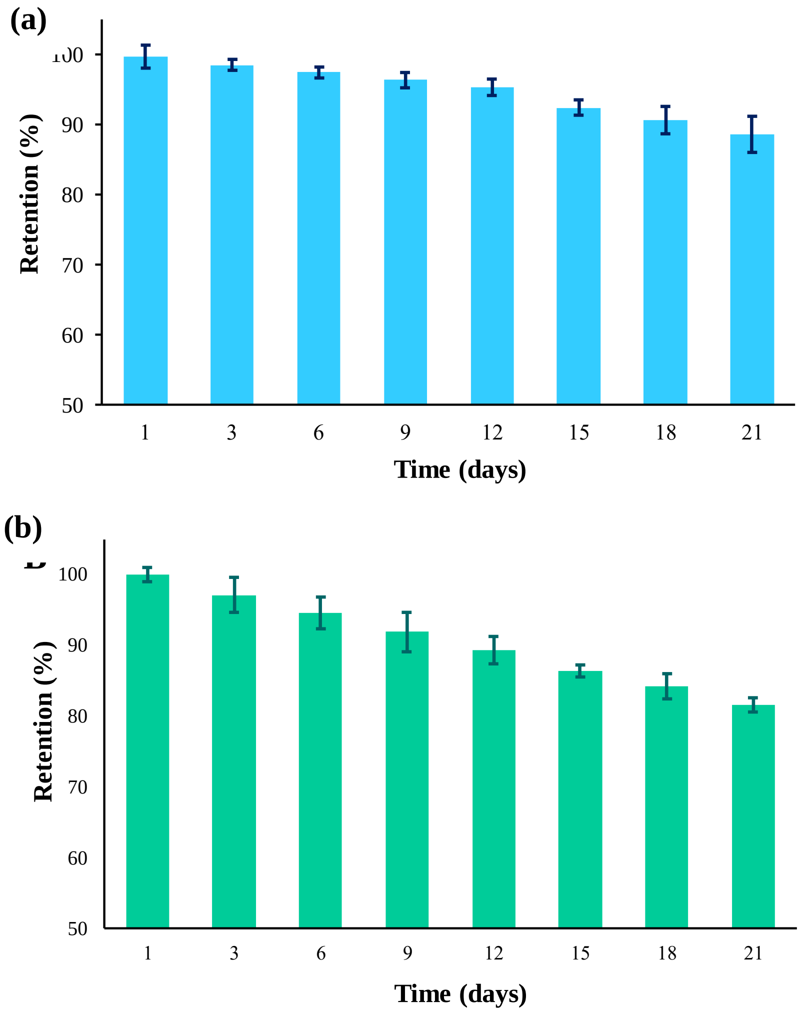

Figure 4.15 The long-term stability of Fe^{II}Fe^{III} LDHNS for colorimetric detection of H_2O_2 by using TMB (a) and ABTS (b) substrate for 21 days.

4.2.8 Determination of H_2O_2 in real samples

To investigate the accuracy and feasibility of the developed colorimetric method, the standard iodometric titration method was employed to compare with the proposed colorimetric method for H_2O_2 analysis in milk and disinfectant samples [59, 62]. Six aseptic milk samples and two disinfectant samples were purchased from the local supermarkets. These samples were treated and prepared as described in section 3.5.7. Proteins were precipitated from all six milk samples and H_2O_2 standard solutions were spiked into the protein free sample. Two disinfectant samples were diluted to ensure that H_2O_2 concentrations were within linearity range. Under the optimized conditions, five replicates for each sample, the concentration of H_2O_2 in all real samples were determined and the results are summarized in Table 4.7. The developed methods provided the recoveries ranged from 97.52 to 102.99 % for TMB substrate and 97.34 to 103.26 % for ABTS substrate, which was consistent with the range from 98.78 to 103.50 % obtained by the standard iodometric titration method. Furthermore, these methods exhibited impressively good precision (% RSD ranging from 1.10 to 2.87). Therefore, the proposed colorimetric method is sufficiently accurate and there is no significant matrix interference that affects the sample measurements, demonstrating that our method is suitable for the quantification of H_2O_2 in real samples.

Table 4.7 Comparison of H_2O_2 concentration in milk and disinfectant samples obtained using the proposed colorimetric method and iodometric titration standard method (Avg. ± SD of five trials).

Methods	Iodometric titration			Proposed method: TMB (Added 0.1 M)			Proposed method: ABTS (Added 0.1 M)		
Samples	Found[d]	Recovery (%)[d]	RSD (%)[d]	Found[d]	Recovery (%)[d]	RSD (%)[d]	Found[d]	Recovery (%)[d]	RSD (%)[d]
M1[a]	0.91 ± 0.02	103.50 ± 1.73	1.67	0.87 ± 0.03	99.12 ± 2.84	2.87	0.90 ± 0.03	101.83 ± 2.84	2.79
M2[a]	0.90 ± 0.02	102.39 ± 2.20	2.15	0.86 ± 0.01	97.52 ± 1.33	1.37	0.87 ± 0.02	99.05 ± 1.88	1.90
M3[a]	0.88 ± 0.03	99.89 ± 3.00	3.00	0.90 ± 0.02	101.87 ± 2.35	2.31	0.90 ± 0.01	102.17 ± 1.24	1.22
M4[a]	0.87 ± 0.02	98.78 ± 2.09	2.12	0.91 ± 0.01	102.99 ± 1.65	1.60	0.86 ± 0.01	97.34 ± 1.07	1.10
M5[a]	0.90 ± 0.01	102.11 ± 0.48	0.47	0.89 ± 0.02	100.43 ± 0.19	2.18	0.90 ± 0.01	102.14 ± 1.40	1.37
M6[a]	0.89 ± 0.01	101.28 ± 1.27	1.25	0.87 ± 0.02	98.30 ± 2.14	2.17	0.91 ± 0.02	103.26 ± 1.87	1.82
6% HP1[b]	0.90 ± 0.03	101.84 ± 2.92	2.87	1.79 ± 0.03	ND	1.78	1.79 ± 0.03	ND	1.62
3% HP2[c]	0.90 ± 0.02	102.11 ± 2.09	2.05	0.90 ± 0.01	ND	1.14	0.89 ± 0.03	ND	1.96

[a] Spike 3% H_2O_2 (0.882 M) in real samples, [b] Hydrogen peroxide disinfectant: concentration of 6% w/v or 1.76 M, [c] Hydrogen peroxide disinfectant: concentration of 3% w/v or 0.882 M, [d] Average of five determinations ± standard deviation.

4.3 Characterization of Fe_3O_4/rGO/ZnAl LDHs

4.3.1 X-Ray Diffractometer (XRD)

X-ray diffraction spectroscopy is a powerful technique used to identify crystalline structure and phase composition of materials. The diffraction peak for graphite (Figure 4.16) was at 2θ angles of 26.3°, which is assigned to (002) plan of graphite [95]. After oxidation of graphite, the diffraction peak for GO (Figure 4.17 (a)) shows two characteristic plans of (002) and (100) at $2\theta = 10.6°$ and 42.5°, which indicated that the graphite was fully oxidized into GO [53, 57, 58, 95, 121]. As can be seen from Figure 4.17 (b), the pattern of Fe_3O_4/rGO showed weak and board diffraction reflections, which were assumed to the random arrangement of the GO sheets and the uneven interlayer spacing after deposition of magnetite nanoparticles [53]. The Fe_3O_4/rGO reveals five characteristic peaks at 2θ angles of 30.3°, 35.7°, 43.9°, 57.7°, and 63.1° corresponding to (220), (311), (400), (511), and (440) reflections, confirming the formation of Fe_3O_4 nanoparticles deposited on GO sheets [57, 58]. Clearly seen that, the XRD pattern of Fe_3O_4/GO did not show diffraction peak corresponding to the GO because of the disorders that occur in GO stacking during the composite formation, according to the previous reports [122, 123]. The sharp diffraction peaks for ZnAl-LDHs (Figure 4.17 (c)) occur at 2θ angles of 11.7°, 23.3°, 34.5°, 39.1°, 46.3°, 60.0°, and 61.3°, which are assigned to the (003), (006), (012), (015), (018), (110), and (113) planes in ZnAl-LDHs, respectively [104, 121, 124]. Figure 4.17 (d) shows the XRD pattern of Fe_3O_4/rGO/ZnAl-LDHs displayed obviously main characteristic peaks of Fe_3O_4/rGO and ZnAl-LDHs. These results confirm that these two components existed in the final product.

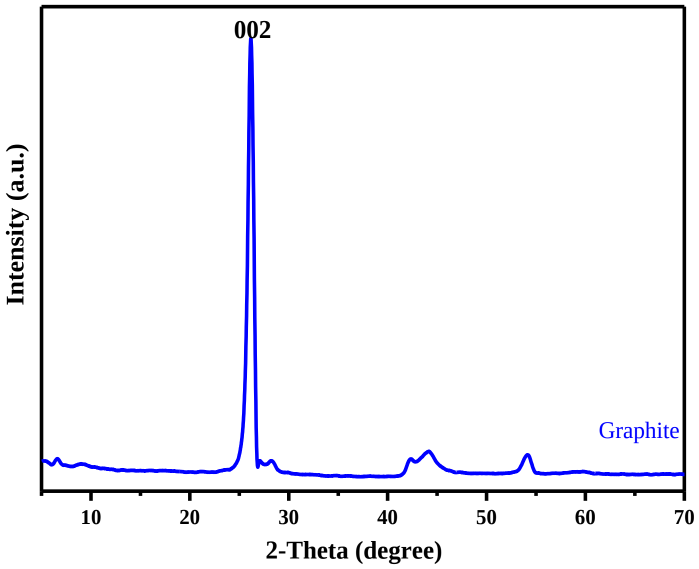

Figure 4.16 XRD pattern of graphite.

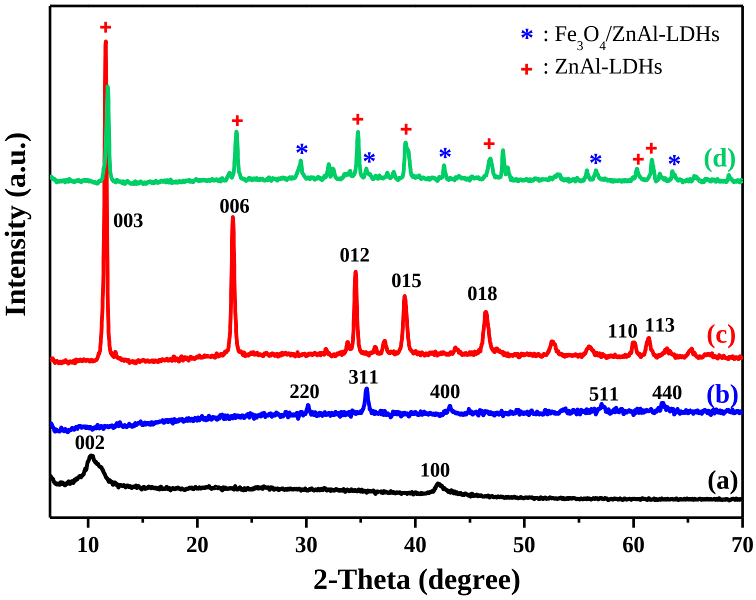

Figure 4.17 XRD patterns of pure GO (a), Fe_3O_4/rGO (b), ZnAl-LDHs (c) and Fe_3O_4/rGO/ZnAl-LDHs (d).

4.3.2 Scanning Electron Microscope (SEM)

The morphologies of the as-prepared products were characterized by SEM. The SEM images in Figure 4.18 represents the surface morphology of the synthesized samples of GO, Fe_3O_4/rGO, ZnAl-LDHs and Fe_3O_4/rGO/ZnAl-LDHs, respectively. Figure 4.18 (a) shows SEM images of the GO have well defined and interlinked three-dimensional rGO sheet-like structure. Clearly seen that, the surface morphology of GO displays highly wrinkled structure [53, 95]. In contrast, the surface of GO which was quite smooth, but the Fe_3O_4 nanoparticles-decorated GO sheets revealed that clearly reveal that the rGO sheets structure with well intercalation of Fe_3O_4 nanoparticles and uniform distribution of nanoparticles on rGO surface as shown in Figure 4.18 (b). It is evident that prepared Fe_3O_4 nanoparticles are nearly spherical in shape at nanoscale with mean diameter around 56 nm. Besides, the surfaces of Fe_3O_4/rGO were rougher than those of the original GO. The results confirmed the rGO oxidize Fe^{2+} to form Fe_3O_4/rGO *via* the spontaneous *in-situ* deposition of Fe_3O_4 nanoparticles onto the self-reduced rGO surface [53, 58]. Figure 4.18 (c) displays the highly regularity disk-like platelets of ZnAl-LDHs similarly to previous work [125, 126], which indicates that the average diameter approximately 2–3 μm and the thickness is about 44.5 nm. The representative SEM image of Fe_3O_4/rGO/ZnAl-LDHs morphology as shown in Figure 4.18 (d). After assembling of Fe_3O_4/rGO/ZnAl-LDHs, the ZnAl-LDHs were randomly formed by co-precipitation method the surface of Fe_3O_4/rGO sheets and intercalated into adjacent rGO sheets, which directly increased the unevenness of the Fe_3O_4/rGO sheets.

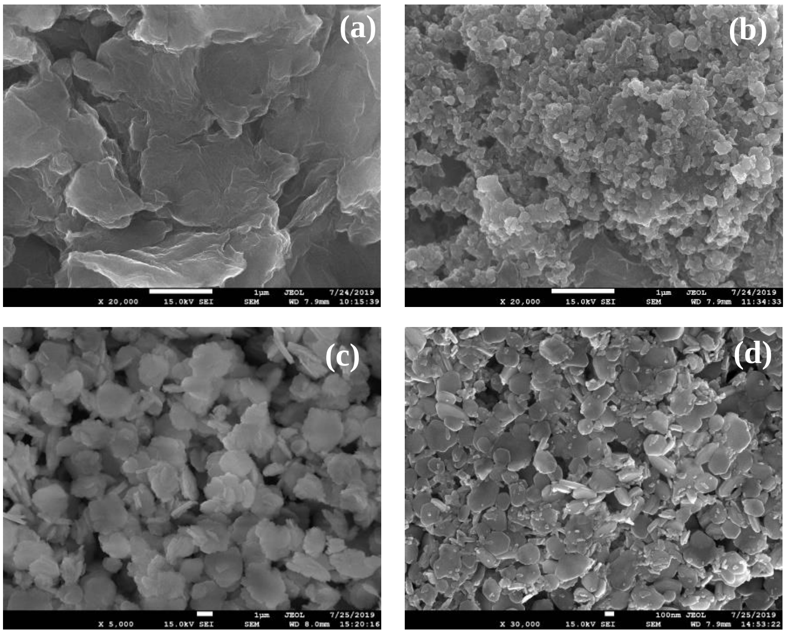

Figure 4.18 SEM image of GO (a), Fe_3O_4/rGO (b), ZnAl-LDHs (c) and Fe_3O_4/rGO/ZnAl-LDHs (d).

4.3.3 Energy Dispersive X-Ray Spectroscopy (EDS)

The EDS spectrum (Figure 4.19) reveals that the final product mainly contains elemental Fe, O, S, and C. In the Fe_3O_4/rGO/ZnAl-LDHs EDS spectrum, peaks at approximately 0.7 ($L_{\alpha 1}$), 6.4 ($K_{\alpha 1}$), and 7.0 ($K_{\beta 1}$) keV, which are associated with the binding energies of iron (Fe), were observed. The peaks around 1.0 ($L_{\alpha 1}$) and 8.6 ($K_{\alpha 1}$) keV relate to the binding energies of zing (Zn). The signal of binding energies of aluminum (Al), oxygen (O), and carbon (C) at approximately 1.5 ($K_{\alpha 1}$), 0.5 ($K_{\alpha 1}$), and 0.3 ($K_{\alpha 1}$) keV, respectively, were also observed. Carbon indicate the component of rGO and carbonate anion is a charge-balancing ion in the product interlayer. Moreover, the few signal binding energies of nitrogen (N) around 0.4 ($K_{\alpha 1}$) keV were assumed the effect of incomplete removal in wash steps. These results are evidencing that the successful assembly of ZnAl-LDHs and Fe_3O_4/rGO. The percentages of all elemental are summarized in Table 4.8. Additionally, the distribution of these elements was investigated with elemental mapping using SEM-EDS, as displayed in Figure 4.20. The elements Zn, Al, Fe, O, C and N appear to be uniformly distributed, and these also confirm the presence of these elements in the adsorbent.

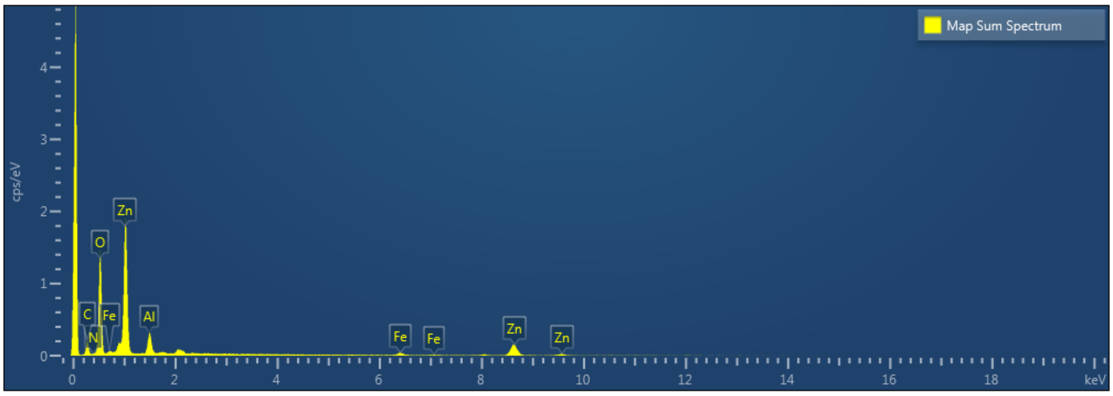

Figure 4.19 EDS spectra of Fe_3O_4/rGO/ZnAl-LDHs.

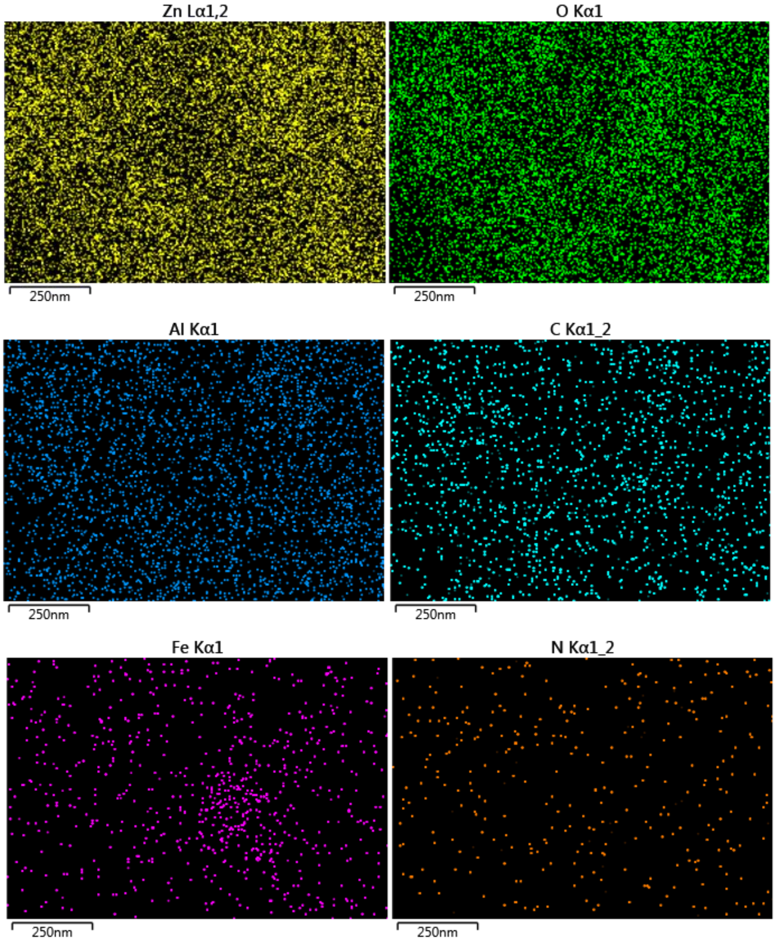

Figure 4.20 SEM-EDS elemental mapping images of Fe_3O_4/rGO/ZnAl-LDHs.

Table 4.8 The elemental quantity of the element normalized for adsorbent (Fe_3O_4/rGO/ZnAl-LDHs).

Total: Element	Weight %	Weight % Sigma
C	14.73	0.62
N	0.60	0.52
O	32.63	0.48
Al	4.99	0.17
Fe	2.84	0.26
Zn	44.22	0.56

4.3.4 Fourier Transform Infrared Spectrophotometer (FTIR)

FTIR was employed to characterize the functional group and the new bands formed by the group. The FTIR spectra of synthesized magnetic adsorbent by co-precipitation method were shown in Figure 4.21. In the spectrum of GO **(**Figure 4.21 (a)), the board band at 3401 cm^{-1} is attributed to O−H stretching of the carboxylic groups and phenolic groups. The other peaks corresponded to oxygen functional group, such as, C=O carbonyl stretching of COOH groups at 1716 cm^{-1}, and the C−O epoxide group stretching at 1245 cm^{-1} and C−OH alkoxy group stretching vibrations at 1043 cm^{-1}. The band at 1611 cm^{-1} is C=C aromatic stretching vibration [53, 57, 58, 95, 121]. The FTIR spectrum of Fe_3O_4/rGO show in Figure 4.21 (b), the bands at 3417 cm^{-1} indicated the O−H stretching vibration. Other peaks at 1764, 1639, 1239 and 1094 cm^{-1} are ascribed to the C=O carbonyl stretching and C=C aromatic stretching, C−O epoxide stretching, and C−OH alkoxy stretching of rGO, respectively. In addition, the strong peak at 539 cm^{-1} can be assigned to Fe−O stretching vibration of Fe_3O_4 nanoparticles [57, 58], which confirm that Fe^{2+} has been oxidized into formation of Fe_3O_4 nanoparticles on rGO sheets [58]. For ZnAl-LDHs **(**Figure 4.21 (c)**)** the strong and board band at 3452 cm^{-1} is attributed to O−H stretching of the hydroxyl groups and water molecules. The weak band at 1660 cm^{-1} corresponded to O−H bending vibration of the interlayer water. The bands observed in the low wavenumber region at 741 and 548 cm^{-1} are ascribed to the Al−OH deformation mode and the Zn/Al−OH translation, respectively [1, 2, 104, 121]. The strong peak at 1360 cm^{-1} can be interpreted as the anti-symmetric stretching mode of the carbonate anion present in the interlayer of ZnAl-LDHs [1, 2]. The spectra of

Fe_3O_4/rGO/ZnAl-LDHs **(**Figure 4.21 (d)**)** mainly presented the same band as ZnAl-LDHs. But the characteristic bands of Fe_3O_4/rGO was not observed clearly and the band of carbonate anion was decrease intensity because of the suspension of the peaks between of Fe_3O_4/rGO and LDHs-phase. It is evidencing that the Fe_3O_4 nanoparticles onto the self-reduced graphene oxide (rGO) sheets and attached with ZnAl-LDHs have been successfully prepared.

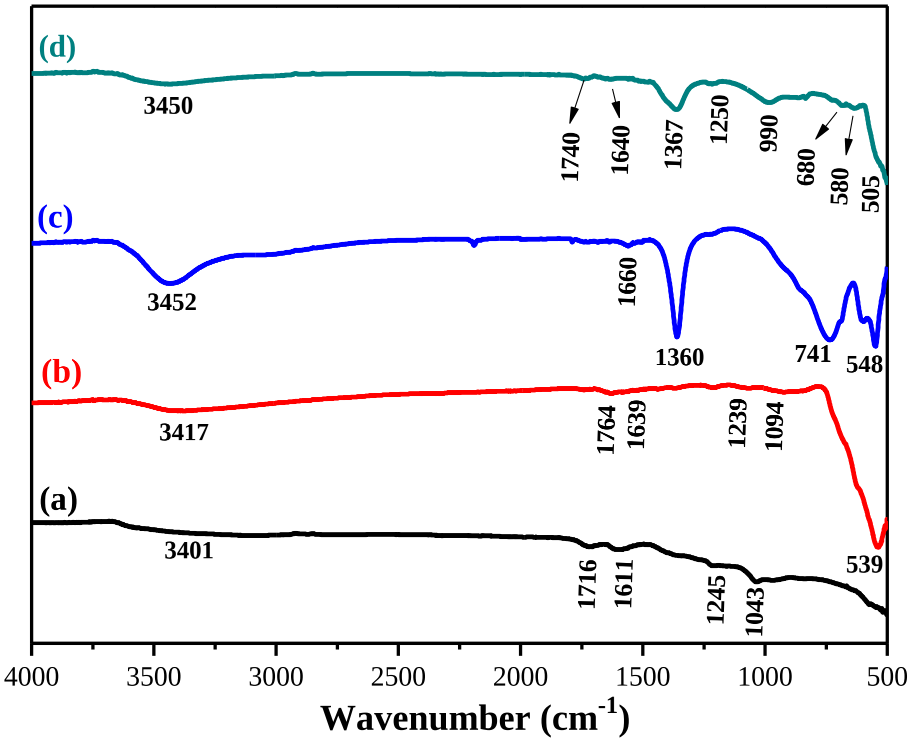

Figure 4.21 FTIR spectra of GO (a), Fe_3O_4/rGO (b), ZnAl-LDHs (c) and Fe_3O_4/rGO/ZnAl-LDHs (d).

4.3.5 Brunauer-Emmett-Teller (BET) surface area analysis

N_2 adsorption–desorption isotherms of BET analysis was reported as an effective tool for investigating the specific surface area of materials. The N_2 adsorption/desorption isotherm of as-synthesized GO, Fe_3O_4/rGO, ZnAl-LDHs and Fe_3O_4/rGO/ZnAl-LDHs exhibited typical IV-type isotherms with H3-hysteresis loops according to the IUPAC classification of adsorption isotherms as shown in Figure 22. This result indicate that the presence of mesopores with many slit holes, which might generate from the gaps between GO sheets or the gaps between Fe_3O_4, rGO and ZnAl-LDHs [126-128]. Pore diameter is in the range of 2.85-7.43 nm which suggests the presence of mesopores and slit pores of plate-like particles due to sheets aggregation of the LDHs [104]. The pore structure parameters of the materials, such as the specific surface area, pore diameter and pore volume are listed in Table 4.9. Note that, the Brunauer–Emmett–Teller (BET) specific surface area of Fe_3O_4/rGO/ZnAl-LDHs (11.13 $m^2\ g^{-1}$) was large than ZnAl-LDHs only (5.32 $m^2\ g^{-1}$), indicating that Fe_3O_4/rGO could improve surface properties of LDHs. The decline in pore diameter should be attributed to the restacking of Fe_3O_4/rGO and ZnAl-LDHs, which will inevitably block the pores and channels of LDHs.

Table 4.9 The specific surface areas and pore characteristics of the adsorbent samples.

Materials	**BET surface area ($m^2\ g^{-1}$)**	**Average pore diameter (nm)**	**Pore volume (cm^3/g)**
rGO	57.42	4.31	5.952
Fe_3O_4/rGO	62.18	2.85	12.87
ZnAl-LDHs	5.32	7.43	0.049
Fe_3O_4/rGO/ZnAl-LDHs	11.13	4.29	0.136

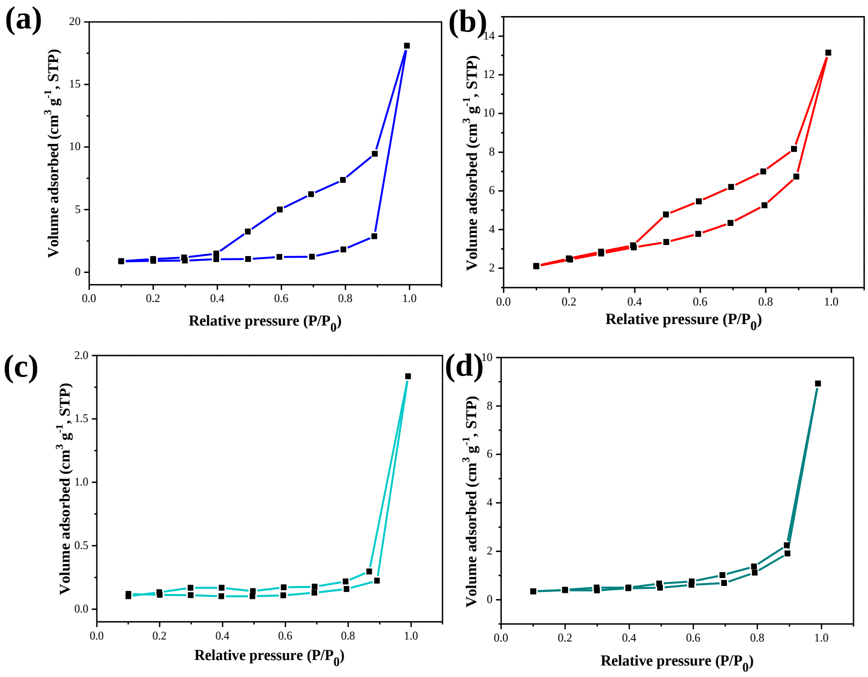

Figure 4.22 **N_2 adsorption–desorption isotherms of GO (a), Fe_3O_4/rGO (b), ZnAl-LDHs (c) and Fe_3O_4/rGO/ZnAl-LDHs (d).**

4.3.6 Zeta potential analysis

Zeta potential is an important indicator to determine the surface charge of the materials and to characterize the stability of dispersions. The zeta potential of synthesized materials suspended in aqueous media and using ultrasonic bath were measured by Zetasizer- NANO-ZS. Figure 4.23 (a) displays the zeta potentials of GO was measured at -19.1 mV. The zeta potential of GO was high due to the presence of negatively charged OH and COOH groups [129]. After Fe_3O_4 nanoparticles deposited onto the self-reduced GO surface as shows in Figure 4.23 (b), resulting to reduce the negative surface at -10.6 mV due to a decrease in oxygen functional groups [130]. Zeta potential for ZnAl LDHs suspension shows in Figure 4.23 (c) is positive charge (+37.2 mV). Figure 4.23 (d) shows that Fe_3O_4/rGO/ZnAl-LDHs exhibited the zeta potentials of + 30.6 mV. These results assumed that the hybrid material was obtained by the electrostatic of negative charge from Fe_3O_4/rGO and positive charge of ZnAl LDHs. Generally, particles with positive zeta potentials greater than +30 mV or those are more negative than -30 mV are considered stable [131]. This result suggests that the surface modification of Fe_3O_4/rGO/ZnAl-LDHs is an effective can promote the stability of dispersions in aqueous media.

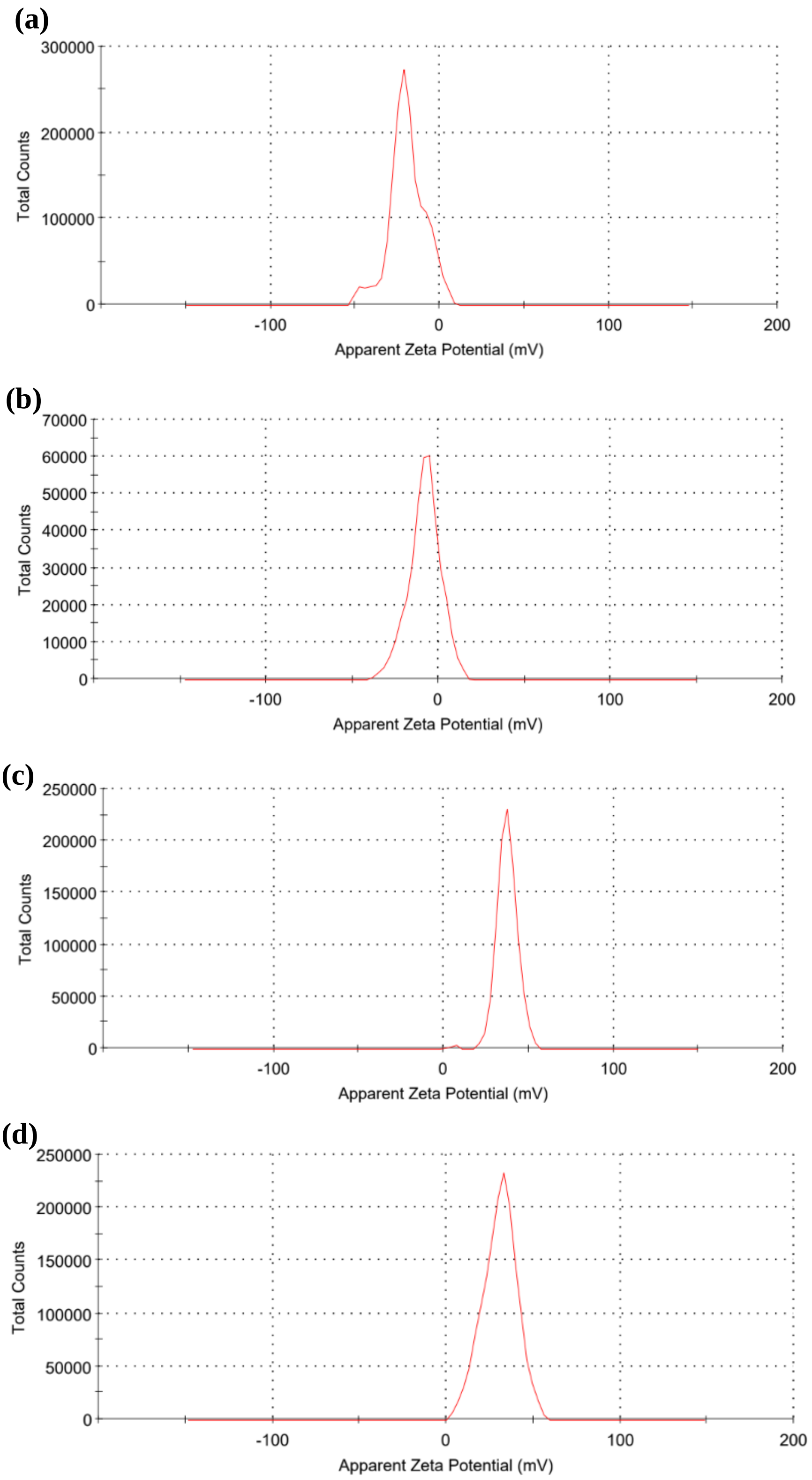

Figure 4.23 **Zeta potential of GO (a), Fe_3O_4/rGO (b), ZnAl-LDHs (c) and Fe_3O_4/rGO/ZnAl-LDHs (d).**

4.3.7 Vibrating sample magnetometer (VSM)

The magnetic properties of the as-obtain materials were characterized by a vibrating sample magnetometer (VSM) at 300 K and the magnetic field variation between −10 and 10 kOe. The magnetization (M) versus field (H) curve for Fe_3O_4/rGO and Fe_3O_4/rGO/ZnAl LDHs is shown in Figure 4.24. It was observed that synthetic Fe_3O_4/rGO and Fe_3O_4/rGO/ZnAl LDHs have a saturation magnetization (M_s) of 90.8 and 57.2 emu g^{-1}, respectively. The decrease of M_s could be due to the existence of ZnAl LDHs on the surface of Fe_3O_4/rGO, which changes the surface magnetic anisotropy and leads to enhancement of the surface spins disorientation [132]. However, the Fe_3O_4/rGO/ZnAl LDHs still exhibited good magnetic properties that can ensure them be easily collected and recycled from aqueous solution by simply putting an external magnetic field. The nature of the magnetic hysteresis loops was "S curves", indicative of the superparamagnetic characteristic of composites [53, 132]. According to the VSM results, both samples showed hysteresis loop was close to S-like curves, and the magnetic remanences are nearly zero. This result indicates that there is almost no remaining magnetization when the external magnetic field is removed which is characteristic of superparamagnetic behavior.

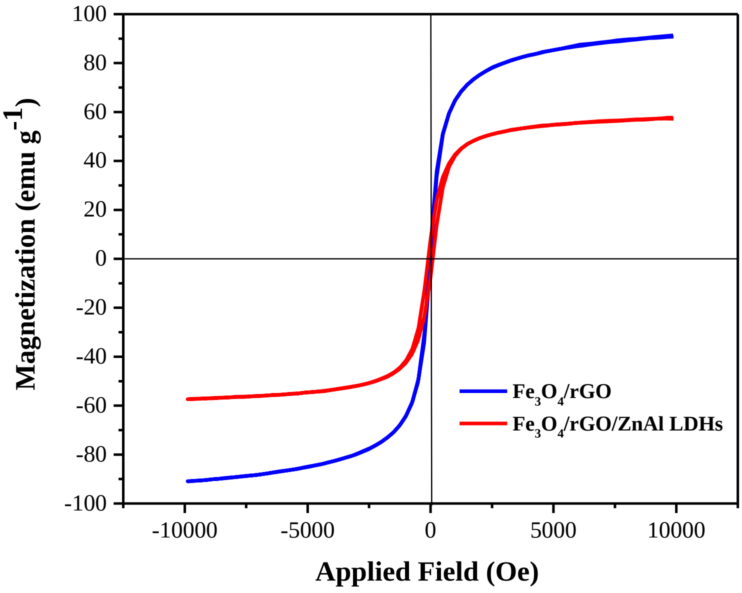

Figure 4.24 Hysteresis loops of adsorbent samples measured at 300 K.

4.4 Adsorption behavior of methyl orange and brilliant green

4.4.1 Effect of contact time and initial dyes concentration

It is well known that the equilibrium time is an important factor for the adsorption of dye molecules, which influences the structure of the dye molecules and the surface properties of adsorbent [34, 35, 105]. Factor influencing equilibrium time for dye adsorption include: i) the binding interactions between the surface of absorbent and dye molecules; ii) the transport of dye molecules caused by associated driving forces (shaking or concentration gradient) ; and iii) the availability of active sites of adsorbent [35, 105]. Effect of contact time with GO, Fe_3O_4/rGO, ZnAl-LDHs and Fe_3O_4/rGO/ZnAl-LDHs for adsorption of MO and BG were assessed at concentration of 100 mg L^{-1} as shown in Figure 4.25 (a) and Figure 4.26 (a), respectively. It was observed that the adsorption capacity rate of MO and BG on all samples was very fast at initial time due to the adsorbent surface bears a lot of available active sites for fast adsorption to takes place. Then the adsorption capacity rate becomes slow and reaches equilibrium finally [36]. In terms of the adsorption capacity, GO performed the best, followed by Fe_3O_4/rGO/ZnAl-LDHs, ZnAl-LDHs and Fe_3O_4/rGO. Especially, the adsorption capacity rate of both dyes adsorption on GO was very fast when compared with other adsorbents and display highest adsorption capacity at equilibrium in short time about 307.45 mg g^{-1} (60 min) and 477.79 mg g^{-1} (90 min) for MO and BG, respectively. For the Fe_3O_4/rGO/ZnAl-LDHs displays adsorption capacity in pseudo-second order for MO and BG of 187.53 mg g^{-1} (60 min) and 445.89 mg g^{-1} (360 min), respectively. It is obvious that adsorption capacity of Fe_3O_4/rGO/ZnAl-LDHs increased when compared with ZnAl-LDHs about 153.59 mg g^{-1} (360 min) and 343.85 mg g^{-1} (360 min) for MO and BG, respectively. Thus, Fe_3O_4-decorated rGO could be enhancements adsorption capacity of ZnAl-LDHs only. This was attributed to the surface functional groups which increased their surface complexation capability and π–π interactions between the aromatic ring of dye molecule and the aromatic structure of rGO. Also, the adsorption was attributed to the electrostatic interactions between surface functional groups of rGO and primary ammonium ion, while the MO adsorption was mainly favored by the van der Waals interactions [133]. The initial concentrations are an important factor, which is used to design dye adsorption in aqueous solution. To investigate the effect of contact time on MO and BG adsorption with different initial concentrations (5, 10, 25, 50, 100, 200, 300 and 500 mg L^{-1}) are operated and presented in Figure 4.25 (b-d) and Figure 4.26 (b-d), respectively. Observably, increasing in the initial dye concentration of both dyes leads to an increase in the adsorption capacity of all eight samples. The adsorption process was rapid during the initial stage. After that, adsorption rate slowed down and remained constant after an equilibrium time was reached. This observation was ascribed to a large number of vacant active sites on the adsorbent surface in the beginning stage, and the remaining sites were difficult to occupy due to repulsive forces between the dye molecules on the adsorbent and the bulk phase [36, 48]. The equilibrium was attained in 60 min and 360 min for MO and BG, respectively.

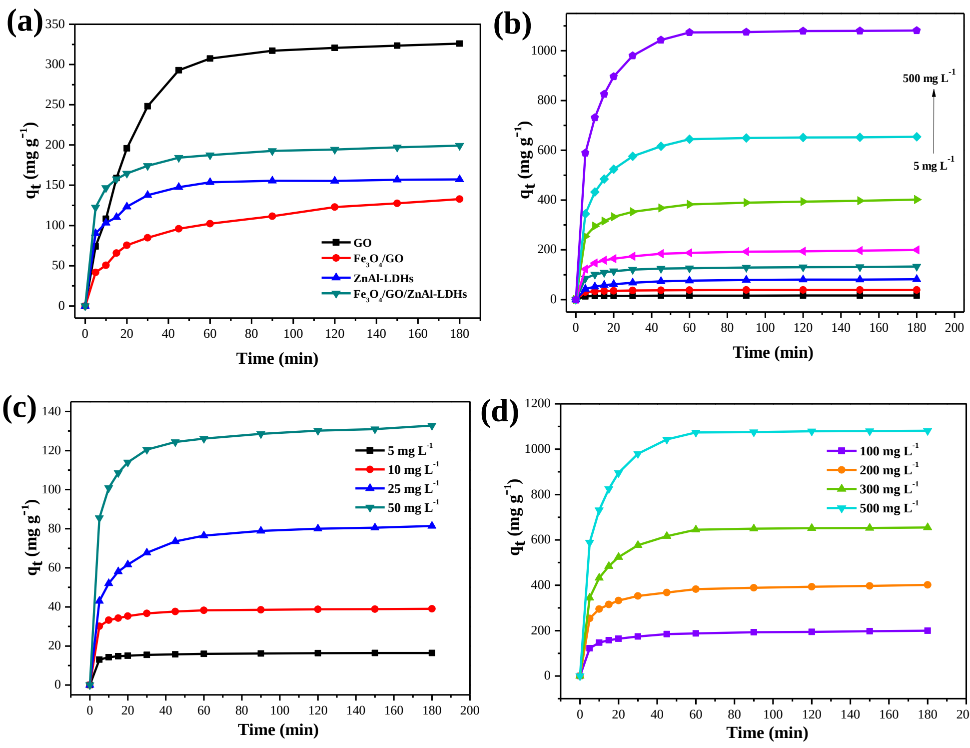

Figure 4.25 Effect of contact time on adsorption kinetics of MO removal by (a) different adsorbents (C_0 = 100 mg L^{-1}, T ≈ 25 °C, pH ≈ 5.6), (b-d) onto Fe_3O_4/rGO/ZnAl-LDHs at different initial concentrations.

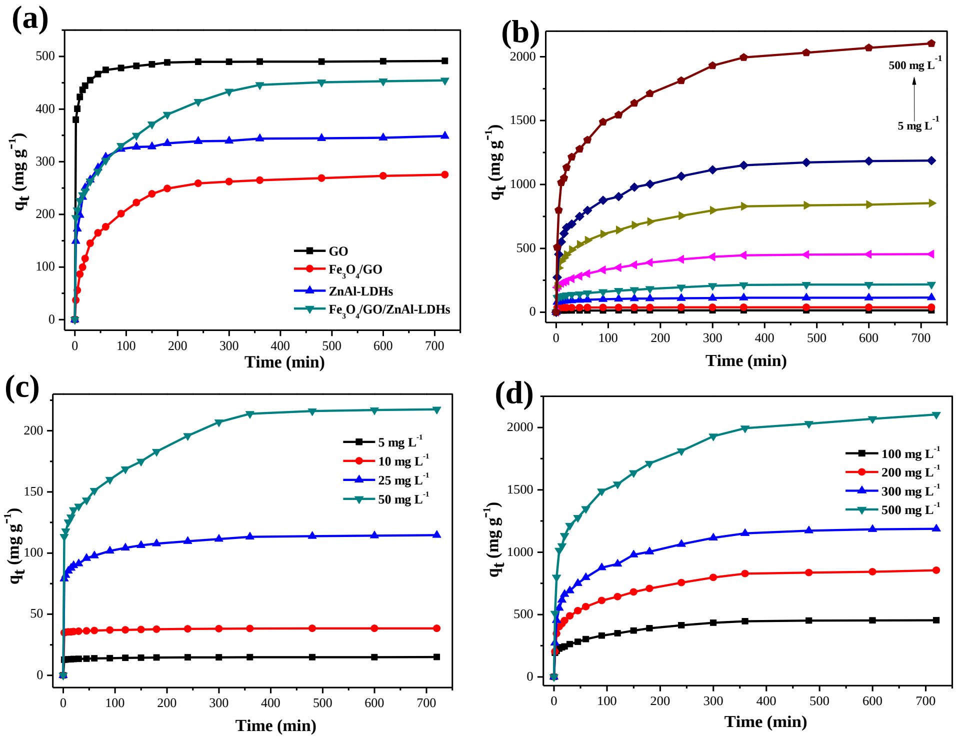

Figure 4.26 Effect of contact time on adsorption kinetics of BG removal by (a) different adsorbents (C_0 = 100 mg L^{-1}, T ≈ 25 °C, pH ≈ 5.6), (b-d) onto Fe_3O_4/rGO/ZnAl-LDHs at different initial concentrations.

4.4.2 Effect of pH

The solution pH is one of most important parameters in adsorption process. It can significantly affect but also the active sites on surface of adsorbents. The surface charge and the degree of ionization of the functional group of dye molecules and charge density around adsorbent are greatly affected by pH parameter, and this in turn controls the extent of adsorption [1, 34, 57]. The effect of pH on dye adsorption was investigated by varying pH within the range 2-12, at 25 ± 1 °C for 60 min and 360 min as an equilibrium time of MO and BG, respectively. The MO solution noticeably change its color from red to orange (inset image in Fig. 6a). Also, the red color of the solution with pH value less than 3 was different from its original orange color [134, 135]. Figure 4.27 (a) shows the effect of initial pH on the adsorption capacities of MO. It is clear that the adsorption capacities of MO on Fe_3O_4/rGO/ZnAl-LDHs was pH dependent and exhibited optimum pH in over the range 4-10. The reduced adsorption capacities of MO observed at pH 2 can be explained by the protonate with sulfonic acid on MO molecule leading to a low attachment of dye molecule. Likewise, the adsorption capacities of MO were lowest at pH 12 presence of excessive OH^- leading to competitive with MO molecules [1, 36]. In addition, the surface of Fe_3O_4/rGO/ZnAl-LDHs would adsorption of OH^-, resulting to the electrostatic repulsion between adsorbent and adsorbate [1, 36]. MO is an anionic dye molecule can be attached on the surface of adsorbent through electrostatic force of ZnAl-LDHs, van der Waal’s force, hydrogen bonding between dye molecule and rGO, π-π stacking interaction between aromatic part of dye and delocalized π-electron system of graphene [44]. The influent of solution pH on the removal of BG by Fe_3O_4/rGO/ZnAl-LDHs is illustrated in Figure 4.27 (b). The original green blue color of BG was observed over the pH range 4-10 (inset image in Fig. 6b). It was found that the color of BG solution was stable at pH 2.9-11 [102, 103]. The trend of BG removal increases with increasing pH until 7, and adsorbent showed a better adsorption capacity in over the range 5.6-7. At low pH (pH = 2), the adsorption capacity decreased due to the surface of adsorbent would charge positively by protonate H^+, resulting in the electrostatic repulsion between dye molecule and adsorbent [106]. At high pH values, increase in the number of OH^- can be attracted with ZnAl-LDHs via hydrogen bonding leading to reduce the active sites for BG adsorption, thereby resulted decrease of MO removal [98]. BG is a cationic molecule can be easily absorbed on the negative surface charge of rGO and excess hydroxyl groups of ZnAl-LDHs by electrostatic interaction, van der Waal’s force, hydrogen boning, π-π stacking interaction between aromatic part of dye and delocalized π-electron system of graphene [44]. In addition, lone pair of nitrogen atom is a partial negative charge can be attracted with ZnAl-LDHs sheets via Lewis acid-base interaction [136].

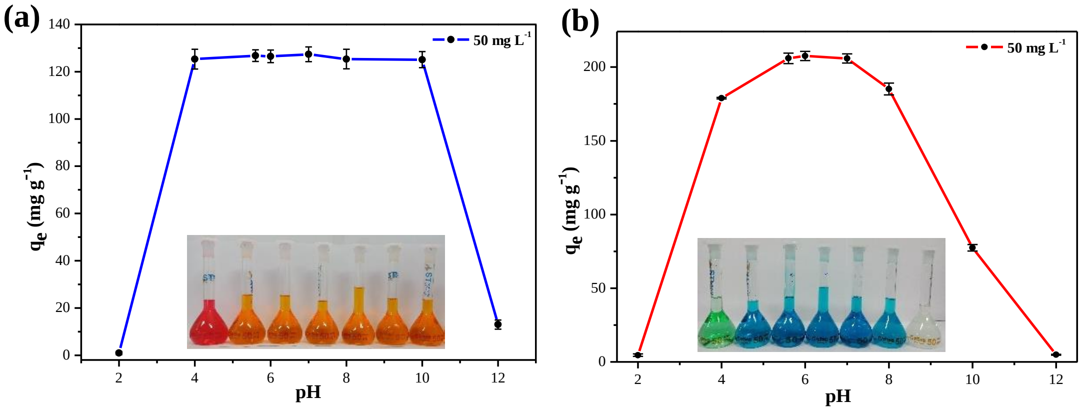

Figure 4.27 **Effect of initial solution pH on MO (a) and BG (b) adsorption onto Fe_3O_4/rGO/ZnAl-LDHs (C_0 = 50 mg L^{-1}, pH of deionized water = 5.6).**

4.4.3 Effect of adsorbent dose

The adsorbent dosage of Fe_3O_4/rGO/ZnAl-LDHs significantly influenced the dye adsorption [57]. To investigate the effect of adsorbent dosage on the adsorption of MO and BG from aqueous solution, adsorbent dosages in range from 0.2-1.2 g L^{-1} of Fe_3O_4/rGO/ZnAl-LDHs were used. As shown in Figure 4.28, it was observed that the adsorption capacity (q_e) and it consistent to the removal efficiency (R; %) of MO and BG at initial concentration of 25 mg L^{-1}. It can be seen that the adsorbent dosage between 0.2-0.6 g L^{-1} lead to the removal efficiency of MO (Figure 4.28 (a)) constant around 67%, then sharply increase until 90% at adsorbent mass 1.0 g L^{-1}. The increase of MO removal is due to more adsorption sites was available to bind MO, and thereby resulted increase of MO adsorption [34, 44]. Besides, the removal efficiency of BG with adsorbent amount as 0.2-1.2 g L^{-1} found that did not differ significantly as shows in Figure 4.28 (b). Nevertheless, the adsorption capacities at equilibrium of MO and BG were decrease from with the increase in the amount of adsorbent. One of the possible reasons is that the decrease of adsorption capacity might be attributed to the competition of the adsorption sites at high adsorbent amount, due to the excess of active sites exceeding the demand of the saturated adsorption [34, 45, 100]. Furthermore, some available sites were unavailable to form complexes with dye molecules, lead the way a large number of effective active sites are not employed, thus resulting to the decreased the adsorption capacity [35, 45, 100]. Therefore, 0.2 g L^{-1} of Fe_3O_4/rGO/ZnAl-LDHs was selected as the optimal adsorbent amount to get the highest adsorption capacity for MO and BG removal.

(a) **(b)**

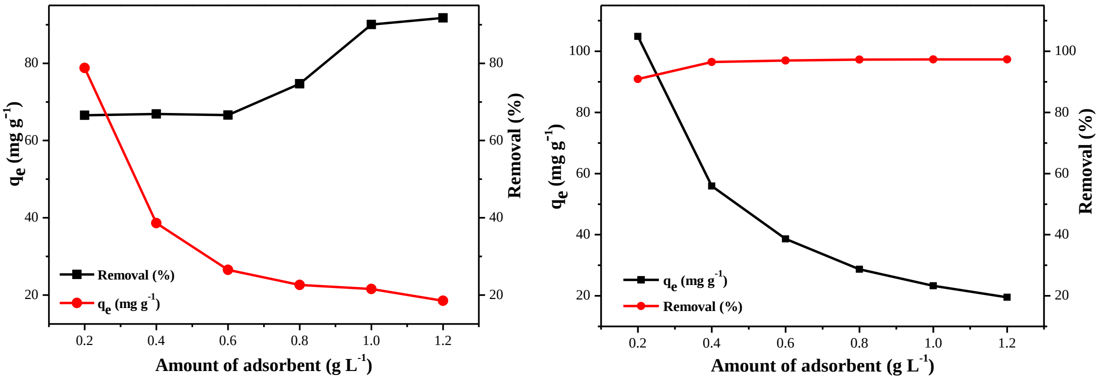

Figure 4.28 Effect of adsorption dosage on the removal of (a) MO and (b) BG by Fe_3O_4/rGO/ZnAl-LDHs (C_0 = 25 mg L^{-1}, pH ≈ 5.6, T = 25 ± 1 °C).

4.4.4 Adsorption kinetics

The adsorption kinetics is important due to it can be describe the adsorption rate and provide valuable data for understanding the mechanism of sorption reactions [99]. The adsorption kinetics of MO and BG on of Fe_3O_4/rGO/ZnAl-LDHs were analyzed by the pseudo-first, pseudo-second kinetic model and Weber-Morris intra-particle mass diffusion model, which are the most common models for the prediction of sorption kinetics [99-102].

The pseudo-first order model suggests a proportional relation for the rate of adsorption, described by the following equations [99-102]:

$$ln(q_e - q_t) = \ln q_e - \left(\frac{k_1}{2.303}\right)t \quad (34)$$

where, q_t (mg g^{-1}) and q_e (mg g^{-1}) represent the amount of MO or BG adsorbed at time t and at equilibrium time, respectively. k_1 (min^{-1}) represents the adsorption rate constant which is calculated from the plot of $\ln(q_e - q_t)$ against t.

The pseudo-second order model suggests a quadratic relation for the rate of adsorption. This model defines the kinetic of adsorption as [99-102]:

$$\frac{t}{q_t} = \frac{1}{k_2 q_e^2} + \frac{t}{q_e} \tag{35}$$

where, k_2 (g (mg•min)$^{-1}$) is the pseudo second-order rate constant of sorption, the q_e and k_2 can be obtained by linear plot of t/qt versus t.

The kinetic parameters of MO and BG adsorption onto Fe_3O_4/rGO/ZnAl-LDHs were conducted at six initial concentrations from 10 to 300 mg g^{-1} and the collection coefficients (r^2) obtained from Figure 4.29 are listed in Table 4.10. It was found that the experimental data could be well fitted with the linear form of the pseudo-second-order model is the much better matching degree ($r^2 > 0.99$) than the pseudo-first order kinetics model and can describe the MO and BG adsorption on Fe_3O_4/rGO/ZnAl-LDHs perfectly. Furthermore, the theoretical adsorption capacities ($q_{e,cal}$) are in good agreement (approximately) with the experimental data ($q_{e,exp}$), implying that the overall rate-limiting step in adsorption process was controlled by chemisorption for both cases *viz* MO and BG [44, 99]. The best fit to that pseudo-second-order model indicated that the adsorption mechanism depended both on the adsorbate and adsorbent [48].

The Weber-Morris intra-particle mass diffusion model describe the process during adsorption internal diffusion determines the adsorption rate in most of the liquid systems. Intra-particle mass diffusion model as the following equation [101-103]:

$$q_t = k_d t^{1/2} + C \tag{36}$$

where k_d is the intra-particle diffusion rate constant (mg g^{-1}·min$^{1/2}$) and C is the intercept which represents the thickness of the boundary layer ((mg g^{-1}). The values of k_{id} and C can be calculated from the slope and the intercept of the linear plot of q_t versus $t^{1/2}$. The value of the intercept C provides information about the thickness of the boundary layer, and the larger the intercept, the greater the boundary layer effect [36, 99]. If the intra-particle diffusion is involved in the adsorption process, the plot of qt versus $t^{1/2}$ will be linear; and if this line passes through the origin, the rate-limiting process is only due to the intra-particle diffusion.

The intra-particle diffusion model has been widely applied to analyze the mechanism of adsorption [99]. The fitting results for both cases *viz* MO and BG are shown in Figure 4.29 (c) and Figure 4.29 (f), respectively. It can be observed that the adsorption process is divided into three sections for both cases *viz* MO and BG. The first stage be ascribed to instantaneous adsorption or external surface adsorption (k_{d1}) due to the high initial concentration of dyes and ample active adsorption sites. The dye molecules diffuse through the solution to the external surface and boundary layer of the Fe_3O_4/rGO/ZnAl-LDHs. The second stage illustrates a gradual adsorption stage (k_{d2}) ascribed to intra-particle diffusion between the dye ions and the adsorbent is related to the rate-determining step, this stage is a controlling step of the whole adsorption. The last stage substitutes the equilibrium stage (k_{d3}), in which intra-particle diffusion further slows down owing to the saturation of active adsorption sites and the decrease in dye concentration [36, 99].

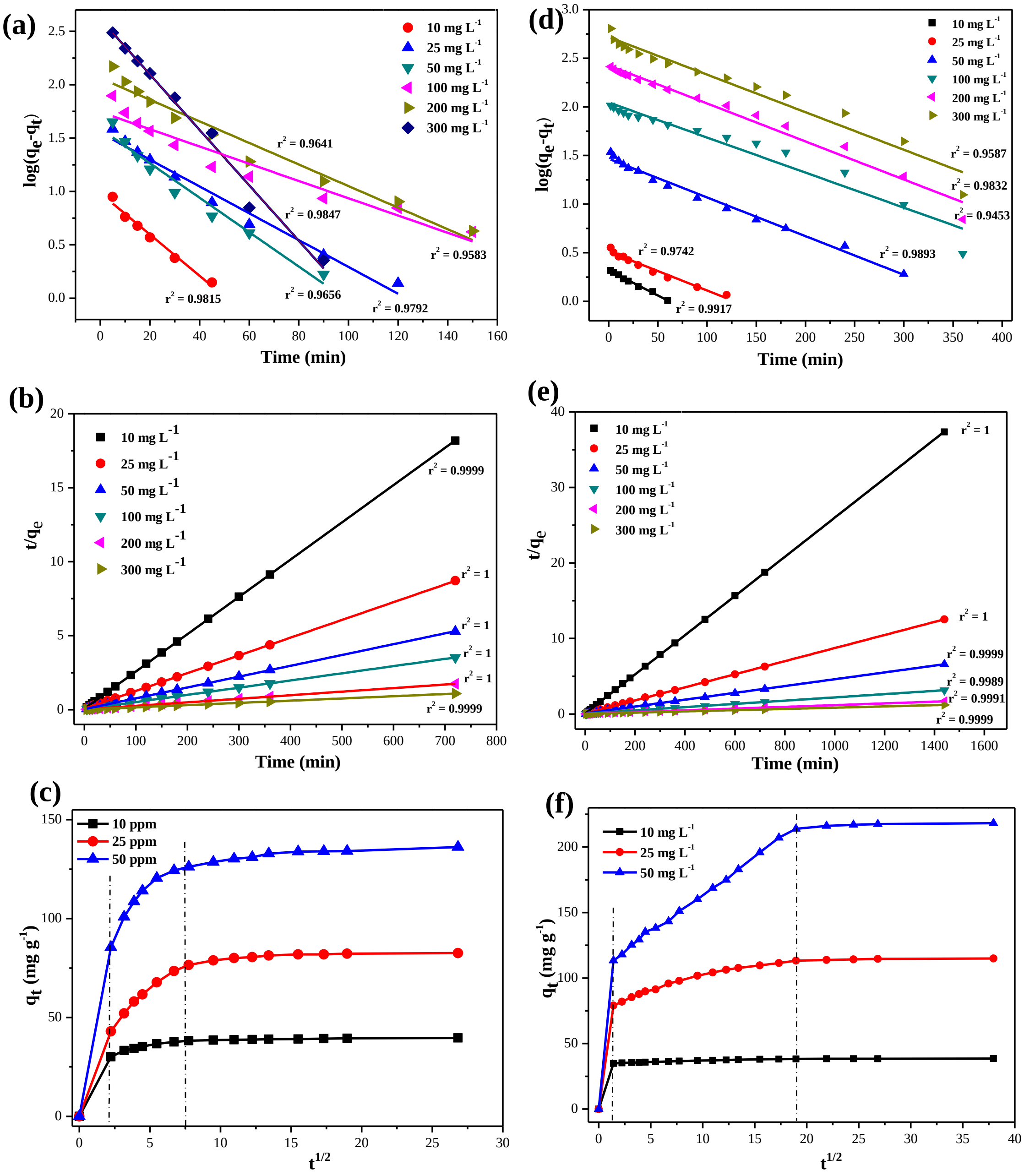

Figure 4.29 Pseudo-first-order model fitting plots for (a) MO and (b) BG adsorption kinetics. Pseudo-second-order model fitting plots for (c) MO and (d) BG adsorption kinetics. Intraparticle diffusion model for (e) MO and (f) BG adsorption at different concentrations.

Table 4.10 Calculated parameters of the pseudo-first and pseudo-second order kinetic models for adsorption of dyes onto Fe_3O_4/rGO/ZnAl-LDHs.

Dyes	Initial concentration (mg g^{-1})	$q_{e,exp}$ (mg g^{-1})	Pseudo-first order kinetic model			Pseudo-second order kinetic model		
			k_1 (min^{-1})	$q_{e,cal}$ (mg g^{-1})	r^2	k_2 (g (mg min)$^{-1}$)	$q_{e,cal}$ (mg g^{-1})	r^2
MO	10	38.26437	0.050896	10.4737	0.9809	0.0658	39.68254	1
	25	76.47947	0.029018	35.40789	0.9792	0.0671	83.33333	1
	50	126.137	0.037078	38.61891	0.9656	0.0349	136.9863	1
	100	187.5289	0.018654	55.51368	0.9583	0.0255	204.0816	1
	200	382.6461	0.02326	115.133	0.9847	0.013	416.6667	1
	300	644.7044	0.059878	412.7623	0.9641	0.0058	666.6667	1
	500	1074.0207	0.062872	606.1778	0.9458	0.0026	1111.111	0.9999
BG	10	38.29327	0.010133	3.324298	0.9761	0.0699	39.0625	1
	25	113.3182	0.009212	29.26847	0.9893	0.0697	114.9425	0.9999
	50	213.924	0.008291	111.0708	0.9453	0.0914	222.2222	0.9989
	100	445.8893	0.009673	279.7049	0.9832	0.0479	454.5455	0.9991
	200	828.6211	0.008982	523.3594	0.9587	0.029	833.3333333	0.999
	300	1150.517	0.029939	558.2131	0.9641	0.0192	1250	0.9992
	500	1994.573	0.376771	1929.301	0.995	0.0132	2000	0.9988

4.4.5 Adsorption isotherms

The adsorption isotherm usually describes the distribution of the adsorbate between the aqueous and solid phase of adsorbent at equilibrium state during the adsorption process. On the basis of the shape of the isotherm, the nature of the studied process can be determined [99]. The adsorption capacity of the adsorbent for the adsorbate can be determined from the equilibrium adsorption isotherm [48].

The Langmuir isotherm is applicable to homogeneous sorption occur on specific homogeneous adsorbent sites where the sorption of each sorbate molecule onto the surface has equal sorption activation energy. Therefore, the Langmuir isotherm assumption that sorption comes from the monolayer coverage of the adsorbate over a homogeneous adsorbent surface [1, 102]. The Langmuir isotherm can be presented in the form [99-106]:

$$q_e = \frac{q_m K_L C_e}{1 + K_L C_e} \tag{37}$$

Linear form of the Langmuir model can be escribed by the following equation [99-106]:

$$\frac{C_e}{q_e} = \frac{1}{q_m K_L} + \frac{C_e}{q_m} \tag{38}$$

where C_e is the equilibrium concentration of dye aqueous solution (mg L^{-1}); q_e is the amount of dye adsorbed by elementary mass of adsorbent (mg g^{-1}); q_m is the maximum adsorption capacity (mg g^{-1}); and K_L is the Langmuir adsorption constant. A plot of C_e/q_e versus C_e gives a straight line with the slope of 1/q_m and the intercept C_e/q_m, as shown in Figure 4.30; the calculated isotherm parameters are shown in Table 4.11.

A dimensionless parameter R_L from the Langmuir model is commonly used to predict the feasibility of the adsorption process. R_L can be represented by Eq. (39):

$$R_L = \frac{1}{1 + K_L C_0} \tag{39}$$

where R_L value indicates the shape and feasibility of isotherm, the isotherm can be unfavourable ($R_L > 1$), linear ($R_L = 1$), favourable ($0 < R_L < 1$) or irreversible ($R_L = 0$) [44, 48, 98]. In this study, values of R_L at different studied temperatures were comprised between 0 and 1; confirm applicability of Langmuir isotherm (Table 4.11).

The Freundlich isotherm is an empirical model based on the assumption that the adsorption process occurs on heterogenous surface of the adsorbent with a non-uniform distribution of heat sorption and means of multilayer adsorption characterized by the heterogeneity factor 1/n. The values of 1/n in the range of 0-1 show favorable adsorption while 1/ n above 1 is an indicative of cooperative adsorption [99]. The Freundlich model is described by [99-106]:

$$q_e = K_F C_e^{1/n} \tag{40}$$

The linear form of the Freundlich isotherm models is represented as follows [99-106]:

$$ln\, q_e = ln\, K_F + \frac{1}{n}\, ln\, C_e \tag{41}$$

where K_F is the Freundlich isotherm constant; q_e and C_e has the same meaning as that in Eq. (41); 1/n is the influence coefficient of solution concentration to the equilibrium adsorbed amount.

The experimental adsorption isotherms of investigated MO and BG dyes on Fe_3O_4/rGO/ZnAl-LDHs, commonly models including Langmuir and Freundlich have been used to analyze the equilibrium adsorption data at ambient temperature of 27 ± 1 °C. The curve-fitting results of the Langmuir model for MO and BG adsorption are shown in Figure 4.30 (a) and Figure 4.30 (b), respectively. It can be seen that the experimental adsorption data of the Fe_3O_4/rGO/ZnAl-LDHs fit well with Langmuir model were collected with the correlation coefficient (r^2) values of 0.9948 and 0.9999 for both cases viz MO and BG, respectively. Freundlich isotherms plots for adsorption of MO and BG onto Fe_3O_4/rGO/ZnAl-LDHs are depicted in Figure 4.31. The parameters as shown in Table 4.11 were obtained. The results indicated that the monolayer Langmuir adsorption isotherm was more suitable for explaining the adsorption process [99-106]. The Langmuir isotherm showed maximum adsorption capacities (q_m) of Fe_3O_4/rGO/ZnAl-LDHs according to the Langmuir fitting result were 294.11 and 312.50 mg g^{-1} for MO and BG, respectively.

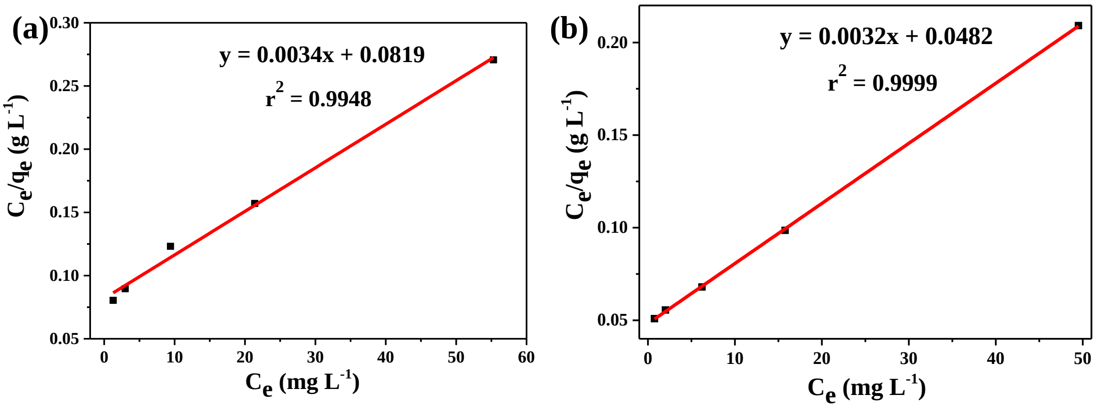

Figure 4.30 Langmuir isotherms model of (a) MO and (b) BG adsorption.

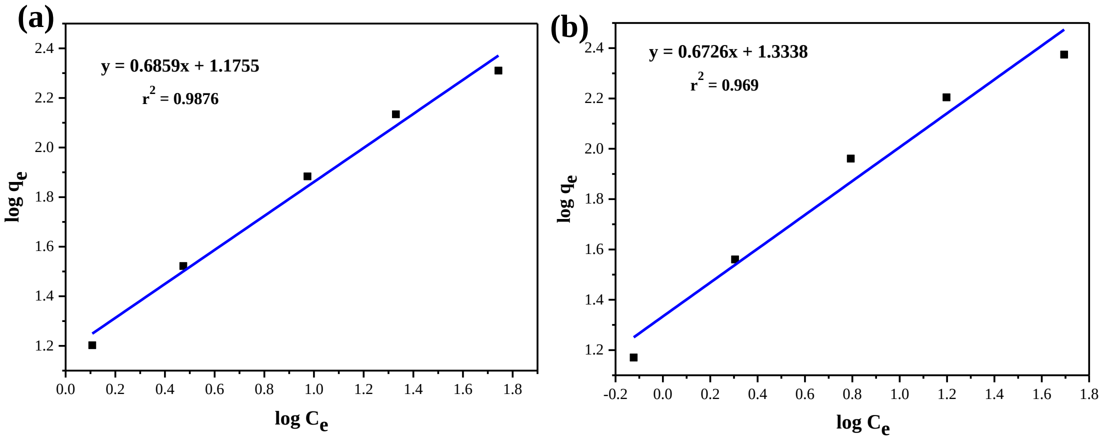

Figure 4.31 Freundlich isotherm model of (a) MO and (b) BG adsorption.

Table 4.11 Langmuir and Freundlich isotherm parameters for MO and BG adsorption onto Fe_3O_4/rGO/ZnAl-LDHs.

Isotherms parameters		MO	BG
Langmuir	q_m (mg g^{-1})	294.11	312.50
	K_L	0.0557	0.0659
	r^2	0.9948	0.9999
	R_L	0.7821-0.1522	0.7521-0.1317
Freundlich	1/n	0.6859	0.5865
	K_F	14.98	27.53
	r^2	0.9876	0.9628

Table 4.12 Comparison of MO adsorption capacity among various adsorbents.

Adsorbent	q_m (mg/g)	Time	Ref.
Chlorine interlayer microsheets ZnAl-LDH	359.71	12 h	[44]
Calcined ZnAl-LDH/Al[OH]$_3$	1015.1	6 h	[45]
Calcined GO/NiAl LDH hybrid	211	16 h	[87]
Graphene oxide/zero-valent	210.8	16 h	[87]
DS-Zn/Al LDHs	114.9	1 h	[142]
Graphene oxide/NiCr-LDH	312.5	24 h	[143]
ZnAl-LDH	1153	6 h	[144]
LDH@Fe_3O_4/PVA magnetic	18.97	5 h	[145]
Starch/NiFe–LDH (2:1)	387.59	3 h	[146]
Starch/NiFe–LDH (1:1)	358.42	3 h	[146]
NiFe-LDH	246.91	1 h	[146]
Fe_3O_4/ZnCr-LDH	240.16	1 h	[147]
CuMgAl-LDH	79.2	3 h	[148]
Fe_3O_4/rGO/ZnAl-LDHs	294.11	1 h	This work

Table 4.13 Comparison of BG adsorption capacity among various adsorbents.

Adsorbent	q_m (mg/g)	Time	Ref.
Modified Saw dust	58.47	3 h	[103]
Red clays	125	4 h	[106]
DS-Zn/Al LDHs	86.95	1 h	[142]
Fe_3O_4@SDBS@MgAl-LDHs	329.1	10 h	[149]
Bagasse fly ash	116.28	5 h	[150]
Kaolin	65.42	90 min	[151]
Saklıkent mud	1.18	150 min	[152]
Acorn	2.11	30 min	[153]
$CoFe_2O_4$	3.58	1 h	[154]
Rice husk ash	26.18	5 h	[155]
Fe_3O_4/rGO/ZnAl-LDHs	312.50	6 h	This work

4.4.6 Adsorption mechanisms

MO and BG dyes adsorption are defined as the accumulation of adsorbent at an interface between the solid surface and the aqueous phases. Various mechanisms for instance electrostatic interaction, hydrogen bond, π–π interaction, and ion exchange may be involved in the whole adsorption process [137, 138]. Mechanism studies of dyes adsorbed by Fe_3O_4/rGO/ZnAl-LDHs have been carried out with either the assistance of the characterization of the structures of the adsorbent before and after adsorption including XRD, FTIR, and SEM. Figure 4.32 shows the XRD pattern onto Fe_3O_4/rGO/ZnAl-LDHs before and after adsorption of MO and BG. The XRD pattern of the synthesized Fe_3O_4/rGO/ZnAl-LDHs before adsorption exhibited characteristic crystalline peaks of the pristine LDHs. It was observed that the intensity of XRD peaks weakened significantly after adsorption for MO and BG onto Fe_3O_4/rGO/ZnAl-LDHs. The post adsorption of MO; XRD pattern of the adsorbent exhibited similar 2-theta values, which indicates that the adsorption of MO dye on Fe_3O_4/rGO/ZnAl-LDHs takes place via surface adsorption [104]. For the BG adsorption onto Fe_3O_4/rGO/ZnAl-LDHs, the features at (003) 2-theta values shifted slightly from 11.81° to 13.27° (7.4845 – 6.6637 nm) compared with the XRD patterns of original adsorbent, which is within the accepted range for a LDHs structure, indicated that the crystal structure of adsorbent was not destroyed in the adsorption process [99]. It was found that the basal spacing at the (003) diffraction peaks for MO adsorption were increased from 7.4845 to 7.6808 Å. The expanse of the interlayer distance indicating that some MO molecules is intercalated into the interlayer of ZnAl LDHs by chemisorption [31, 35, 36, 45].

The FTIR analysis of adsorbents after adsorption of MO and BG as shown in Figure 4.33 (a) and Figure 4.33 (b), respectively. The board vibration bands located at around 3450 cm^{-1} is attributed to the stretching vibrations of O–H of the hydroxyl group on the adsorbent and hydrogen-bonded surface water molecules. The O–H peak of adsorbent after MO and BG adsorption did not change, suggesting that hydrogen bonding did not participate in MO and BG adsorption on Fe_3O_4/rGO/ZnAl-LDHs. Creation of new bands in the case of after adsorption dyes in the region from 550–1600 cm^{-1}, evidences the adsorption of both cases viz MO and BG over the surface of Fe_3O_4/rGO/ZnAl-LDHs. The bands observed at 1605 cm^{-1} could be attributed to the stretching vibration of C=C of the benzene ring of MO and BG. The new bands at 1050, 1152 and 1377 cm^{-1} were attributed to S–O and S=O vibrations of sulfonic acid group ($\mathrm{S}O_3^-$) on MO molecules [36, 44, 45]. After BG adsorption on Fe_3O_4/rGO/ZnAl-LDHs showed vibrations bands region from 1360–1521 cm^{-1} might be ascribed to the N–C groups [98, 100]. Besides, several adsorption peaks that emerged in the range below of 1000 cm^{-1} known as fingerprint region which does not interact with dye appreciably, which assigned to Al–OH deformation mode and Zn/Al–OH translation of adsorbent. Hence, we can conclude that MO and BG are adsorbed to the surface of Fe_3O_4/rGO/ZnAl-LDHs.

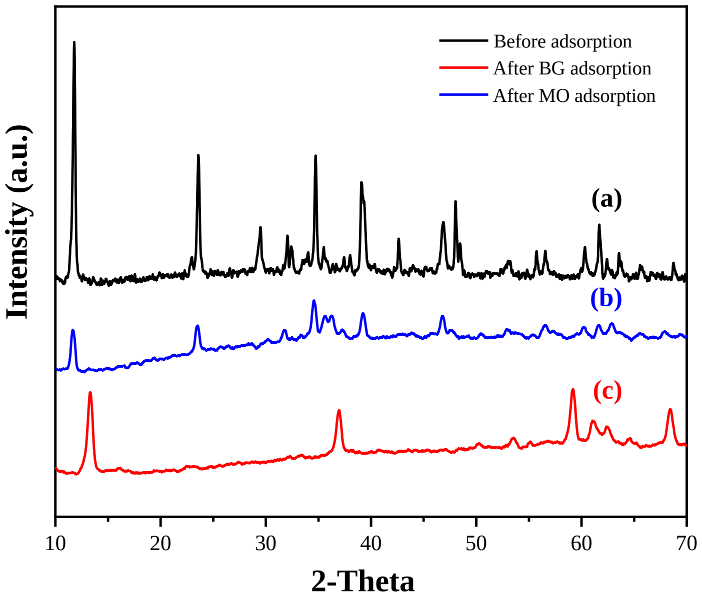

Figure 4.32 XRD patterns for Fe_3O_4/rGO/ZnAl-LDHs of before and after MO and BG adsorption.

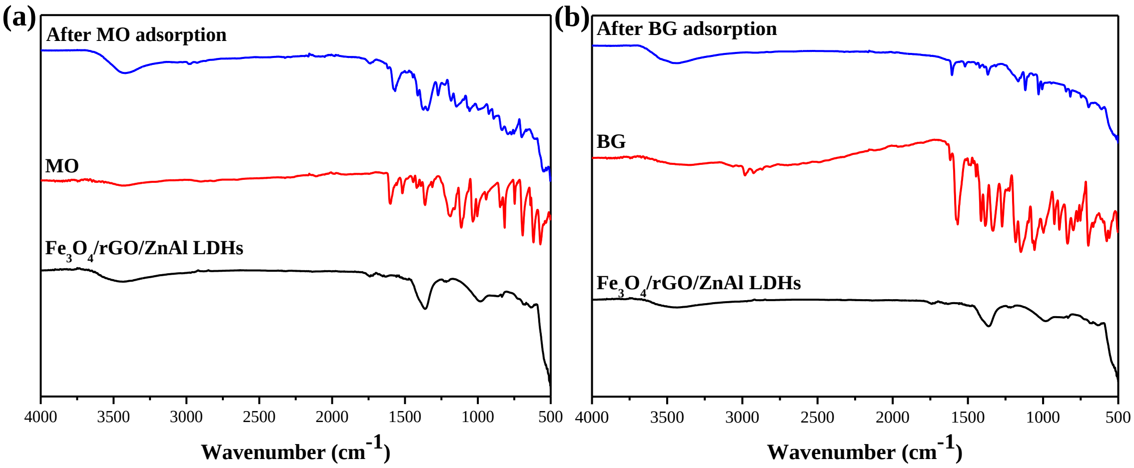

Figure 4.33 FTIR spectra of after adsorption for MO (a) and BG (b).

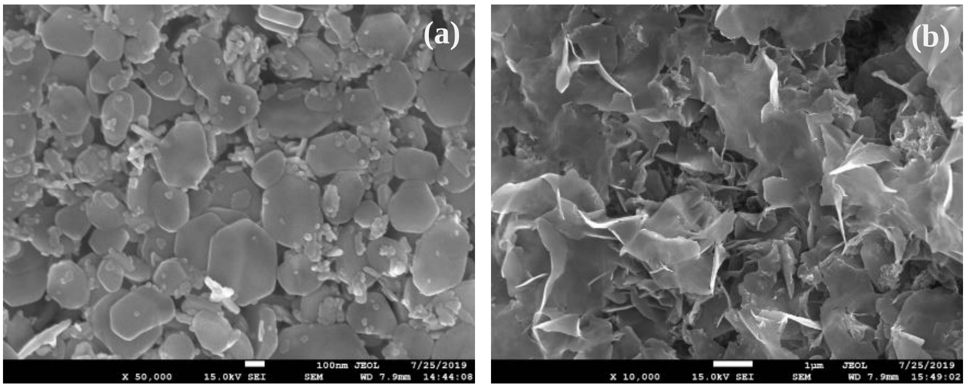

Figure 4.35 SEM image of Fe_3O_4/rGO/ZnAl-LDHs adsorbent before (a) and after (b) adsorption of MO.

Table 4.14 The elemental quantity of Fe_3O_4/rGO/ZnAl-LDHs adsorbent for after adsorption of MO.

Element	Weight %	Weight % Sigma
C	29.42	0.93
N	4.12	0.93
O	21.03	0.58
Na	4.49	0.52
Al	3.05	0.17
S	3.26	0.16
Fe	2.54	0.32
Zn	32.10	0.75
Total:	100.00	

SEM technique is widely used to study the morphological features and surface characteristics of the adsorbent materials. In the present study, SEM images were used to evidence the adsorption of MO and BG around the surface of the Fe_3O_4/rGO/ZnAl-LDHs by comparison with the untreated in dyes solution. Figure 4.34 shows the SEM images of adsorbent material after adsorption of MO. It can be seen that the adsorbent consist of uniform microplates displays smooth surface, after they were in contact with MO solution on the surface of Fe_3O_4/rGO/ZnAl-LDHs exhibit crumpled structure cover on the surface of absorbent.

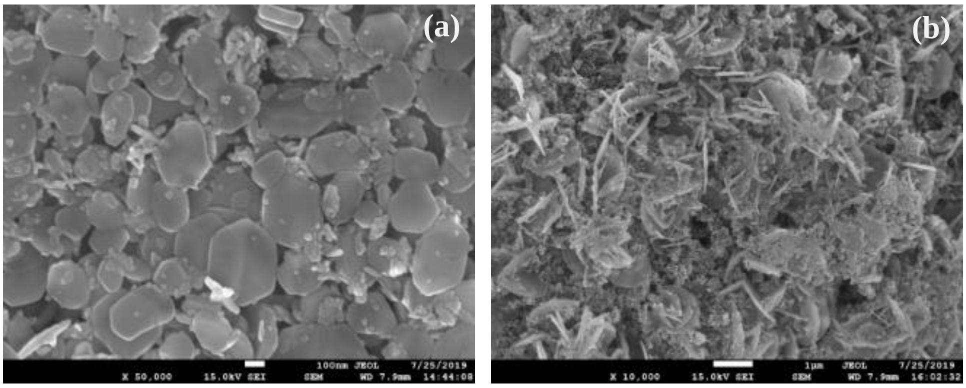

Figure 4.35 SEM image of Fe_3O_4/rGO/ZnAl-LDHs adsorbent before (a) and after (b) adsorption of BG.

Table 4.15 The elemental quantity of Fe_3O_4/rGO/ZnAl-LDHs adsorbent for after adsorption of BG.

Element	Weight %	Weight % Sigma
C	15.65	0.58
N	0.59	0.45
O	27.59	0.41
Na	5.02	0.48
Al	3.64	0.13
S	0.11	0.06
Fe	1.80	0.18
Zn	45.59	0.57
Total:	100.00	

The surface of adsorbent after treatment with BG shows in Figure 4.35. After BG adsorption, the surface of the BG-treated Fe_3O_4/rGO/ZnAl-LDHs was altered as evidenced by its relatively jagged surface. These results confirm that the Fe_3O_4/rGO/ZnAl-LDHs adsorbent could be adsorb MO and BG dye molecule was successfully.

4.4.7 Desorption and Regeneration of Fe_3O_4/rGO/ZnAl-LDHs

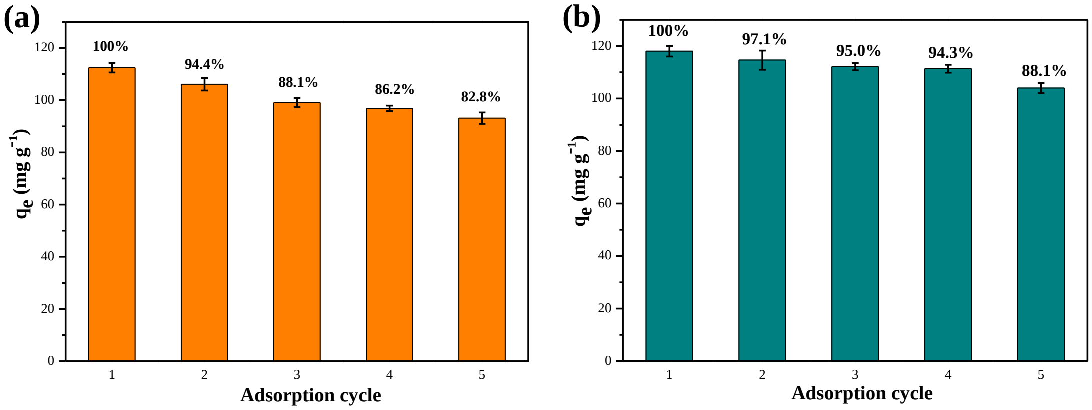

Figure 4.36 After regeneration of Fe_3O_4/rGO/ZnAl-LDHs adsorbent for MO and BG adsorption (three cycles).

Regeneration and reusability of sorbent is an important factor for practical applications and large-scale in industrial field. In order to study the reusability of the Fe_3O_4/rGO/ZnAl-LDHs as an adsorbent were studied through sorption-description cycles according to Section 3.8.5. Adsorption results of MO and BG using the regenerated Fe_3O_4/rGO/ZnAl-LDHs after the recycling are shown in Figure 4.36. It can be found that, after five consecutive cycles, the removal adsorption capacity decreased from 112.4 to 93.1 mg g^{-1} for MO and 118.0 to 104.0 mg g^{-1} for BG, when compared with the original Fe_3O_4/rGO/ZnAl-LDHs. At the same time, the percentage removal efficiency was reduced and remained more than 80 % after five cycles for both cases viz MO and BG. The results showed that there was slight decrease in the percentage removal efficiency after five cycles can be explained to lose some adsorbent during the adsorption-description cycles. These results confirmed that the Fe_3O_4/rGO/ZnAl-LDHs adsorbent can be regenerated easily and has potential to be reused in multiple adsorption cycles.

CHAPTER 5

CONCLUSIONS

Part I: Development of H_2O_2 colorimetric assay based on $Fe^{II}Fe^{III}$ LDHNs

In this work, $Fe^{II}Fe^{III}$ layered double hydroxide nanosheets ($Fe^{II}Fe^{III}$ LDHNS) have been successfully prepared by co-precipitation method. The prepared $Fe^{II}Fe^{III}$ LDHNS possesses the superior intrinsic peroxidase-like activity, which can catalyze the oxidation of TMB and ABTS chromogenic substrates in the presence of H_2O_2 to produce a blue and green colored product of oxidized TMB and $ABTS^{\bullet+}$, respectively. For TMB substrate, the catalytic activity was dependent on the pH, reaction time and H_2O_2 concentration. Whereas the catalytic activity for ABTS only affected by reaction time and H_2O_2 concentration; therefore, as it was not influenced by pH, the reaction can be carried out in water medium. The peroxidase-like catalytic activity originates from the $Fe^{II}Fe^{III}$ LDHNS not the leached Fe^{2+}. The kinetics analysis indicated that the process is in accordance with the typical Michaelis-Menten kinetics and the $Fe^{II}Fe^{III}$ LDHNS exhibited high affinity towards TMB, ABTS and H_2O_2 substrate. On the basis of these findings, a colorimetric method with high sensitivity and selectivity for H_2O_2 detection has been developed. The colorimetric method showed good response towards H_2O_2 detection with a linear range from 0.1-50 µM (LOD of 0.05 µM) for TMB, and 0.5-20 µM (LOD of 0.2 µM) for ABTS. This selective approach could be applied for H_2O_2 detection in real milk and disinfectant samples. $Fe^{II}Fe^{III}$ LDHNS as peroxidase mimics exhibited several advantages when compared to natural enzyme for instant; ease of preparation, low-cost, robustness, long-term stability and good biocompatibility. The proposed method is expected to be more potential for exact detection of H_2O_2 in biotechnology, food industry, clinical diagnosis life process and other industries.

Part II: Synthesis of Fe_3O_4/rGO/ZnAl for the removal of methyl orange and brilliant green from aqueous solution

In summary, a novel of magnetic adsorbent consisting of magnetite nanoparticles (Fe_3O_4 NPs), reduced graphene oxide (rGO), and ZnAl layered double hydroxides (ZnAl-LDHs), denoted as Fe_3O_4/rGO/ZnAl-LDHs have been successfully prepared. The magnetic adsorbent was employed as adsorbents for the qualitative removal of anionic methyl orange (MO) and cationic brilliant green (BG) from aqueous solution. Therefore, this simple modification of ZnAl-LDHs was modified by using Fe_3O_4-decorated rGO has been proposed for the improvement the magnetic properties and adsorption capacity of magnetic adsorbent. This magnetic adsorbent can easily be separated and regenerated from aqueous solutions by using external magnet. As a word, this work provides some new scientific in rational design of desirable bifunctional adsorbent for anionic and cationic dyes. Adsorption capacity of dyes much depend on pH of solutions and the best results are obtained at the pH range from 4-10 and 6-7 for MO and BG, respectively. The experimental data fitted for MO and BG dyes well to the pseudo-second order kinetic model, indicating the chemisorption process. The Langmuir isotherm provided the best correlation of both organic dyes on the Fe_3O_4/rGO/ZnAl-LDHs, implying the adsorption is mainly a monolayer adsorption process. Adsorption capacity calculated according to the Langmuir isotherm were 1111.11 and 2000.00 mg g^{-1} at initial concentration of 1000 mg L^{-1} for MO and BG, respectively. The mechanism of adsorption proposed according to the XRD and FTIR data, are consistent with an anion exchange process into the interlayer of ZnAl LDHs and adsorbed to the surface of Fe_3O_4/rGO/ZnAl-LDHs. The reusability of the Fe_3O_4/rGO/ZnAl-LDHs as an adsorbent were studied through sorption-description cycles by using ethanol and NaOH, respectively. The percentage removal efficiency was reduced and remained more than 80 % after five cycles for both cases viz MO and BG. In common, we can be concluded that the magnetic adsorbent studied here could be successfully applied in the cleaning of the wastewaters of the dyeind industry.

REFERRENCES

REFERRENCES

[1] Mahjoubi, F.Z. and et al. "Zn–Al layered double hydroxides intercalated with carbonate, nitrate, chloride and sulphate ions: Synthesis, characterization and dye removal properties", **Journal of Taibah University for Science.** 2017(11): 90-100; January, 2017.

[2] Liu, J. and et al. "Synthesis and thermal properties of ZnAl layered double hydroxide by urea hydrolysis", **Powder Technology.** 2014(253): 41-45; February 2014.

[3] Liu, Z. and et al. "Synthesis, anion exchange, and delamination of Co-Al layered double hydroxide: assembly of the exfoliated nanosheet/polyanion composite films and magneto-optical studies", **Journal of the American Chemical Society.** 128(14): 4872-80; March, 2006.

[4] Iyi, N. and et al. "A Novel Synthetic Route to Layered Double Hydroxides Using Hexamethylenetetramine", **Chemistry Letters.** 2004(33): 1122-1123; September, 2004.

[5] Iyi, N. and et al. "Deintercalation of Carbonate Ions from a Hydrotalcite-Like Compound: Enhanced Decarbonation Using Acid−Salt Mixed Solution", **Chemistry of Materials.** 16(15): 2926-2932; June, 2004.

[6] Fu, G. and et al. "Cost-effective and sensitive colorimetric immunosensing using an iron oxide-to-Prussian blue nanoparticle conversion strategy", **The Analyst.** 141(12): 3883-3889; May, 2016.

[7] Liu, H., et al., "Colorimetric and ultrasensitive detection of H_2O_2 based on Au/Co_3O_4-CeO_x nanocomposites with enhanced peroxidase-like performance", **Sensors and Actuators B: Chemical.** 2018(271): 336-345; October, 2018.

[8] Liu, Q. and et al. "Higher catalytic activity of porphyrin functionalized Co_3O_4 nanostructures and colorimetric detection of H_2O_2 and glucose", **Materials Science and Engineering: C.** 2014(43): 321-329; October, 2014.

[9] Martin, N. and et al. "Peroxide Test Strips Detect Added Hydrogen Peroxide in Raw Milk at Levels Affecting Bacterial Load", **Journal of food protection.** 2014(77): 1809-1813; October, 2014.

REFERRENCES (CONTINUED)

[10] Amin, V.M. and Olson N.F. “Spectrophotometric Determination of Hydrogen Peroxide in Milk1”, **Journal of Dairy Science.** 50(4): 461-464; April, 1967.

[11] Arefin, S. and et al. “Use of Hydrogen Peroxide (H_2O_2) in raw cow's milk preservation”, **Journal of Advanced Veterinary and Animal Research.** 2017(4): 371-377; December, 2017.

[12] Touyz, R.M. and Schiffrin E.L. “Reactive oxygen species in vascular biology: implications in hypertension”, **Histochem Cell Biol.** 122(4): 339-352; August, 2004.

[13] Cai, H. “Hydrogen peroxide regulation of endothelial function: origins, mechanisms, and consequences”, **Cardiovascular Research.** 68(1): 26-36; October, 2005.

[14] Reuter, S. and et al. “Oxidative stress, inflammation, and cancer: how are they linked?”, **Free Radical Biology and Medicine.** 49(11): 1603-1616; December, 2010.

[15] Wen, F. and et al. “Horseradish Peroxidase Functionalized Fluorescent Gold Nanoclusters for Hydrogen Peroxide Sensing”, **Analytical Chemistry.** 83(4): 1193-1196; January, 2011.

[16] Kim, J.-H. and et al. “Single-Molecule Detection of H_2O_2 Mediating Angiogenic Redox Signaling on Fluorescent Single-Walled Carbon Nanotube Array”, **ACS Nano.** 5(10): 7848-7857; September, 2011.

[17] Yue, H. and et al. “Quantitative determination of trace levels of hydrogen peroxide in crospovidone and a pharmaceutical product using high performance liquid chromatography with coulometric detection”, **International Journal of Pharmaceutics.** 375(1-2): 33-40; April, 2009.

[18] Lim, C.-K. and et al. “Chemiluminescence-Generating Nanoreactor Formulation for Near-Infrared Imaging of Hydrogen Peroxide and Glucose Level in vivo”, **Advanced Functional Materials.** 2010(20): 2644-2648; August, 2010.

REFERRENCES (CONTINUED)

[19] Tahirović, A. and et al. “A chemiluminescence sensor for the determination of hydrogen peroxide”, **Talanta.** 72(4): 1378-1385; June, 2007.

[20] Shu, Y., et al. “Cube-like $CoSn(OH)_6$ nanostructure for sensitive electrochemical detection of H_2O_2 in human serum sample”, **Sensors and Actuators B: Chemical.** 2017(241): 528-533; March, 2017.

[21] Shu, Y. and et al. “Ni and NiO Nanoparticles Decorated Metal–Organic Framework Nanosheets: Facile Synthesis and High-Performance Nonenzymatic Glucose Detection in Human Serum”, **ACS Applied Materials & Interfaces.** 9(27): 22342-22349; June, 2017.

[22] Sun, L. and et al. “Montmorillonite-loaded ceria nanocomposites with superior peroxidase-like activity for rapid colorimetric detection of H_2O_2”, **Sensors and Actuators B: Chemical.** 2017(239): 848-856; February, 2017.

[23] Bhave, C. “A review on the synthesis and applications of green rust for environmental pollutant remediation”, **International journal of environmental science and technology.** 15(6): 1243-1248; August, 2017.

[24] Gao, L. and et al. “Intrinsic peroxidase-like activity of ferromagnetic nanoparticles”, **Nature Nanotechnology.** 2(9): 577-853; September, 2007.

[25] Xie, J. and et al. “Analytical and environmental applications of nanoparticles as enzyme mimetics”, **TrAC Trends in Analytical Chemistry.** 2012(39): 114-129; October, 2012.

[26] Wei H. and Wang E. “Fe_3O_4 Magnetic Nanoparticles as Peroxidase Mimetics and Their Applications in H_2O_2 and Glucose Detection”, **Analytical Chemistry.** 80(6): 2250-2254; February, 2008.

[27] Zhang, W., Ma D. and Du, J. “Prussian blue nanoparticles as peroxidase mimetics for sensitive colorimetric detection of hydrogen peroxide and glucose”, **Talanta.** 2014(120): 362-367; March, 2014.

[28] Liu, Q. and et al. “Glucose-sensitive colorimetric sensor based on peroxidase mimics activity of porphyrin-Fe_3O_4 nanocomposites”, **Materials Science and Engineering: C.** 2014(41): 142-151; August, 2014.

REFERRENCES (CONTINUED)

[29] Zhu, Y. and et al. “Synthesis of hierarchical Co_3O_4@NiO core-shell nanotubes with a synergistic catalytic activity for peroxidase mimicking and colorimetric detection of dopamine”, **Talanta.** 2018(181): 431-439; May, 2018.

[30] Hai, B. and Zou, Y. “Carbon cloth supported NiAl-layered double hydroxides for flexible application and highly sensitive electrochemical sensors”, **Sensors and Actuators B: Chemical.** 2015(208): 143-150; March, 2015.

[31] Zhang, Y. and et al. “Novel application of CoFe layered double hydroxide nanoplates for colorimetric detection of H_2O_2 and glucose”, **The Analyst.** 2012(137): 1325-1328; January, 2012.

[32] Su, L. and et al. “One-step analysis of glucose and acetylcholine in water based on the intrinsic peroxidase-like activity of Ni/Co LDHs microspheres”, **Journal of Materials Chemistry B.** 5(1): 116-122; January, 2016.

[33] Géhin, A. and et al. “Synthesis of Fe(II-III) hydroxysulphate green rust by coprecipitation”, **Solid State Sciences.** 4(1): 61-66; January, 2002.

[34] Zheng, Y.-M. “Preparation of nanostructured microspheres of Zn–Mg–Al layered double hydroxides with high adsorption property”, **Colloids and Surfaces A: Physicochemical and Engineering Aspects.** 2012(415): 195-201; December, 2012.

[35] Zhang, P. and et al. “Enhanced removal of ionic dyes by hierarchical organic three-dimensional layered double hydroxide prepared via soft-template synthesis with mechanism study”, **Chemical Engineering Journal.** 2019(360): 1137-1149; March, 2019.

[36] Guan, T. “A facile approach to synthesize 3D flower-like hierarchical NiCo layered double hydroxide microspheres and their enhanced adsorption capability A Physicochemical and engineering aspects”, **Colloids and Surfaces A: Physicochemical and Engineering Aspects.** 2017(529): 907-915; September, 2017.

REFERRENCES (CONTINUED)

[37] dos Santos, A.B., F.J. Cervantes and van Lier, J.B. “Review paper on current technologies for decolourisation of textile wastewaters: Perspectives for anaerobic biotechnology”, **Bioresource Technology.** 98(12): 2369-2385; September ,2007.

[38] Eftekhari, S., Habibi-Yangjeh A. and Sohrabnezhad, S. “Application of AlMCM-41 for competitive adsorption of methylene blue and rhodamine B: Thermodynamic and kinetic studies”, **Journal of Hazardous Materials.** 178(1): 349-355; June, 2010.

[39] Wu, J., Eiteman Mark, A. and Law, S.E. “Evaluation of Membrane Filtration and Ozonation Processes for Treatment of Reactive-Dye Wastewater”, **Journal of Environmental Engineering.** 124(3): 272-277; March, 1998.

[40] Sureshkumar, M.V. and Namasivayam, C. “Adsorption behavior of Direct Red 12B and Rhodamine B from water onto surfactant-modified coconut coir pith”, **Colloids and Surfaces A: Physicochemical and Engineering Aspects.** 317(1): 277-283; March 2008.

[41] Banković, P. and et al. “Al, Fe-pillared clays in catalytic decolorization of aqueous tartrazine solutions”, **Applied Clay Science.** 2012(58): 73-78; April, 2012.

[42] Aarthi, T., Narahari, P. and Madras, G. “Photocatalytic degradation of Azure and Sudan dyes using nano TiO_2”, **Journal of Hazardous Materials.** 149(3): 725-734; November, 2019.

[43] Ravikumar, K. and et al. “Optimization of process variables by the application of response surface methodology for dye removal using a novel adsorbent”, **Dyes and Pigments.** 72(1): 66-74; December, 2007.

[44] Kumar, N. and et al. “Controlled synthesis of microsheets of ZnAl layered double hydroxides hexagonal nanoplates for efficient removal of Cr(VI) ions and anionic dye from water”, **Journal of Environmental Chemical Engineering.** 5(2): 1718-1731; April, 2017.

REFERRENCES (CONTINUED)

[45] Guo, X., Yin, P. and Yang, H. “Superb adsorption of organic dyes from aqueous solution on hierarchically porous composites constructed by ZnAl-LDH/Al(OH)$_3$ nanosheets. **Microporous and Mesoporous Materials.** 2017(259): 123-133; March, 2018.

[46] Shao, M. and et al. “Hierarchical Structures Based on Functionalized Magnetic Cores and Layered Double-Hydroxide Shells: Concept, Controlled Synthesis, and Applications”, **Chemistry - A European Journal.** 19(13): 4100-4108; 19 February, 2013.

[47] Starukh, H. and Levytska, S. “The simultaneous anionic and cationic dyes removal with ZnAl layered double hydroxides”, **Applied Clay Science.** 2019(180): 105183- 105192; November, 2019.

[48] Lu, L. and et al. “Synthesis of novel hierarchically porous Fe$_3$O$_4$@MgAl–LDH magnetic microspheres and its superb adsorption properties of dye from water”, **Journal of Industrial and Engineering Chemistry.** 2017(46): 315-323; February, 2017.

[49] Gong, J.-L. and et al. “Removal of cationic dyes from aqueous solution using magnetic multi-wall carbon nanotube nanocomposite as adsorbent”, **Journal of Hazardous Materials.** 164(2): 1517-1522; May 2009.

[50] Solvay Interox, Inc. “Chances are, some of the foods and beverages you had today were treated with hydrogen peroxide (H_2O_2). If you had margarine, cheese, instant tea, wine or aseptically packaged milk or juice, odds are that hydrogen peroxide improved the product”, **Food Processing.** 2000: 1-8.

[51] Teo, P.S. and et al. “Room temperature in situ chemical synthesis of Fe$_3$O$_4$/graphene”, **Ceramics International.** 38(8): 6411-6416; December, 2012.

[52] Vikesland, P.J. and et al. “Aggregation and sedimentation of magnetite nanoparticle clusters”, **Environmental Science: Nano.** 2016(3): 567-577; March, 2016.

REFERRENCES (CONTINUED)

[53] Zhang, B. and et al. "Fabrication of Magnetite-Graphene Oxide/MgAl-Layered Double Hydroxide Composites for Efficient Removal of Emulsified Oils from Various Oil-in-Water Emulsions", **Journal of Chemical & Engineering Data.** 63(12): 4689-4702; October, 2018.

[54] Stoller, M.D. and et al. "Graphene-based ultracapacitors", **Nano Letters.** 8(10): 3498-3502; September, 2008.

[55] Mishra, A.K. and Ramaprabhu, S. "Removal of metals from aqueous solution and sea water by functionalized graphite nanoplatelets based electrodes", **Journal of Hazardous Materials.** 185(1): 322-328; January, 2011.

[56] Wen, T. and et al. "One-Pot Synthesis of Water-Swellable Mg–Al Layered Double Hydroxides and Graphene Oxide Nanocomposites for Efficient Removal of As(V) from Aqueous Solutions", **ACS Applied Materials & Interfaces.** 5(8): 3304-3311; March, 2013.

[57] Zhang, F. and et al. "Synthesis of Magnetite–Graphene Oxide-Layered Double Hydroxide Composites and Applications for the Removal of Pb(II) and 2,4-Dichlorophenoxyacetic Acid from Aqueous Solutions", **ACS Applied Materials & Interfaces.** 7(13): 7251-7263; March, 2015.

[58] Xue, Y. and et al. "Oxidizing metal ions with graphene oxide: The in situ formation of magnetic nanoparticles on self-reduced graphene sheets for multifunctional applications", **Chemical communications.** 2011(47): 11689-11691; September, 2011.

[59] He J. and et al. "Preparation of Layered Double Hydroxides", In **Structure and Bonding.** Duan X. and Evans D.G. Editors. p 89-119. Berlin: Springer-Verlag Berlin Heidelberg, 2005.

[60] Goh, K.-H., Lim, T.-T. and Dong, Z. "Application of layered double hydroxides for removal of oxyanions: A review", **Water Research.** 42(6): 1343-1368; March, 2008.

REFERRENCES (CONTINUED)

[61] Wang, Q. and O'Hare, D. "Recent Advances in the Synthesis and Application of Layered Double Hydroxide (LDH) Nanosheets", **Chemical Reviews.** 112(7): 4124-4155; March, 2012.

[62] Feng L. and Xue D. "Applications of Layered Double Hydroxides", Part of the Structure and Bonding book series, **Springer, Berlin, Heidelberg.** 2005(119): 193-223; September, 2005.

[63] Jin, W. "Recent Advances in the Synthesis of Layered, Double- Hydroxide-Based Materials and Their Applications in Hydrogen and Oxygen Evolution", **Energy Technology.** 4(3): 354-368; March, 2016.

[64] Rives, V. "Characterisation of layered double hydroxides and their decomposition products", **Materials Chemistry and Physics.** 2002(75):19-25; April, 2002.

[65] Erickson, K.L., Bostrom, T.E. and Frost, R.L. "A study of structural memory effects in synthetic hydrotalcites using environmental SEM", **Materials Letters.** 59(2): 226-229; February 2005.

[66] Cavani, F., Trifirò, F. and Vaccari, A. "Hydrotalcite-type anionic clays: Preparation, properties and applications", **Catalysis Today.** 11(2): 173-301; December, 1991.

[67] Jiang, X., Evans, D. and Duan, X. "Structure and Basicity of Mesoporous Materials from Mg/Al/In Layered Double Hydroxides Prepared by Separate Nucleation and Aging Steps Method", **Journal of Porous Materials.** 2005(12): 55-63; January, 2005.

[68] Evans, D. and Duan, X. "Preparation of Layered Double Hydroxides and Their Applications as Additives in Polymers, as Precursors to Magnetic Materials and in Biology and Medicine", **Chemical communications.** 2006(37): 485-96; November, 2005.

[69] Benício, L.P. and et al. "Layered double hydroxides: Nanomaterials for applications in agriculture", **Revista Brasileira de Ciência do Solo.** 2015(39): 1-13; February, 2015.

REFERRENCES (CONTINUED)

[70] Yun, S.K. and Pinnavaia, T.J. “Water Content and Particle Texture of Synthetic Hydrotalcite-like Layered Double Hydroxides”, **Chemistry of Materials.** 7(2): 348-354; February, 1995.

[71] Vaccari, A. “Layered double hydroxides: present and future”, In **Applied Clay Science.** V. Rives Editors. p. 75-76. New York: Nova Science Publishers, Inc., 2002.

[72] Costa, F.R. and et al. “Morphology and fracture behaviour of polyethylene/Mg–Al layered double hydroxide (LDH) nanocomposites”, **European Polymer Journal.** 42(9): 2140-2152; September, 2006.

[73] Wang, X. and et al. “CO_2 Induced Synthesis of Zn-Al Layered Double Hydroxide Nanostructures towards Efficiently Reducing Fire Hazards of Polymeric Materials”, **Nano Advances.** 2018(3): 12-17; March ,2018.

[74] Miyata, S. “Anion-Exchange Properties of Hydrotalcite-Like Compounds” **Clays and Clay Minerals.** 31(4): 305-311; August, 1983.

[75] Rahmanian, O., Maleki, M.H. and Dinari, M. “Ultrasonically assisted solvothermal synthesis of novel Ni/Al layered double hydroxide for capturing of Cd(II) from contaminated water”, **Journal of Physics and Chemistry of Solids.** 2017(110): 195-201; November, 2017.

[76] Taviot-Gueho, C. and et al. “Tailoring Hybrid Layered Double Hydroxides for the Development of Innovative Applications”, **Advanced Functional Materials.** 2017(28): 1703868-1703874; November 2017.

[77] Chen, L. and et al. “2D ultrathin nanosheets of Co–Al layered double hydroxides prepared in L-asparagine solution: enhanced peroxidase-like activity and colorimetric detection of glucose”, **Journal of Materials Chemistry B.** 2013(1): 2268-2274; Mar, 2013.

[78] Chen, L. and et al. “DNA-enhanced peroxidase-like activity of layered double hydroxide nanosheets and applications in H_2O_2 and glucose sensing”, **Nanoscale.** 2013(5): 10982-10988; August, 2013.

REFERRENCES (CONTINUED)

[79] Guo, Y. and et al. “Carbon Dots/NiAl-layered double hydroxide hybrid material: facile synthesis, intrinsic peroxidase-like catalytic activity and its application”, **RSC Advances.** 2015(5): 95495-95503; October, 2015.

[80] Zhan, T. and et al. “NiFe layered double hydroxide nanosheets as an efficiently mimic enzyme for colorimetric determination of glucose and H_2O_2”, **Sensors and Actuators B: Chemical.** 2017(255): 2635-2642; February, 2018.

[81] Chen, C. and et al. “Layered double hydroxide derived ultrathin 2D Ni-V mixed metal oxide as a robust peroxidase mimic”, **Chemical Engineering Journal.** 2019(369): 161-169; August, 2019.

[82] Li, H. and et al. “A Novel Heterostructure of MXene@NiFe-LDH Nanohybrid with Superior Peroxidase-like Activity for Sensitive Colorimetric Detection of Glutathione”, **ACS Sustainable Chemistry & Engineering.** 2019(8): 520-526; December, 2019.

[83] Ponlakhet, K. and et al. “Development of sensitive and selective glucose colorimetric assay using glucose oxidase immobilized on magnetite-gold-folate nanoparticles”, **Analytical Methods.** 2016(8): 8288-8298; November, 2016.

[84] Gong, J. and et al. “Efficient Removal of Heavy Metal Ions from Aqueous Systems with the Assembly of Anisotropic Layered Double Hydroxide Nanocrystals@Carbon Nanosphere”, **Environmental science & technology.** 2011(45): 6181-6187; June, 2011.

[85] Wu, X.-L. and et al. “Water-dispersible magnetite-graphene-LDH composites for efficient arsenate removal”, **Journal of Materials Chemistry.** 2011(21): 17353-17359; September, 2011.

[86] Zhang, M. and et al. “Phosphate removal ability of biochar/MgAl-LDH ultra-fine composites prepared by liquid-phase deposition, **Chemosphere.** 92(8): 1042-1047; August, 2013.

REFERRENCES (CONTINUED)

[87] Yang, Z. and et al. “Magnetic nanomaterial derived from graphene oxide/layered double hydroxide hybrid for efficient removal of methyl orange from aqueous solution”, **Journal of Colloid and Interface Science.** 2013(408): 25-32; October, 2013.

[88] Li, S.-S. and et al. “Competitive adsorption behavior toward metal ions on nano-Fe/Mg/Ni ternary layered double hydroxide proved by XPS: Evidence of selective and sensitive detection of Pb(II)”, **Journal of Hazardous Materials.** 2017(338): 1-10; September, 2017.

[89] Peng, F.F. Zhang, Y. and Gu, N. “Size-dependent peroxidase-like catalytic activity of Fe3O4 nanoparticles”, **Chinese Chemical Letters.** 19(6): 730-733; June, 2008.

[90] Ruby, C. and et al. “Coprecipitation of Fe(II) and Fe(III) cations in sulphated aqueous medium and formation of hydroxysulphate green rust”, **Solid State Sciences.** 5(7): 1055-1062; July, 2003.

[91] Roohi, H. and Rajabi, M. “Iodometric Determination of Hydroperoxides in Hydrocarbon Autoxidation Reactions Using Triphenylphosphine Solution as a Titrant: A New Protocol”, **Industrial & Engineering Chemistry Research.** 57(20): 6805-6814; May, 2018.

[92] Graves Lab. “Peroxide Quantification via Iodometric Titration”, **Department of Chemical and Biomolecular Engineering.** http://www.graveslab.org/lab-resources/procedures/peroxide-quantification-via-iodometric-titration. June, 2020

[93] Xu, Y. and et al. “Chemically Converted Graphene Induced Molecular Flattening of 5,10,15,20-Tetrakis(1-methyl-4-pyridinio)porphyrin and Its Application for Optical Detection of Cadmium(II) Ions”, **Journal of the American Chemical Society.** 131(37): 13490-13497; August, 2009.

[94] Hummers, W.S. and Offeman, R.E. “Preparation of Graphitic Oxide”, **Journal of the American Chemical Society.** 80(6): 1339-1339; March, 1958.

[95] Alazmi, A. and et al. “Comparative study of synthesis and reduction methods for graphene oxide”, **Polyhedron.** 2016(116): 153-161; September, 2016.

REFERRENCES (CONTINUED)

[96] Lv, F. and et al. “Structure and magnetic properties of soft organic ZnAl-LDH/polyimide electromagnetic shielding composites”, **Journal of Materials Science.** 2012(47): 2033-2039; October, 2011.

[97] Wang, J. and et al. “Synthesis, sustained release properties of magnetically functionalized organic–inorganic materials: Amoxicillin anions intercalated magnetic layered double hydroxides via calcined precursors at room temperature”, **Solid State Sciences.** 11(9): 1597-1601; September 2009.

[98] Rehman, R., Mahmud, T. and Irum, M. “Brilliant Green Dye Elimination from Water Using Psidium guajava Leaves and Solanum tuberosum Peels as Adsorbents in Environmentally Benign Way”, **Journal of Chemistry.** 2015(2015): 126036; January, 2015.

[99] Lu, Y. and et al. “High performance NiFe layered double hydroxide for methyl orange dye and Cr(VI) adsorption”, **Chemosphere.** 2016(152): 415-422; June, 2016.

[100] Salleh, M.A.M. and et al. “Cationic and anionic dye adsorption by agricultural solid wastes: A comprehensive review”, **Desalination.** 280(1): 1-13; October, 2011.

[101] Guan, T. and et al. “A facile approach to synthesize 3D flower-like hierarchical NiCo layered double hydroxide microspheres and their enhanced adsorption capability”, **Colloids and Surfaces A: Physicochemical and Engineering Aspects.** 2017(529): 907-915; September, 2017.

[102] Mane, V.S., Deo Mall, I. and Chandra Srivastava, V. “Kinetic and equilibrium isotherm studies for the adsorptive removal of Brilliant Green dye from aqueous solution by rice husk ash”, **Journal of Environmental Management.** 84(4): 390-400; October, 2007.

[103] Mane, V.S. and Babu, P.V.V. “Studies on the adsorption of Brilliant Green dye from aqueous solution onto low-cost NaOH treated saw dust”, **Desalination.** 273(2): 321-329; June ,2011.

REFERRENCES (CONTINUED)

[104] Chilukoti, S. and Thangavel, T. “Enhanced adsorption of Congo red on microwave synthesized layered Zn-Al double hydroxides and its adsorption behaviour using mixture of dyes from aqueous solution”, **Inorganic Chemistry Communications.** 2019(100): 107-117; February, 2019.

[105] Huang, M., Mishra, S.B. and Liu, S. “Waste Glass Fiber Fabric as a Support for Facile Synthesis of Microporous Carbon To Adsorb Cr(VI) from Wastewater”, **ACS Sustainable Chemistry & Engineering.** 5(9): 8127-8136; August, 2017.

[106] Saif Ur Rehman, M. and et al. “Adsorption of Brilliant Green dye from aqueous solution onto red clay”, **Chemical Engineering Journal.** 2013(228): 54-62; July, 2013.

[107] Refait, P. and et al. “Coprecipitation thermodynamics of iron(II–III) hydroxysulphate green rust from Fe(II) and Fe(III) salts”, **Corrosion Science.** 45(4): 659-676; April, 2003.

[108] Bernal, J.D., Dasgupta, D.R. and Mackay, A.L. “The oxides and hydroxides of iron and their structural inter-relationships”, **Clay Minerals Bulletin.** 4(21): 15-30; August, 1959.

[109] Ahmed, I.A.M. and et al. “Formation of Green Rust Sulfate: A Combined in Situ Time-Resolved X-ray Scattering and Electrochemical Study”, **Langmuir.** 26(9): 6593-6603; February, 2010.

[110] Kim, M.S. and et al. “A novel synthesis of an Fe^{3+}/Fe^{2+} layered double hydroxide ('green rust') via controlled electron transfer with a conducting polymer”, **Dalton Transactions.** 46(24): 7656-7659; May, 2017.

[111] Zegeye, A. and et al. “Formation of Hydroxysulphate Green Rust 2 as a Single Iron(II-III) Mineral in Microbial Culture”, **Geomicrobiology Journal.** 2005(22): 389-399; October, 2005.

[112] Duesterberg, C.K., Mylon, S.E. and Waite, T.D. “pH Effects on Iron-Catalyzed Oxidation using Fenton’s Reagent”, **Environmental Science & Technology.** 42(22): 8522-8527; October, 2008.

REFERRENCES (CONTINUED)

[113] Cohen, G. and Sinet, P.M. “The fenton reaction between ferrous-diethylenetriaminepentaacetic acid and hydrogen peroxide”, **FEBS Letters.** 138(2): 258-260; February, 1982.

[114] Rodríguez-López, J.N. and et al. “Mechanism of Reaction of Hydrogen Peroxide with Horseradish Peroxidase: Identification of Intermediates in the Catalytic Cycle”, **Journal of the American Chemical Society.** 123(48): 11838-11847; November, 2001.

[115] Masud, M.K. and et al. “Gold-Loaded Nanoporous Ferric Oxide Nanocubes with Peroxidase-Mimicking Activity for Electrocatalytic and Colorimetric Detection of Autoantibody”, **Analytical Chemistry.** 89(20): 11005-11013; September, 2017.

[116] Sekher Pannala, A. and et al. “Flavonoid B-Ring Chemistry and Antioxidant Activity: Fast Reaction Kinetics”, **Biochemical and Biophysical Research Communications.** 282(5): 1161-1168; April, 2001.

[117] Qian, J. and et al. “Facile preparation of Fe_3O_4 nanospheres/reduced graphene oxide nanocomposites with high peroxidase-like activity for sensitive and selective colorimetric detection of acetylcholine”, **Sensors and Actuators B: Chemical.** 2014(201): 160-166; October, 2014.

[118] Su, L. and et al. “Colorimetric Detection of Urine Glucose Based $ZnFe_2O_4$ Magnetic Nanoparticles”, **Analytical Chemistry.** 84(13): 5753-5758; June, 2012.

[119] Gallati, H. “Peroxidase aus Meerrettich: Kinetische Studien sowie Optimierung der Aktivitätsbestimmung mit den Substraten H_2O_2 und 2,2′-Azino-di-(3-ethyl-benzthiazolinsulfonsäure-(6)) (ABTS)”, **Clinical Chemistry and Laboratory Medicine (CCLM).** 17(1): 1-8; October, 1979.

[120] Liu, Y. and Yu, F. “Substrate-specific modifications on magnetic iron oxide nanoparticles as an artificial peroxidase for improving sensitivity in glucose detection”, **Nanotechnology.** 22(14): 145704; April, 2011.

REFERRENCES (CONTINUED)

[121] Lonkar, S.P., Raquez, J.-M. and Dubois, P. "One-Pot Microwave-Assisted Synthesis of Graphene/Layered Double Hydroxide (LDH) Nanohybrids", **Nano-Micro Letters.** 7(4): 332-340; June, 2015.

[122] Gong, X.-B. "Degradation of dye wastewater by persulfate activated with Fe_3O_4/graphene nanocomposite", **Journal of Water Reuse and Desalination.** 6(4): 553-561; January, 2016.

[123] Ganesan, V., Louis, C. and Damodaran, S.P. "Graphene oxide-wrapped magnetite nanoclusters: A recyclable functional hybrid for fast and highly efficient removal of organic dyes from wastewater", **Journal of Environmental Chemical Engineering.** 6(2): 2176-2190; April, 2018.

[124] Inayat, A., Klumpp, M. and Schwieger, W. "The urea method for the direct synthesis of ZnAl layered double hydroxides with nitrate as the interlayer anion", **Applied Clay Science.** 51(4): 452-459; March, 2011.

[125] Wei, Y., Li, F. and Liu, L. "Liquid exfoliation of Zn–Al layered double hydroxide using NaOH/urea aqueous solution at low temperature", **RSC Advances.** 2014(4): 18044-18051; March, 2014.

[126] Hu, M. and et al. "High-capacity adsorption of benzotriazole from aqueous solution by calcined Zn-Al layered double hydroxides", **Colloids and Surfaces A: Physicochemical and Engineering Aspects.** 2018(540): 207-214; March, 2018.

[127] Hoan, N. and et al. "Fe_3O_4/Reduced Graphene Oxide Nanocomposite: Synthesis and Its Application for Toxic Metal Ion Removal", **Journal of Chemistry.** 2016(1):1-10; January, 2016.

[128] Yu, L. and et al. "Degradation of phenol using Fe_3O_4-GO nanocomposite as a heterogeneous photo-Fenton catalyst", **Separation and Purification Technology.** 2016(171): 80-87; July, 2016.

[129] Gurunathan, S. and et al. "Enhanced green fluorescent protein-mediated synthesis of biocompatible graphene", **Journal of Nanobiotechnology.** 12(1): 1-16; October, 2014.

REFERRENCES (CONTINUED)

[130] Tran, D., Kabiri, S. and Losic, D. “A green approach for the reduction of graphene oxide nanosheets using non-aromatic amino acids”, **Carbon.** 2014(76): 193-202; September, 2014.

[131] Technical note. “Zetasizer Nano series technical note”, **Zeta Potential An Introduction in 30 Minutes.** https://caliscc.org/images/presentations/ Morante_Zeta_Potential. June, 2020

[132] Ge, Y. and et al. “Effect of surface charge and agglomerate degree of magnetic iron oxide nanoparticles on KB cellular uptake in vitro”, **Colloids Surf B Biointerfaces.** 73(2): 294-301; October, 2009.

[133] Upadhyay, R. “Role of graphene/metal oxide composites as photocatalysts, adsorbents and disinfectants in water treatment: a review”, **RSC Advances.** 2014(4): 3823–3851; November, 2013.

[134] What color is methyl orange in basic/alkali, acidic and neutral solutions? https://www.enotes.com/homework-help/what-colour-methyl-orange-base-alkali-acid-neutral-318001. May, 2020.

[135] Methyl Orange Indicator. https://www.sciencesource.com/archive/Methyl-Orange-Indicator-SS2732929.html. May, 2020.

[136] Wei, W. and et al. “Fast removal of methylene blue from aqueous solution by adsorption onto poorly crystalline hydroxyapatite nanoparticles”, **Digest Journal of Nanomaterials and Biostructures.** 2015(10): 1343-1363; November, 2015.

[137] Kumar, R., Ansari, M.O. and Barakat, M.A. “Adsorption of Brilliant Green by Surfactant Doped Polyaniline/MWCNTs Composite: Evaluation of the Kinetic, Thermodynamic, and Isotherm”, **Industrial & Engineering Chemistry Research.** 2014. 53(17): 7167-7175; April, 2014.

[138] Yang, Z. and et al. “Utilization of LDH-Based Materials as Potential Adsorbents and Photocatalysts for the Decontamination of Dyes Wastewater: A Review”, **RSC Advances.** 2016(6): 79415-79436; August 2016.

REFERRENCES (CONTINUED)

[139] İşlek, Y., Aksuner, N. and Yanik, J. “Sandpaper Wastes as Adsorbent for the Removal of Brilliant Green and Malachite Green Dye”, **Acta Chimica Slovenica.** 2019 (66): 402-413; June 2019.

[140] Jeffrey Paulo H.P. and et al. “The interfacial reactivity of arsenic species with green rust sulfate (GR_{SO4})”, **Science of The Total Environment.** 2019(648): 1161-1170; January 2019.

[141] Asfaw, Z. and et al. “Biogenic hydroxysulfate green rust, a potential electron acceptor for SRB activity”, **Geochimica et Cosmochimica Acta.** 71(22): 5450-5462; November 2007.

[142] Aman, G. and et al. “Zn-Al layered double hydroxides intercalated with surfactant: Synthesis and applications for efficient removal of organic dyes”, **Journal of Cleaner Production.** 2019(240): 118090-118100; December 2019.

[143] Xiuxiu, R. and et al. “Sorption behavior of methyl orange from aqueous solution on organic matter and reduced graphene oxides modified Ni–Cr layered double hydroxides”, **Chemical Engineering Journal.** 2016(297): 295-303; August 2016.

[144] Huang, G. and et al. “Water–n-BuOH solvothermal synthesis of ZnAl–LDHs with different morphologies and its calcined product in efficient dyes removal”, **Journal of Colloid and Interface Science.** 2017(494): 215-222; May 2017.

[145] Shadpour M. and Masoud H. “An effective, low-cost and recyclable bio-adsorbent having amino acid intercalated LDH@Fe_3O_4/PVA magnetic nanocomposites for removal of methyl orange from aqueous solution”, **Applied Clay Science.** 2019(174): 127-137; July 2019.

[146] Zubair, M. and et al. “Starch-NiFe-layered double hydroxide composites: Efficient removal of methyl orange from aqueous phase”, **Journal of Molecular Liquids.** 2018(249): 254-264; January 2018.

REFERRENCES (CONTINUED)

[147] Chen, D. and et al. “Efficient removal of dyes by a novel magnetic Fe_3O_4/ZnCr-layered double hydroxide adsorbent from heavy metal wastewater”, **Journal of Hazardous Materials.** 2012(243): 152-160; December 2012.

[148] Dipshikha, B. and Ramesh, C.D. “Preferential adsorption of various anionic and cationic dyes from aqueous solution over ternary CuMgAl layered double hydroxide”, **Colloids and Surfaces A: Physicochemical and Engineering Aspects.** 2017 (525): 64-76; July 2017.

[149] Dan, Z. and et al. “Effective removal of brilliant green from aqueous solution with magnetic Fe_3O_4@SDBS@LDHs composites”, **Transactions of Nonferrous Metals Society of China.** 2017(27): 2673-2681; December 2017.

[150] Venkat, S.M. and et al. “Use of bagasse fly ash as an adsorbent for the removal of brilliant green dye from aqueous solution”, **Dyes and Pigments.** 73(3): 269-278; November, 2007.

[151] Nandi, B.K., Goswami, A. and Purkait, M.K. “Removal of cationic dyes from aqueous solutions by kaolin: Kinetic and equilibrium studies”, **Applied Clay Science.** 2009(42): 583-590; January 2009.

[152] Kismir, Y. and Ayse Z. A. “Adsorption characteristics of the hazardous dye Brilliant Green on Saklıkent mud”, **Chemical Engineering Journal.** 172(1): 199-206; August 2011.

[153] Ghaedi, M. and et al. “A novel acorn based adsorbent for the removal of brilliant green”, **Desalination.** 2011(281): 226-233; October 2011.

[154] Lei, Z. and et al. “Studies on the treatment of brilliant green solution by combination microwave induced oxidation with $CoFe_2O_4$”, **Separation and Purification Technology.** 62(2): 458-463; September 2008.

[155] VenKat, S.M. and et al. “Kinetic and equilibrium isotherm studies for the adsorptive removal of Brilliant Green dye from aqueous solution by rice husk ash”, **Journal of Environmental Management.** 84(4): 390-400; September 2007.

APPENDIX

CONFERENCES

Poster presentation

1. Kitayanan Ponlakhet, Purim Jarujamrus, Maliwan Amatatongchai and Suparb Tamuang. $Fe^{II}Fe^{III}$ Layered Double Hydroxide Nanosheets ($Fe^{II}Fe^{III}$ LDHNS) as an Enzyme Mimic for Colorimetric Detection of H_2O_2. Mini-symposium on Science and Technology for Science Achievement Scholarship of Thailand, 7 September 2019, U Place Hotel Ubon Ratchathani University, Ubon Ratchathani, Thailand.

Oral presentation

1. Kitayanan Ponlakhet, Purim Jarujamrus, Maliwan Amatatongchai and Suparb Tamuang. $Fe^{II}Fe^{III}$ Layered Double Hydroxide Nanosheets ($Fe^{II}Fe^{III}$ LDHNS) as an Enzyme Mimic for Colorimetric Detection of H_2O_2. Mini-symposium on Science and Technology for Science Achievement Scholarship of Thailand, 7 September 2019, U Place Hotel Ubon Ratchathani University, Ubon Ratchathani, Thailand.
2. Kitayanan Ponlakhet, and Suparb Tamuang. Synthesis a novel Fe_3O_4-decorated rGO/ZnAl-layered double hydroxide (Fe_3O_4/rGO/ZnAl-LDHs) composites for the removal of methyl orange from aqueous solution. Pure and Applied Chemistry International Conference 2020 (PACCON 2020), 13-14 February 2020, IMPACT Forum, Muangthong Thani, Bangkok, Thailand.

Publication

1. Kitayanan Ponlakhet, Purim Jarujamrus, Maliwan Amatatongchai and Suparb Tamuang. $Fe^{II}Fe^{III}$ layered double hydroxide nanosheets ($Fe^{II}Fe^{III}$ LDHNS) as an enzyme mimic for colorimetric detection of H_2O_2. Journal of Analytical Methods, Volume: 11, Pages: 4785-4794, Received 2nd July 2019, First published online 26th August 2019.

Analytical Methods

PAPER

Check for updates

Cite this: *Anal. Methods*, 2019, 11, 4785

$Fe^{II}Fe^{III}$ layered double hydroxide nanosheets ($Fe^{II}Fe^{III}$ LDHNS) as an enzyme mimic for colorimetric detection of H_2O_2†

Kitayanan Ponlakhet, Purim Jarujamrus, Maliwan Amatatongchai and Suparb Tamuang*

Received 2nd July 2019
Accepted 26th August 2019

DOI: 10.1039/c9ay01387c

rsc.li/methods

In this study, a new, rapid, sensitive, and convenient approach for colorimetric detection of H_2O_2 using $Fe^{II}Fe^{III}$ layered double hydroxide nanosheets ($Fe^{II}Fe^{III}$ LDHNS) is reported. The $Fe^{II}Fe^{III}$ LDHNS were constructed from a mixture of divalent and trivalent Fe ions by a co-precipitation method. $Fe^{II}Fe^{III}$ LDHNS were found to possess superior intrinsic peroxidase-like activity. They were used to catalyze the oxidation of a peroxidase substrate 3,3′,5,5′-tetramethylbenzidine (TMB) and 2,2′-azino-bis(3-ethylbenzothiazoline-6-sulfonic acid) (ABTS) diammonium salt in the presence of H_2O_2 to produce a blue and green solution product, respectively, that provided colorimetric detection of H_2O_2. The colorimetric detection of H_2O_2 was conveniently carried out by incubating at room temperature. Moreover, for the ABTS substrate, the experiment was facilely and successfully carried out in deionized water at a pH of approximately 5.6. The colorimetric assays displayed linearity for H_2O_2 determination by using TMB and ABTS systems in the range of 0.1–50 μM and 0.5–20 μM, respectively, and the corresponding limits of detection were found to be 0.05 μM and 0.2 μM, respectively. The catalytic reaction follows Michaelis–Menten kinetics and exhibits strong affinity towards TMB, ABTS, and H_2O_2 substrates. This selective approach could be applied for H_2O_2 detection in real milk and disinfectant samples. It is expected that there is great potential for the proposed method for exact detection of H_2O_2 in biotechnology, clinical diagnoses, the food industry, and other industries.

Introduction

Hydrogen peroxide (H_2O_2) is a well-documented powerful oxidizing agent and is regarded as a major reactive oxygen species (ROS) component of living cells. It is an essential intermediate in pharmaceutical, clinical, industrial, and environmental fields. Moreover, it is widely used as an equipment and packaging sanitizer in industrial processes such as water treatment, milk production, and electrical circuit cleaning to prolong the shelf life of products, and for medical purposes such as wound cleaning.[1–5] However, high levels of H_2O_2, usually ≥50 μM, are regarded as cytotoxic. High concentrations of H_2O_2 in living organisms could induce serious disorders such as cardiovascular disease,[6,7] cancer,[8] *etc.* In addition, H_2O_2 is one of the products from the reaction of glucose and the glucose oxidase enzyme, detection of H_2O_2 leads to the determination of glucose in glucose bioassay. Therefore, due to the significance of H_2O_2 in various fields, the development of efficient and accurate methods for H_2O_2 determination is of interest.

There are several analytical techniques that have been developed for monitoring H_2O_2, such as fluorescence,[9,10] chromatography,[11] chemiluminescence,[12–15] and electrochemical techniques.[16,17] However, each technique has its limitations such as high cost, high complexity, or strict requirements for equipment. Another technique for the detection of H_2O_2 is the colorimetric method,[18,19] and it has attracted more attention since it provides a simple and convenient platform for analyte determination. Additionally, it is less dependent on equipment, timesaving, inexpensive, and easy to perform as well as convenient for practical applications. A major advantage of this technique is that the color change of a specific substance can be rapidly observed by the naked eye for qualitative analysis and is also easily monitored by UV-Vis spectrophotometer for accurate quantification. Typically, H_2O_2 can be utilized for catalytic oxidation and coloration of chromogenic agents with the aid of horseradish peroxidase (HRP) as a catalyst.[20,21] Chromogenic agents, including 3,3′,5,5′-tetramethylbenzidine (TMB) and 2,2′-azino-bis-(3-ethylbenzothiazoline)-6-sulfonic acid (ABTS), immediately react with H_2O_2 in the presence of HRP to produce blue- and green-colored products, respectively, which serve as a colorimetric output signal.[20–22]

Department of Chemistry, Faculty of Science, Ubon Ratchathani University, Ubon Ratchathani 34190, Thailand. E-mail: suparb.t@ubu.ac.th; Fax: +66 45 288 379; Tel: +66 45 353 407 ext. 4634

† Electronic supplementary information (ESI) available. See DOI: 10.1039/c9ay01387c

HRP is a natural enzyme with a great practical application based on its satisfactory selectivity and high sensitivity under mild conditions. However, there are numerous disadvantages of natural enzymes, including high cost, inherent instability, and easy denaturation under extreme conditions (*e.g.*, in strong acidic and basic conditions or high temperature) or digestion by proteases,[23] and these have often limited their practical applications.[24] Moreover, the preparation, purification, and storage of natural enzymes are usually expensive, difficult, and time-consuming, and these limitations have inevitably restricted their widespread applications.[23–25] Therefore, it is interesting and challenging to develop novel and efficient artificial peroxidase enzyme mimetics that can overcome certain drawbacks of natural enzymes.

Since Gao *et al.* found in 2007 that Fe_3O_4 nanoparticles (NPs) possessed an intrinsic enzyme mimetic activity similar to that found in HRP natural enzyme,[20] Fe_3O_4 nanoparticles were subsequently used as natural enzyme replacements. Natural HRP enzyme contains Fe^{2+} or Fe^{3+} in its reaction centers,[24] and these metal centers are also found in Fe_3O_4 NPs. Thus, there has been extensive research performed to design nanomaterials with enzyme-like catalytic activity. A variety of Fe-based nanomaterials and composites including metal particles,[26–29] metal oxides,[24,30] layered structures[31,32] and carbon based nanostructures[33] have been explored as efficient enzyme mimics. Amongst these inorganic nanomaterials, layered materials are one of the promising candidates for being used as a catalyst for colorimetric assays due to its low cost, environmental friendliness, high conductivity, and high redox activity.[34]

Layered double hydroxides (LDHs), also known as hydrotalcite-like compounds, are a class of anionic clays with two-dimensional (2D) structure. There is great interest in these materials because they are non-toxic, stable, easy to prepare, and also because of their good biocompatibility, large surface area, good adsorption ability, and anion exchange. LDHs have been applied in a wide range of applications such as antacid precursors, ion exchangers, adsorbents, and catalysts.[35–37] The general formula of LDHs is $[M_{1-x}{}^{2+}M_x{}^{3+}(OH)_2]^{x+}(A^{n-})_{x/n}\cdot mH_2O$, where M^{2+} and M^{3+} denote divalent and trivalent cations, respectively (*e.g.*, Mg^{2+}, Fe^{2+}, Zn^{2+}, Ni^{2+}, Al^{3+}, and Fe^{3+}). Each cation is octahedrally surrounded by six OH^- ions, and the different octahedra share edges to form a 2D layer.[17] A^{n-} denotes the interlayer anion of valence n (*e.g.*, $CO_3{}^{2-}$, $NO_3{}^-$, and Cl^-). The value of x represents the molar ratio of $M^{3+}/(M^{2+} + M^{3+})$ within the hydroxide sheets, and it has been reported that the value of x in the range from 0.2 to 0.4 will enable a pure LDH phase to be formed. The value of m indicates the extent of water molecules in the structure. An outstanding feature of LDHs is that multi-inorganic metal cations can be simultaneously incorporated into the brucite-like layer to prepare multi-component LDHs by rationalizing the x value to be in the valid range.[38]

Several LDH materials were found to exhibit intrinsic enzyme mimetic activity. In 2012, Zhang *et al.* reported CoFe-LDH as an effective peroxidase mimetic to catalyze the oxidation of TMB in the presence of H_2O_2 to produce a blue solution.[31] In 2017, NiCo-LDH microspheres were used to catalyze the oxidation of ABTS in the presence of H_2O_2 to generate a green-colored solution of $ABTS^{•+}$.[39]

$Fe^{II}Fe^{III}$ layered double hydroxides ($Fe^{II}Fe^{III}$ LDHs), as shown in Fig. 1, contain a mixture of Fe^{2+} and Fe^{3+} ions with the ratio of $Fe^{3+} : Fe^{2+}$ at 0.25–0.33, have been reported[41] but they have never been used in the application as described herein. To the best of our knowledge, the present work is the first report of Fe^{2+} and Fe^{3+} ions in the LDHs that have the same activity as active reaction centers in HRP natural enzyme.

Herein, we present a new colorimetric method for the detection of H_2O_2 using $Fe^{II}Fe^{III}$ layered double hydroxide nanosheets ($Fe^{II}Fe^{III}$ LDHNS), which act as a peroxidase mimetic. The $Fe^{II}Fe^{III}$ LDHNS were constructed from a mixture of divalent and trivalent Fe ions with simple procedures and green solvent (aqueous medium). $Fe^{II}Fe^{III}$ LDHNS were prepared by a co-precipitation method and were used as peroxidase mimetics to catalyze the oxidation of TMB and ABTS chromogenic substrates in the presence H_2O_2 to produce a blue- and green-colored product of oxidized TMB and $ABTS^{•+}$, respectively. Furthermore, the developed colorimetric assays can be applied for detection of H_2O_2 in real milk and disinfectant samples.

Experimental details

Chemicals and materials

All chemicals were of analytical grade and were used as received without further purification. Ferrous sulfate heptahydrate ($FeSO_4\cdot 7H_2O$), ferric sulfate monohydrate ($Fe_2(SO_4)_3\cdot H_2O$), sodium hydroxide (NaOH), sodium acetate trihydrate ($CH_3COONa\cdot 3H_2O$), glacial acetic acid (CH_3COOH), 30% hydrogen peroxide (H_2O_2), and 2,2′-azino-bis(3-

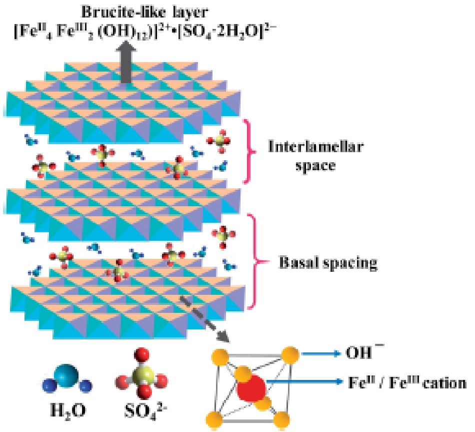

Fig. 1 $Fe^{II}Fe^{III}$ layered double hydroxide structure. Anions and water are presented in the interlayer space, and Fe^{II} or Fe^{III} ions are surrounded by six hydroxides in distorted octahedral coordination (lower right).

ethylbenzothiazoline-6-sulfonic acid) diammonium salt (ABTS) were purchased from Sigma-Aldrich (St. Louis, MO, USA); 3,5,3′5′-tetramethylbenzidine (TMB) was purchased from Acros Organics (Nidderau, Germany). Ethanol was purchased from Carlo Erba (de Valdonne, France). Deionized water was used in all experiments.

Instruments

UV-Visible absorption spectra were collected using a double beam spectrophotometer (UV-2600, Shimadzu, Japan) with a 10 mm micro quartz cell (700 μL). X-ray diffraction (XRD) patterns of powder samples were recorded from 2θ of 15° to 80° by an X-ray diffractometer (X′ Pert PAN, Philip, Finland) with Cu K_α radiation; the applied voltage and current were 35 kV and 25 mA, respectively. X-ray photoelectron spectroscopy (XPS; AXIS ULTRA^{DLD}, Kratos Analytical, Manchester, UK) was employed to investigate the valence of Fe. The samples were excited with Al K_α radiation. Scanning electron microscopy (SEM) was performed with a model JSM 7610F Plus microscope (JEOL, Japan) to examine the morphology of prepared materials. Nanosheets were attached on SEM stubs and coated with platinum (20 mA, 60 s) prior to the SEM study. The SEM was operated at 15 kV in a vacuum atmosphere. Energy dispersive X-ray spectroscopy (EDS) using model X-Stream-2 (Oxford Instruments, UK) in conjunction with SEM was used to investigate the elemental composition. Nanosheets were also attached on SEM stubs prior to the study of elemental composition using EDS.

Preparation of $Fe^{II}Fe^{III}$ LDHNS

$Fe^{II}Fe^{III}$ LDHNS were synthesized by a co-precipitation method from a mixture of divalent and trivalent Fe ions, which were mixed with a sodium hydroxide solution (0.3 M NaOH), as described in detail by A. Géhin *et al.* (2002).[40] In brief, a mixed solution of Fe^{2+} and Fe^{3+} ions was prepared by dissolving $FeSO_4 \cdot 7H_2O$ and $Fe_2(SO_4)_3 \cdot H_2O$ in 50 mL of deionized water. A $[Fe^{2+}]/[Fe^{3+}]$ ratio of 3 and total Fe concentration ($[Fe^{2+}] + [Fe^{3+}]$) of 0.2 M were required. Then, 50 mL of 0.3 M NaOH with a $[OH^-]/([Fe^{2+}] + [Fe^{3+}])$ ratio of 3/2 was added to the mixed Fe^{2+}–Fe^{3+} solution. Due to the fact that Fe^{2+} ions can easily be oxidized, the reaction was performed under N_2 gas, and magnetic stirring (approximately 500 rpm) was applied to ensure a fast and complete dissolution. The reaction process is described as follows:[40,41]

$$4Fe_{(aq)}^{2+} + 2Fe_{(aq)}^{3+} + 12OH^- + SO_4^{2-} \rightarrow Fe^{II}{}_4Fe^{III}{}_2(OH)_{12}SO_4 \quad (1)$$

Upon reaction, a black-brown precipitate immediately appeared. After complete addition, the pH was maintained at approximately 6.9. Then, the precipitate was aged for 24 hours under N_2 gas at room temperature. Finally, the solid product was separated from the solution by centrifugation and washed three times with deionized water; a green-brown powder was obtained. The expected final product was $Fe^{II}Fe^{III}$ LDHNS of formula $[Fe^{II}{}_4Fe^{III}{}_2(OH)_{12}]^{2+} \cdot [SO_4 \cdot mH_2O]^{2-}$.

H_2O_2 detection using $Fe^{II}Fe^{III}$ LDHNS as peroxidase mimetics

To investigate the peroxidase-like catalytic activity of $Fe^{II}Fe^{III}$ LDHNS, the as-synthesized $Fe^{II}Fe^{III}$ LDHNS were directly employed to catalyze the oxidation of chromogenic substrates ABTS and TMB in the presence of H_2O_2 by a facile step at ambient temperature. Using this method, colorimetric detection of H_2O_2 can be achieved.

For the TMB substrate, H_2O_2 detection was carried out in an air-saturated solution, according to the protocol from a previous study.[42–44] In a typical experiment, 50 μL of 0.3 mg mL^{-1} $Fe^{II}Fe^{III}$ LDHNS, 100 μL of different concentrations of H_2O_2, 200 μL of 1 mM TMB (in ethanol), and 400 μL of 0.1 M pH 4.0 acetate buffer solution were mixed. The mixture was then allowed to react for 30 min at ambient temperature (25 ± 1 °C), and then, the absorbance was measured by UV-Vis spectrophotometry at 652 nm.

For the ABTS substrate, H_2O_2 detection was performed using a facile step in deionized water. The solution, which included 50 μL of 0.3 mg mL^{-1} $Fe^{II}Fe^{III}$ LDHNS, 100 μL of different concentrations of H_2O_2, 100 μL of 20 mM ABTS, and 500 μL of deionized water, was mixed and then reacted at ambient temperature (25 ± 1 °C) for 30 min. Then, the absorbance was measured by UV-Vis spectrophotometry at 418 nm.

Kinetic analysis

The experiments for kinetics study were also performed at ambient temperature (25 ± 1 °C) by using 0.3 mg mL^{-1} of $Fe^{II}Fe^{III}$ LDHNS with ABTS and TMB substrate in the presence of H_2O_2 under optimal conditions. The apparent steady-state kinetics were observed by varying the concentration of ABTS or TMB at a fixed concentration of H_2O_2, or varying the H_2O_2 concentration while fixing the ABTS or TMB concentration. The Michaelis–Menten equation (eqn (2)) describes the kinetic properties of isolated enzymes.[42–45] It is also used in modeling the dynamics of enzyme systems and displays oscillatory behavior. If a low oscillatory reaction is shown, many biochemical processes catalyzed by enzymes take place. The Michaelis–Menten constant (K_m) can be calculated by the Lineweaver–Burk equation, which is shown in eqn (3):

$$\nu = V_{max}\frac{[S]}{[S] + K_m} \quad (2)$$

$$\frac{1}{\nu} = \left(\frac{K_m}{V_{max}}\right)\left(\frac{1}{[S]}\right) + \frac{1}{V_{max}} \quad (3)$$

where ν denotes the initial velocity, V_{max} denotes the maximal reaction velocity, and [S] represents the substrate concentration.[42–45]

Real sample application

Two disinfectant samples purchased from a local pharmacy were used for H_2O_2 colorimetric detection to validate the method. The H_2O_2 concentrations designated on the packages were 3% and 6% (w/v). These disinfectants were appropriately diluted with deionized water before measurement. In addition, nine brands of milk that were sterilized and then packaged were purchased from local supermarkets, and samples were used in these experiments. Before detection, the milk samples were initially treated with 20% (w/w) trichloroacetic acid (TCA) to precipitate protein from solution.[44] The mixed solution was vigorously stirred at 500 rpm for 40 min to ensure the completion of protein precipitation. The solution was then filtered through a 0.45-micron syringe ultra-filter membrane. The final solution was split into 2 portions, one for direct detection and another for method validation by the addition of H_2O_2 to a standard solution.

Results and discussion

Characterization of $\mathrm{Fe^{II}Fe^{III}}$ LDHNS

The XRD pattern of $\mathrm{Fe^{II}Fe^{III}}$ LDHNS recorded from 2θ of 15° to 80° (Fig. S1 (ESI†)) reveals the main diffraction peaks for $\mathrm{Fe^{II}}$-$\mathrm{Fe^{III}}$ LDHNS at 2θ angles of 21.03°, 26.63°, 32.93°, 36.39°, 40.69°, 53.03°, 62.55°, 68.31°, and 70.73°, which were assigned to a series of planes (002), (003), (004), (101), (102), (104), (105), (110), and (111), respectively, according to that proposed by Bernal *et al.*[46] Various small lines (*) indicate that some ordering of sulphate ions occurs inside the interlayers of the structure.[46,47] Thus, all main lines found in the XRD pattern are correlated with crystalline structures of $\mathrm{Fe^{II}Fe^{III}}$ LDHNS.

SEM was employed to investigate the morphologies of $\mathrm{Fe^{II}}$-$\mathrm{Fe^{III}}$ LDHNS. Fig. 2 illustrates the SEM image of $\mathrm{Fe^{II}Fe^{III}}$ LDHNS, and the figure reveals that the product clearly exhibits a plate-like morphology, which is a stereotype of the LDHs.[48–50] In addition, it is seen that the plate-like form of this product appears to possess an irregular shape. The EDS spectrum (Fig. S2 (ESI†)) reveals that the $\mathrm{Fe^{II}Fe^{III}}$ LDHNS mainly contain elemental Fe, O, S, and C. In the $\mathrm{Fe^{II}Fe^{III}}$ LDHNS EDS spectrum, peaks at approximately 0.7, 6.4, and 7.0 keV, which are associated with the binding energies of iron (Fe), were observed. The signal of binding energies of oxygen (O) and sulfur (S) at approximately 0.5 and 2.3 keV, respectively, were also observed, as sulfate is a charge-balancing ion in the product interlayer.[50] Moreover, the peak at approximately 0.3 keV, which relates with the binding energies of carbon (C), is influenced by carbon film on the SEM stub holder. The percentages of elemental Fe, O, S, and C are summarized in Table S1 (ESI†). Additionally, the distribution of these elements was investigated with elemental mapping using SEM-EDS, as displayed in Fig. S3 (A–D) (ESI†). The elements C, O, S, and Fe appear to be uniformly distributed, and these also confirm the presence of Fe, S, and O in the nanosheet product. XPS was also used to verify the valence of Fe in the synthesized materials. The XPS data in Fig. S4A (ESI†) indicate the presence of Fe (2p), O (1s), and S (2p). The binding energy of iron observed at 725.4 and 711.5 eV (Fig. S4B, (ESI†)) corresponds to the characteristics of Fe(II) and Fe(III), respectively.[51,52] Three peaks of O (1s) at 530.2, 531.6, and 532.5 eV (Fig. S4C, (ESI†)) were assigned to O–Fe, O–H, and adsorbed water, respectively.[51] Note that the S (2p) at 168.8 and 170.0 eV (Fig. S4D, (ESI†)) indicates the presence of $SO_4^{\ 2-}$ in the interlayers of the sample.[51,52]

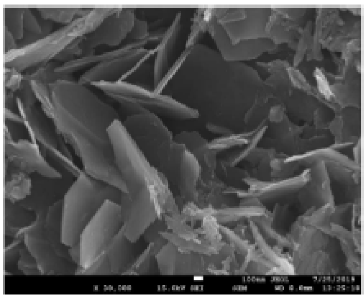

Fig. 2 SEM image of $\mathrm{Fe^{II}Fe^{III}}$ LDHNS.

The peroxidase-like catalytic activity of $\mathrm{Fe^{II}Fe^{III}}$ LDHNS

To investigate the catalytic activity of $\mathrm{Fe^{II}Fe^{III}}$ LDHNS, the chromogenic substrates ABTS and TMB were chosen because they are normally used to study the peroxidase-like activity of enzymes.[21,40] Only a system that includes H_2O_2, $\mathrm{Fe^{II}Fe^{III}}$ LDHNS, and chromogenic substrate (Fig. 3(c) for TMB and Fig. 4(c) for ABTS) could produce the colored product and can easily be observed by the naked eye (inset image). The results indicate that the $\mathrm{Fe^{II}Fe^{III}}$ LDHNS possess peroxidase-like activity and can catalyze the oxidation reaction of TMB and ABTS in the presence of H_2O_2.[21,30,53]

These reactions proceed *via* Fenton's mechanism as shown in the following equations:

$$H_2O_2 \xrightarrow{\mathrm{Fe^{II}Fe^{III}\ LDHNS}} HO^- + HO^{\cdot} \tag{4}$$

$$HO^{\cdot} + TMB \xrightarrow{\mathrm{Fe^{II}Fe^{III}\ LDHNS}} H_2O + TMB(ox) \tag{5}$$

$$HO^{\cdot} + ABTS \xrightarrow{\mathrm{Fe^{II}Fe^{III}\ LDHNS}} 2H_2O + ABTS^{\cdot +} \tag{6}$$

The $\mathrm{Fe^{II}Fe^{III}}$ LDHNS catalyze H_2O_2 decomposition to produce $HO^{\cdot}$, as shown in eqn (4).[53–55] Then, the produced $HO^{\cdot}$

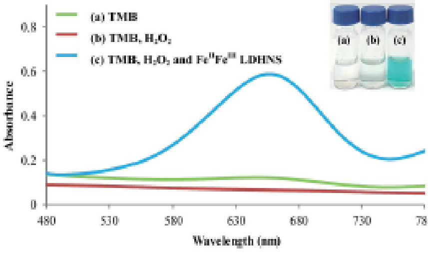

Fig. 3 UV-Vis absorption spectra of TMB solution (1 mM in ethanol) in 0.1 M acetate buffer solution pH 4. The reactions were incubated at 25 ± 1 °C for 30 min in different reaction systems: (a) TMB, (b) TMB and H_2O_2, and (c) TMB, H_2O_2, and $\mathrm{Fe^{II}Fe^{III}}$ LDHNS. The H_2O_2 concentration was 50.0 μM. The inset image shows typical photographs of the different TMB colored products.

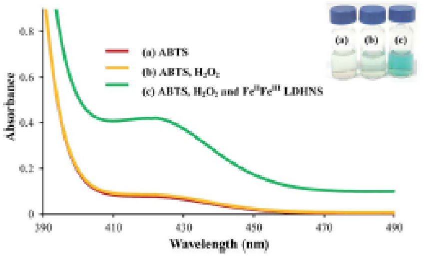

Fig. 4 UV-Vis absorption spectra of ABTS solution (20 mM) in deionized water. The reactions were incubated at 25 ± 1 °C (30 min) in different reaction systems: (a) ABTS, (b) ABTS and H_2O_2, and (c) ABTS, H_2O_2, and $Fe^{II}Fe^{III}$ LDHNS. The H_2O_2 concentration was 20.0 μM. The inset image shows typical photographs of different ABTS reaction solutions.

oxidizes TMB to provide the blue-colored solution of the oxidized products of TMB, as shown in eqn (5). This system displays the characteristic absorbance at 652 nm (Fig. 3: blue line (c)) originating from its distinctive charge-transfer of diamine/diimine complex.[56] The H_2O_2 concentration corresponds to the color change and absorbance signal at 652 nm. Similarly, in the case of ABTS substrate, the $HO^{\cdot}$ oxidizes ABTS to produce the green-colored product of $ABTS^{\cdot+}$, as shown in eqn (6), exhibiting the maximum absorbance at 418 nm (Fig. 4: green line (c)).[57] The results reveal that $Fe^{II}Fe^{III}$ LDHNS can catalyze the oxidation of TMB and ABTS in the presence of H_2O_2. The principle of the detection system is described in Scheme 1. The color change and the corresponding reaction mechanisms for the oxidation of TMB and ABTS are in accordance with results from previous reports.[21,30,53] However, according to J. Lian *et al.*,[58] $O_2^{\cdot-}$ might be produced due to the dissolved O_2 in solution, and it probably played a role similar to that of $HO^{\cdot}$ species. These results strongly suggest that $Fe^{II}Fe^{III}$ LDHNS possess an intrinsic peroxidase-like activity, which is derived from electron transfer between pairs of metal cations with different oxidation states (*e.g.*, Fe^{2+} and Fe^{3+}) on the brucite-like layer.[53]

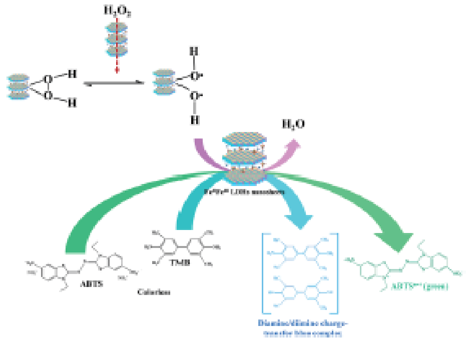

Scheme 1 The principle of the colorimetric detection of H_2O_2 by using an enzyme mimic consisting of $Fe^{II}Fe^{III}$ LDHNS.[56,57]

Optimization of the experimental conditions

To study the effect of pH, experiments were performed by varying pH in the range from 3 to 7.5 using 0.1 M acetate buffer. The results are shown in Fig. S5A and S5B (ESI†) for TMB and ABTS substrate, respectively. For both TMB and ABTS substrate, $Fe^{II}Fe^{III}$ LDHNS exhibited greater activity in acidic solution than that of neutral pH, as had also been observed for Fe_3O_4 NPs[21,22] and Fe_3O_4 NSs/rGO nanocomposites[20] for TMB substrate. Additionally, the results indicated that the maximum catalytic efficiency of $Fe^{II}Fe^{III}$ LDHNS was at pH 3.0 for both TMB and ABTS substrate. The absorbance dramatically decreased to nearly zero at pH > 5 for TMB, while remaining almost constant from pH 4 to 5.5, and then decreased at higher pH for ABTS. As in neutral or basic solutions, H_2O_2 tends to decompose into H_2O and O_2 rather than producing ROS to react with the substrates.

It has been proven that alkaline conditions inhibit the combination and dissociation rates between both substrate and the nanosheets.[59] However, according to a previous study reported by H. Wei *et al.*,[22] $Fe^{II}Fe^{III}$ LDHNS were unstable at pH ≤ 3.0. As a consequence, at low pH, the Fe^{2+} ions in the nanosheets might leach into the reaction solution and subsequently play a catalytic role.[22] Therefore, the optimal pH of $Fe^{II}Fe^{III}$ LDHNS for the TMB system was at approximately pH 4 in an acetate buffer solution to ensure that the observed catalytic activity originated from the nanosheets and not from leached Fe^{2+} ions. Notably, the optimal pH solution for $Fe^{II}Fe^{III}$ LDHNS was similar to those for HRP natural enzyme.[20] However, the optimal pH for the ABTS system could be varied from 4 to 5.5. Because the pH of the ABTS system with deionized (DI) water medium was approximately 5.6, with results in approximately the same as those for pH 5.5 (Fig. S5B†). Therefore, DI medium was chosen for the ABTS system to reduce the complexity of buffer preparation.

The effect of the reaction time on the catalytic activity was studied in the time period of 2–30 min for both TMB and ABTS substrate; the results are shown in Fig. S5C and S5D (ESI†), respectively. In Fig. S5C (ESI†) for TMB substrate, the absorbance significantly increased when increasing the reaction time from 20 to 30 min. The reaction time of 30 min was chosen as optimal to maximize the sensitivity of H_2O_2 colorimetric detection with TMB substrate. In Fig. S5D (ESI†) for ABTS substrate, the absorption dramatically increased when the reaction time increased from 2 to 10 min, with a slow increase from 15 to 30 min. Therefore, 15 min was chosen as the optimum reaction time to maximize the sensitivity towards H_2O_2 detection while minimizing the time required for analysis. Moreover, experiments with both chromogenic substrates were carried out by incubating at room temperature, which thus reduced the time and facilities required for the experimental process.

Optimization of the concentration of the $Fe^{II}Fe^{III}$ LDHNS was performed by varying the concentration from 0.1–2.0 mg mL^{-1}.

The results are shown in Fig. S6 and S7 (ESI†) for TMB and ABTS, respectively. For both substrates, the absorbance increased when the $Fe^{II}Fe^{III}$ LDHNS concentration was increased; however, baseline signals were also increased. Thus, the concentration of 0.3 mg mL^{-1} was chosen as optimal for the $Fe^{II}Fe^{III}$ LDHNS due to the lowest baseline signal as well as reasonable absorbance. In addition, since the concentration was low, catalyst separation was not required.

Steady-state kinetic assay of $Fe^{II}Fe^{III}$ LDHNS

The peroxidase-like activity of $Fe^{II}Fe^{III}$ LDHNS was further studied based on a steady-state kinetics analysis using TMB, ABTS, and H_2O_2 as substrate under optimal reaction conditions. The kinetic data were obtained by fixing one substrate concentration while varying another substrate concentration; *i.e.*, fixing the H_2O_2 concentration while varying the concentration of TMB or ABTS, or conversely, fixing TMB or ABTS while varying the H_2O_2 concentration. A series of experiments was carried out, and the absorbance data were used to calculate the concentration of the oxidized form of both peroxidase substrates based on a molar absorption coefficient of 39 000 and 36 000 M^{-1} cm^{-1} for the TMB- and ABTS-derived oxidation product, respectively.[21,60] The concentration was calculated from the absorbance data using Beer–Lambert's law following eqn (7):[60]

$$A = \varepsilon bc \tag{7}$$

where A denotes the measured absorbance, ε denotes the molar absorptivity coefficient (M^{-1} cm^{-1}), b denotes the path length (cm), and c denotes the analyte concentration (M). Michaelis–Menten constants (K_m) and the maximal reaction velocity (V_{max}) of the $Fe^{II}Fe^{III}$ LDHNS enzyme mimic were calculated from the Lineweaver–Burk plots following eqn (3), where the intercept provides V_{max} and the slope provides K_m. Fig. 5 shows the TMB–H_2O_2 (A and B)- and ABTS–H_2O_2 (C and D)-dependent reaction rates, respectively. The K_m value is an indicator of the affinity of an enzyme towards its substrate, and a lower K_m value indicates a stronger affinity between the enzyme and its substrate. The kinetics parameters for TMB and ABTS were calculated and are summarized in Table 1.

For the TMB–H_2O_2 system, the K_m values for the $Fe^{II}Fe^{III}$ LDHNS when TMB and H_2O_2 were used as the substrate are 0.23 and 3.07 mM, which are lower than that of HRP (0.434 and 3.7 mM).[20] These results indicate the strong affinity of $Fe^{II}Fe^{III}$ LDHNS towards TMB and H_2O_2 and are comparable to those for HRP. For the ABTS–H_2O_2 system, the K_m value for $Fe^{II}Fe^{III}$ LDHNS with ABTS as the substrate is 0.68 mM, and this value was found to be lower than that of HRP (1.56 mM).[61]

These results indicate that $Fe^{II}Fe^{III}$ LDHNS have a higher affinity towards ABTS than HRP. This can be understood because a HRP molecule contains only one iron ion that decomposes H_2O_2 to generate OH$^{\bullet}$, while the surface of nanosheets is decorated with many iron ions. However, the K_m value of $Fe^{II}Fe^{III}$ LDHNS with H_2O_2 as the substrate in the ABTS–H_2O_2 system is 2.26 mM, which is higher than that for HRP (0.24 mM),[62] suggesting that the affinity of $Fe^{II}Fe^{III}$ LDHNS towards H_2O_2 is lower than that of HRP. From these results, it is clearly seen that $Fe^{II}Fe^{III}$ LDHNS show improved catalytic activity for colorimetric detection of H_2O_2 by using TMB and ABTS peroxidase substrates compared to HRP. Thus, we conclude that

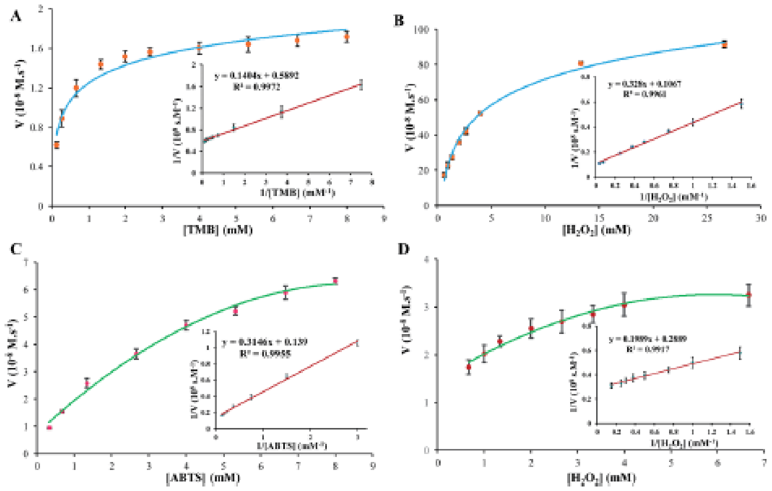

Fig. 5 Michaelis–Menten model and Lineweaver–Burk model (inset curve). (A) and (C) Fixed concentration of H_2O_2 (1.0 μM) with varied concentrations of peroxidase substrate from 0.1–8.0 μM and 0.3–8.0 μM for TMB and ABTS, respectively. (B) Fixed concentration of TMB (100 μM) with varied concentrations of H_2O_2 from 0.5–200 μM. (D) Fixed concentration of ABTS (10 mM) with varied concentrations of H_2O_2 from 0.5–100 μM. The error bars represent the standard deviation of three measurements.

Table 1 Comparison of the Michaelis–Menten constant (K_m) obtained from $Fe^{II}Fe^{III}$ LDHNS for TMB and ABTS substrate

	K_m (mM)				K_m (mM)		
Catalyst[a]	TMB	H_2O_2	Reference	Catalyst[a]	ABTS	H_2O_2	Reference
HRP	0.434	3.7	20	HRP	1.56	0.24	62
Fe_3O_4 NPs	0.098	154	20	Fe_3O_4–NH_2–SH	0.25	5.7	63
NiFe-LDHNS	0.5	2.4	32	$NiFe_2O_4$	0.46	2.60	21
CoAl ELDH	0.37	22.13	42	Prussian blue NPs	157.45	0.028	23
DNA/CuAl-LDHs	1.78	10.24	43	Fe_3O_4@Au–Cys–FA NPs	0.44	0.36	30
C-dot/NiAl-LDHs	0.34	4.72	44	NiCo–LDHs	3.43	13.2	39
$Fe^{II}Fe^{III}$ LDHNS	0.23	3.07	This work	$Fe^{II}Fe^{III}$ LDHNS	0.68	2.26	This work

[a] Catalyst: HRP (horseradish peroxidase), NPs (nanoparticles), ELDHs (exfoliated layered double hydroxides), LDHs (layered double hydroxides), LDHNS (layered double hydroxide nanosheets).

$Fe^{II}Fe^{III}$ LDHNS are promising materials for applications requiring high-sensitivity H_2O_2 detection and analysis.

Analytical feature of $Fe^{II}Fe^{III}$ LDHNS for H_2O_2 detection

The analytical performance of the developed colorimetric method to detect H_2O_2 was investigated using a UV-Vis spectrophotometer. Fig. 6 displays the UV-Vis spectra of (A) TMB and (B) ABTS obtained from solutions in the presence of different H_2O_2 concentrations. The absorbance increased upon increasing the concentration of H_2O_2, and corresponded to the solution color that gradually changed from colorless to blue (inset image A) and green (inset image B), respectively. As shown in Fig. 6(C) and (D), the linearity range of the analytical system was studied by using different concentrations of standard H_2O_2 in both the TMB and ABTS substrate system. For TMB substrate, signals for different H_2O_2 concentrations as well as a linear calibration curve are shown in Fig. 6(C). The linear calibration curve for H_2O_2 ranges from 0.1–50 µM. It is clearly seen that this method provides the lowest detection limit of 0.05 µM (3SD/slope) when compared with a previous report, as shown in Table 2. Fig. 6(D) shows the linear calibration curve for ABTS substrate, which is in a range from 0.5–20 µM with a limit of detection (LOD) of 0.2 µM (3SD/slope). The outstanding features of the proposed method for ABTS substrate are not only a lower limit of detection, but this method also provides simple reaction conditions (in DI water), a convenient process, less chemicals used, and is environmentally friendly. Furthermore, a catalyst separation procedure for both proposed methods is not required, as very small amounts of $Fe^{II}Fe^{III}$ LDHNS (0.3 mg mL^{-1}) were used, and they do not interfere with the absorbance measured by a UV-Vis spectrophotometer. The analytical performance of the $Fe^{II}Fe^{III}$ LDHNS system is comparable to

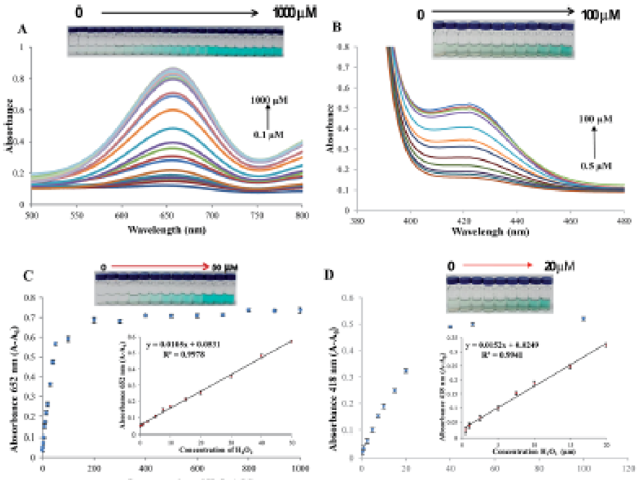

Fig. 6 (A and B) A dose–response curve for H_2O_2 detection using $Fe^{II}Fe^{III}$ LDHNS with TMB and ABTS substrate, respectively. (C and D) The linear calibration plot for H_2O_2 in the range of 0.1–50 µM and 0.5–20 µM for TMB and ABTS substrate, respectively. The upper insets show the corresponding photographs of different solutions. Error bars represent the standard deviation based on three repeated measurements.

Table 2 Colorimetric detection of H_2O_2 with various nanomaterials as peroxidase mimics

Nanomaterials[a]	Peroxidase substrate	H_2O_2 (μM) Linear range	H_2O_2 (μM) LOD	Reference
CoFe-LDHs	TMB	1–20	0.4	31
CoAl-ELDHs	TMB	10–200	10	42
DNA/CuAl-LDHs	TMB	20–2000	10	43
NiFe-LDHNS	TMB	10–500	4.4	32
C-dot/NiAl-LDHs	TMB	0.2–20	0.11	44
Fe_3O_4@Au–Cys–FA NPs	ABTS	5–10 000	2.9	30
Fe_3O_4 NPs	ABTS	5–100	3	30
$Fe^{II}Fe^{III}$ LDHNS	TMB	0.1–50	0.05	This work
$Fe^{II}Fe^{III}$ LDHNS	ABTS	0.5–20	0.2	This work

[a] Nanomaterials: LDHs (layered double hydroxides), ELDHs (exfoliated layered double hydroxides), LDHNS (layered double hydroxide nanosheets), NPs (nanoparticles), LDHNS (layered double hydroxide nanosheets).

that of other reported nanomaterial-based colorimetric assays reported in Table 2.

Study of interference and selectivity

The selectivity is very important in real sample application because there probably are other substances in the sample that might affect the measurement. The considered substances in this study that could cause interference were glucose, maltose, lactose, fructose, ascorbic acid (AA), Na^+, Zn^{2+}, and Mg^{2+}, which are the components in milk samples. The concentrations of the interfering compounds (100 μM) were five-fold higher than that of standard H_2O_2 (20 μM). The experiments were performed under optimized conditions for TMB and ABTS substrate. It can be clearly seen that the absorbance obtained from these ions is relatively weak compared to H_2O_2 and can be neglected for both TMB (Fig. 7(A)) and ABTS (Fig. 7(B)). These results clearly indicate that the $H_2O_2/Fe^{II}Fe^{III}$ LDHNS/TMB and $H_2O_2/Fe^{II}Fe^{III}$ LDHNS/ABTS systems exhibited high selectivity towards H_2O_2 detection.

Stability

The long-term stability of $Fe^{II}Fe^{III}$ LDHNS is significant for continuous and reliable monitoring of H_2O_2. To evaluate the stability of the developed methods, the $Fe^{II}Fe^{III}$ LDHNS were dispersed in deionized water (0.3 mg mL^{-1}) and stored at 4 °C. They were used to measure the absorbance response for 20 μM of H_2O_2 every three days for 21 days. As shown in Fig. S8A (ESI†), the absorbance for the $H_2O_2/Fe^{II}Fe^{III}$ LDHNS/TMB system slightly decreased over time. However, it retained 90% of the original response until week 3. For the $H_2O_2/Fe^{II}Fe^{III}$ LDHNS/ABTS system, the absorbance also slightly decreased over the storage time. Its absorbance response retained approximately 92% of the original value over a storage period of 9 days. In addition, 80% of the original activity remained until day 21 (Fig. S8B (ESI†)). These results indicated that the $Fe^{II}Fe^{III}$ LDHNS exhibited better long-term stability towards H_2O_2 detection with the TMB system than that with the ABTS system.

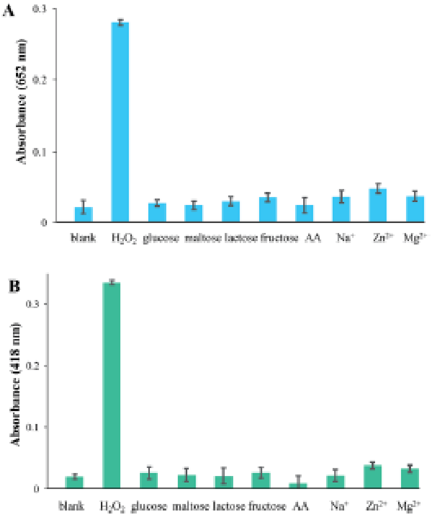

Fig. 7 Selectivity of the colorimetric method of the (A) $H_2O_2/Fe^{II}Fe^{III}$ LDHNS/TMB and (B) $H_2O_2/Fe^{II}Fe^{III}$ LDHNS/ABTS systems for H_2O_2 detection by measuring absorbance at 418 nm and 652 nm, respectively. The error bars represent the standard deviation for three measurements.

Nevertheless, both systems demonstrate good stability, with more than 90% of the original absorbance being retained for a storage period of longer than a week.

Determination of H_2O_2 in real samples

To investigate the accuracy and feasibility of the developed colorimetric method, the standard iodometric titration method was employed to compare with the proposed colorimetric method for analysis of milk and disinfectant samples for H_2O_2.[60,61] Six aseptic milk samples and two disinfectant samples were purchased from the local supermarkets. These samples were treated and prepared as described in Experimental section. Proteins were precipitated from all six milk samples, and H_2O_2 standard solutions were added to the protein-free samples. Two disinfectant samples were diluted to ensure that H_2O_2 concentrations were within a linear range. Under optimized conditions and using five replicates for each sample, the concentration of H_2O_2 in all real samples was determined, and the results are summarized in Table 3. The developed methods provided recoveries ranging from 97.52 to 102.99% for TMB substrate and 97.34 to 103.26% for ABTS substrate, which was consistent with the range from 98.78 to 103.50% obtained by the standard iodometric titration method. Furthermore, these methods exhibited impressively good precision (% relative standard deviation (RSD) ranging from 1.10 to 2.87). Therefore, the proposed colorimetric method is sufficiently accurate and there is no significant matrix interference that affects the sample

Table 3 Comparison of the H_2O_2 concentration in milk and disinfectant samples obtained using the proposed colorimetric method and the iodometric titration standard method (avg. ± SD of five trials)

Methods	Iodometric titration			Proposed method: TMB (added 0.1 M)			Proposed method: ABTS (added 0.1 M)		
Samples	Found[d]	Recovery[d] (%)	RSD[d] (%)	Found[d]	Recovery[d] (%)	RSD[d] (%)	Found[d]	Recovery[d] (%)	RSD[d] (%)
M1[a]	0.91 ± 0.02	103.50 ± 1.73	1.67	0.87 ± 0.03	99.12 ± 2.84	2.87	0.90 ± 0.03	101.83 ± 2.84	2.79
M2[a]	0.90 ± 0.02	102.39 ± 2.20	2.15	0.86 ± 0.01	97.52 ± 1.33	1.37	0.87 ± 0.02	99.05 ± 1.88	1.90
M3[a]	0.88 ± 0.03	99.89 ± 3.00	3.00	0.90 ± 0.02	101.87 ± 2.35	2.31	0.90 ± 0.01	102.17 ± 1.24	1.22
M4[a]	0.87 ± 0.02	98.78 ± 2.09	2.12	0.91 ± 0.01	102.99 ± 1.65	1.60	0.86 ± 0.01	97.34 ± 1.07	1.10
M5[a]	0.90 ± 0.01	102.11 ± 0.48	0.47	0.89 ± 0.02	100.43 ± 0.19	2.18	0.90 ± 0.01	102.14 ± 1.40	1.37
M6[a]	0.89 ± 0.01	101.28 ± 1.27	1.25	0.87 ± 0.02	98.30 ± 2.14	2.17	0.91 ± 0.02	103.26 ± 1.87	1.82
6% HP1[b]	0.90 ± 0.03	101.84 ± 2.92	2.87	1.79 ± 0.03	ND	1.78	1.79 ± 0.03	ND	1.62
3% HP2[c]	0.90 ± 0.02	102.11 ± 2.09	2.05	0.90 ± 0.01	ND	1.14	0.89 ± 0.03	ND	1.96

[a] Addition of 3% H_2O_2 (0.882 M) to real samples. [b] Hydrogen peroxide disinfectant: concentration of 6% w/v or 1.76 M. [c] Hydrogen peroxide disinfectant: concentration of 3% w/v or 0.882 M. [d] Average of five determinations ± standard deviation.

measurements, demonstrating that our method is suitable for the quantification of H_2O_2 in real samples.

Conclusions

In this work, $Fe^{II}Fe^{III}$ layered double hydroxide nanosheets ($Fe^{II}Fe^{III}$ LDHNS) were successfully prepared by a co-precipitation method. The prepared $Fe^{II}Fe^{III}$ LDHNS possess superior intrinsic peroxidase-like activity, which can catalyze the oxidation of TMB and ABTS chromogenic substrates in the presence of H_2O_2 to produce a blue- and green-colored product of oxidized TMB and $ABTS^{\cdot+}$, respectively. The colorimetric detection of H_2O_2 experiments were carried out at room temperature; and for ABTS substrate, the experiment was carried out in deionized water at pH around 5.6. The peroxidase-like catalytic activity originates from the $Fe^{II}Fe^{III}$ LDHNS, not the leached Fe^{2+}. The kinetics analysis indicated that the process is in accordance with the typical Michaelis–Menten kinetics, and the $Fe^{II}Fe^{III}$ LDHNS exhibited high affinity towards TMB, ABTS, and H_2O_2 substrates. On the basis of these findings, a colorimetric method with high sensitivity and selectivity for H_2O_2 detection has been developed. The colorimetric method showed good response towards H_2O_2 detection, with a linear range from 0.1–50 µM (LOD of 0.05 µM) for TMB, and 0.5–20 µM (LOD of 0.2 µM) for ABTS. This selective approach could be applied for H_2O_2 detection in real milk and disinfectant samples. $Fe^{II}Fe^{III}$ LDHNS as peroxidase mimics exhibited several advantages when compared to natural enzyme, such as ease of preparation, low cost, robustness, long-term stability, and good biocompatibility. The proposed method is expected to have great potential for the exact detection of H_2O_2 in biotechnology, clinical diagnosis, the food industry, and other industries.

Conflicts of interest

There are no conflicts to declare.

Acknowledgements

The authors gratefully acknowledge financial support received from the Commission on Higher Education, the Ministry of Education, the instrumental facility of the Department of Chemistry, and the Faculty of Science at Ubon Ratchathani University. We also gratefully acknowledge a scholarship from the Science Achievement Scholarship of Thailand (SAST) that was awarded to K. Ponlakhet.

Notes and references

1 H. Liu, Y. Ding, B. Yang, Z. Liu, Q. Liu and X. Zhang, *Sens. Actuators, B*, 2018, **271**, 336–345.

2 Q. Liu, R. Zhu, H. Du, H. Li, Y. Yang, Q. Jia and B. Bian, *Mater. Sci. Eng., C*, 2014, **43**, 321–329.

3 N. H. Martin, A. Friedlander, A. Mok, D. Kent, M. Wiedmann and K. J. Boor, *J. Food Prot.*, 2014, **77**, 1809–1813.

4 V. M. Amin and N. F. Olson, *J. Dairy Sci.*, 1967, **50**, 461–464.

5 S. Arefin, Md. A. H. Sarker, M. A. Islam, Md. Harun-ur-Rashid and Md. N. Islam, *J. Adv. Vet. Anim. Res.*, 2017, **4**, 371–377.

6 R. M. Touyz and E. L. Schiffrin, *Histochem. Cell Biol.*, 2004, **122**, 339–352.

7 H. Cai, *Cardiovasc. Res.*, 2005, **68**, 26–36.

8 S. Reuter, S. C. Gupta, M. M. Chaturvedi and B. B. Aggarwal, *Free Radical Biol. Med.*, 2010, **49**, 1603–1616.

9 F. Wen, Y. Dong, L. Feng, S. Wang, S. Zhang and X. Zhang, *Anal. Chem.*, 2011, **83**, 1193–1196.

10 J. H. Kim, C. R. Patra, J. R. Arkalgud, A. A. Boghossian, J. Zhang, J. H. Han, N. F. Reuel, J. H. Ahn, D. Mukhopadhyay and M. S. Strano, *ACS Nano*, 2011, **5**, 7848–7857.

11 H. Yue, X. Bu, M. H. Huang, J. Young and T. Raglione, *Int. J. Pharm.*, 2009, **375**, 33–40.

12 C. K. Lim, Y. D. Lee, J. Na, J. M. Oh, S. Her, K. Kim and I. C. Kwon, *Adv. Funct. Mater.*, 2010, **20**, 2644–2648.

13 A. Tahirovic, A. Copra, E. Omanovic-Miklicanin and K. Kalcher, *Talanta*, 2007, 72, 1378–1385.

14 J. Xieab and Y. Huang, *Anal. Methods*, 2011, **3**, 1149–1155.

15 W. Shi, X. Zhang, S. Hea and Y. Huang, *Chem. Commun.*, 2011, **47**, 10785–10787.

16 Y. Shu, B. Li, Q. Xu, P. Gu, X. Xiao, F. Liu, L. Yu, H. Pang and X. Hu, *Sens. Actuators, B*, 2017, **241**, 528–533.

17 Y. Shu, Y. Yan, J. Chen, Q. Xu, H. Pang and X. Hu, *ACS Appl. Mater. Interfaces*, 2017, **9**, 22342–22349.

18 L. Sun, Y. Ding, Y. Jiang and Q. Liu, *Sens. Actuators, B*, 2017, **239**, 848–856.

19 C. Bhave and S. Shejwalkar, *Int. J. Environ. Sci. Technol.*, 2018, **15**, 1243–1248.

20 L. Z. Gao, J. Zhuang, L. Nie, J. Zhang, Y. Zhang, N. Gu, T. Wang, J. Feng, D. Yang, S. Perrett and X. Yan, *Nat. Nanotechnol.*, 2007, **2**, 577–583.

21 J. Xie, X. Zhang, H. Wang, H. Zheng and Y. Huang, *TrAC, Trends Anal. Chem.*, 2012, **39**, 114–129.

22 H. Wei and E. Wang, *Anal. Chem.*, 2008, **80**, 2250–2254.

23 W. Zhang, D. Ma and J. Du, *Talanta*, 2014, **120**, 362–367.

24 Q. Liu, H. Li, Q. Zhao, R. Zhu, Y. Yang, Q. Jia, B. Bian and L. Zhuo, *Mater. Sci. Eng., C*, 2014, **41**, 142–151.

25 Y. Zhu, Z. Yang, M. Chi, M. Li, C. Wang and X. Lu, *Talanta*, 2018, **181**, 431–439.

26 Q. Chen, C. Liang, X. Zhang and Y. Huang, *Talanta*, 2018, **182**, 476–483.

27 J. Zhao, W. Dong, X. Zhang, H. Chai and Y. Huang, *Sens. Actuators, B*, 2018, **263**, 575–584.

28 H. Liu, Y.-N. Ding, B. Yang, Z. Liu, X. Zhang and Q. Liu, *ACS Sustainable Chem. Eng.*, 2018, **6**, 14383–14393.

29 Y. Ding, H. Liu, L.-N. Gao, M. Fu, X. Luo, X. Zhang, Q. Liu and R.-C. Zeng, *J. Alloys Compd.*, 2019, **785**, 1189–1197.

30 K. Ponlakhet, M. Amatatongchai, W. Sroysee, P. Jarujamrus and S. Chairam, *Anal. Methods*, 2016, **8**, 8288–8298.

31 Y. Zhang, J. Tian, S. Liu, L. Wang, X. Qin, W. Lu, G. Chang, Y. Luo, A. M. Asiri, A. O. Al-Youbi and X. Sun, *Analyst*, 2012, **137**, 1325–1328.

32 T. Zhan, J. Kang, X. Li, L. Pan, G. Li and W. Hou, *Sens. Actuators, B*, 2018, **255**, 2635–2642.

33 M. Chen, B. Yang, J. Zhu, H. Liu, X. Zhang, X. Zheng and Q. Liu, *Mater. Sci. Eng., C*, 2018, **90**, 610–620.

34 B. Hai and Y. Zou, *Sens. Actuators, B*, 2015, **208**, 143–150.

35 B. Saifullah and M. Z. B. Hussein, *Int. J. Nanomed.*, 2015, **10**, 5609–5633.

36 K.-H. Goh, T.-T. Lim and Z. Dong, *Water Res.*, 2008, **42**, 1343–1368.

37 F. Li and X. Duan, *Struct. Bonding*, 2006, **119**, 193–223.

38 Z. P. Xu, J. Zhang, M. O. Adebajo, H. Zhang and C. Zhou, *Appl. Clay Sci.*, 2011, **53**, 139–150.

39 L. Su, X. Yu, W. Qin, W. Dong, C. Wu, Y. Zhang, G. Mao and S. Feng, *J. Mater. Chem. B*, 2017, **5**, 116–122.

40 A. Géhin, C. Ruby, M. Abdelmoula, O. Benali, J. Ghanbaja, P. Refait and J.-M. R. Génin, *Solid State Sci.*, 2002, **4**, 61–66.

41 C. Ruby, A. Géhin, M. Abdelmoula, J.-M. R. Génina and J.-P. Jolivet, *Solid State Sci.*, 2003, **5**, 1055–1062.

42 L. Chen, B. Sun, X. Wang, F. Qiao and S. Ai, *J. Mater. Chem. B.*, 2013, **1**, 2268–2274.

43 L. Chen, K. Sun, P. Li, X. Fan, J. Sun and S. Ai, *Nanoscale*, 2013, **5**, 10982–10988.

44 Y. Guo, X. Liu, X. Wang, A. Iqbal, C. Yang, W. Liu and W. Qin, *RSC Adv.*, 2015, **5**, 95495–95503.

45 J. Chen, Y. Shu, H. Li, Q. Xu and X. Hu, *Talanta*, 2018, **189**, 254–261.

46 J. D. Bernal, D. R. Dasgupta and A. L. Mackay, *Clay Miner. Bull.*, 1959, **4**, 15–30.

47 Ph. Refait, A. Géhin, M. Abdelmoula and J.-M. R Génin, *Corros. Sci.*, 2003, **45**, 659–676.

48 I. A. M. Ahmed, L. G. Benning, G. Kakonyi, A. D. Sumoondur, N. J. Terrill and S. Shaw, *Langmuir*, 2010, **26**, 6593–6603.

49 M.-S. Kim, T.-H. Kim, Y. S. Seo, J.-M. Oh and J. K. Park, *Dalton Trans.*, 2017, **46**, 7656–7659.

50 Z. Asfaw, O.-N. Georges, C. Cédric, H. Lucie, A. Mustapha and J. Frédéric, *Geomicrobiol. J.*, 2005, **22**, 389–399.

51 J. P. H. Perez a, H. M. Freeman, J. A. Schuessler and L. G. Benning, *Sci. Total Environ.*, 2019, **648**, 1161–1170.

52 A. Zegeye, L. Huguet, M. Abdelmoula, C. Carteret, M. Mullet and F. Jorand, *Geochim. Cosmochim. Acta*, 2007, **71**, 5450–5462.

53 C. K. Duesterberg, S. E. Mylon and T. D. Waite, *Environ. Sci. Technol.*, 2008, **42**, 8522–8527.

54 G. Cohen and P. M. Sinet, *FEBS Lett.*, 1982, **138**, 258–260.

55 J. N. Rodríguez-López, D. J. Lowe, J. Hernández-Ruiz, A. N. P. Hiner, F. García-Cánovas and R. N. F. Thorneley, *J. Am. Chem. Soc.*, 2001, **123**, 11838–11847.

56 M. K. Masud, S. Yadav, M. N. Islam, N.-T. Nguyen, C. Salomon, R. Kline, H. R. Alamri, Z. A. Alothman, Y. Yamauchi, M. S. A. Hossain and M. J. A. Shiddiky, *Anal. Chem.*, 2017, **89**, 11005–11013.

57 A. S. Pannala, T. S. Chan, P. J. O'Brien and C. A. Rice-Evans, *Biochem. Biophys. Res. Commun.*, 2001, **282**, 1161–1168.

58 J. Lian, P. Liu, C. Jin, Z. Shi, X. Luo and Q. Liu, *Microchim. Acta*, 2019, **186**, 332–340.

59 J. Qian, X. Yang, L. Jiang, C. Zhu, H. Mao and K. Wang, *Sens. Actuators, B*, 2014, **201**, 160–166.

60 Solvay Interox, Inc., *Food Processing*, 2000, pp. 1–8.

61 Solvay Chemicals, Inc., www.solvaychemicals.us, 2008, pp. 1–3.

62 H. Gallati, *Clin. Chem. Lab. Med.*, 1979, **17**, 1–8.

63 Y. Liu and F. Yu, *Nanotechnology*, 2011, **22**, 145704.

$Fe^{II}Fe^{III}$ Layered Double Hydroxide Nanosheets ($Fe^{II}Fe^{III}$ LDHNS) as an Enzyme Mimic for Colorimetric Detection of H_2O_2

Kitayanan Ponlakhet, Purim Jarujamrus, Maliwan Amatatongchai and Suparb Tamuang*
Department of Chemistry and Center of Excellence for Innovation in Chemistry, Faculty of Science,
Ubon Ratchathani University, Ubon Ratchathani 34190, Thailand.
Corresponding author: Tel.; +66 45-353407 ext. 4634, fax; +66 45-288 379
**E-mail: suparb.t @ubu.ac.th*

Introduction

Hydrogen peroxide (H_2O_2) is widely used as equipment and packaging sanitizer in industrial processes such as water treatment, milk production and electrical circuit cleaning to prolong the shelf life of products, and for medical purposes like wound cleaning. However, high level of H_2O_2, usually ≥ 50 μM, is regarded as a cytotoxic agent. Therefore, due to the significance of H_2O_2 in various fields, the development of efficient and accurate methods for H_2O_2 determination is of interest. Layered double hydroxides (LDHs), also known as hydrotalcite-like compounds, are class of anionic clays with two-dimensional (2D) structure (**Scheme 1.**). These materials have received much attention because they are non-toxic, easy to prepare and also their good biocompatibility and large surface area. Several LDHs materials were found to exhibit intrinsic enzyme mimetic activity. Herein, we present a new colorimetric method for detection of H_2O_2 by using $Fe^{II}Fe^{III}$ layered double hydroxide nanosheets ($Fe^{II}Fe^{III}$ LDHNS) which act as peroxidase mimetic. The $Fe^{II}Fe^{III}$ LDHNS were constructed from a mixture of divalent and trivalent Fe ions with simple procedures and green solvent (aqueous medium). $Fe^{II}Fe^{III}$ LDHNS were prepared by co-precipitation method and were used as peroxidase mimetic to catalyze the oxidation of 2,2'-azino-bis-(3-ethylbenzothiazoline)-6-sulfonic acid (ABTS) chromogenic substrates in the presence H_2O_2 to produce a blue and green color product of $ABTS^{\bullet+}$.

Experimental

Preparation of $Fe^{II}Fe^{III}$ LDHNS

$Fe^{II}Fe^{III}$ LDHNS were synthesized by co-precipitation method from a mixture of divalent and trivalent Fe ions in the ratio $[Fe^{2+}]/[Fe^{3+}]$ of 3. The reaction process is as follows:

$$4Fe^{2+}_{aq} + 2Fe^{3+}_{aq} + 12OH^- + SO_4^{2-} \rightarrow Fe^{II}_4 Fe^{III}_2 (OH)_{12}SO_4 \quad (1)$$

The expected final product was $Fe^{II}Fe^{III}$ LDHNS of formula $[Fe^{II}_4Fe^{III}_2(OH)_{12}]^{2+}\cdot[SO_4\cdot mH_2O]^{2-}$.

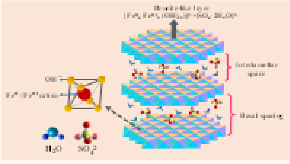

Scheme 1. Schematic illustration of $Fe^{II}Fe^{III}$ layered double hydroxide structure. Anions and water are presented in the interlayer space, and Fe^{II} or Fe^{III} ions are surrounded by six hydroxides in distorted octahedral coordination (lower right).

H_2O_2 detection using $Fe^{II}Fe^{III}$ LDHNS as peroxidase mimetics

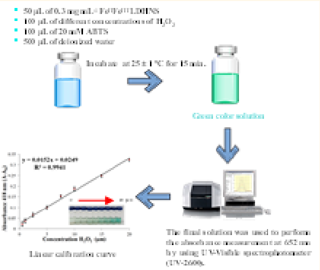

- 50 μL of 0.3 mg mL⁻¹ $Fe^{II}Fe^{III}$ LDHNS
- 100 μL of different concentrations of H_2O_2
- 100 μL of 20 mM ABTS
- 500 μL of deionized water

Incubate at 25 ± 1 °C for 15 min.

Green color solution

Linear calibration curve

The final solution was used to perform the absorbance measurement at 652 nm by using UV-Visible spectrophotometer (UV-2600).

Results: Characterization

Fig. 1 SEM image of $Fe^{II}Fe^{III}$ LDHNS.

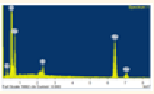

Fig. 2 EDS spectra of $Fe^{II}Fe^{III}$ LDHNS.

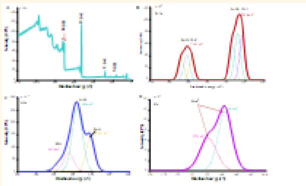

Fig. 3 (A) X-ray Photoelectron Spectroscopy (XPS) survey spectra and high resolution XPS spectra of (B) Fe (2p), (C) O (1s) and (D) S (2p) of $Fe^{II}Fe^{III}$ LDHNS .

Results: Colorimetric method for H_2O_2 detection

The peroxidase-like catalytic activity of $Fe^{II}Fe^{III}$-LDHNS

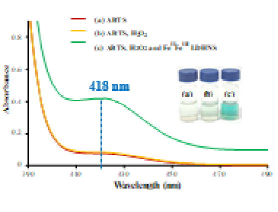

Fig. 4 UV-vis absorption spectra of ABTS solution (20 mM) in deionized water. The reactions were incubated at 25 ± 1 °C (30 min) in different reaction systems: (a) ABTS, (b) ABTS and H_2O_2, (c) ABTS, H_2O_2 and $Fe^{II}Fe^{III}$ LDHNS. The H_2O_2 concentration was 20.0 μM. Inset image: typical photographs of different ABTS reaction solution.

The principle of the colorimetric detectionof H_2O_2 by using $Fe^{II}Fe^{III}$ LDHNS

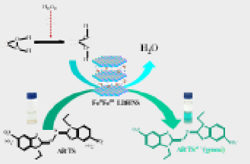

These reactions proceed via the Fenton's mechanism as shown in the following equations:

$$H_2O_2 \longrightarrow HO^- + HO^\bullet \quad (2)$$

$$HO^\bullet + ABTS \longrightarrow 2H_2O + ABTS^{\bullet+} \quad (3)$$

The $Fe^{II}Fe^{III}$ LDHNS catalyze H_2O_2 decomposition to produce $HO^\bullet$ as shown in Eq. (2). Then, the produced $HO^\bullet$ oxidizes ABTS to produce the green colored product of $ABTS^{\bullet+}$ in Eq. (3), exhibiting the maximum absorbance at 418 nm (Fig. 5: green line (c)). The results reveal that $Fe^{II}Fe^{III}$ LDHNS can catalyze the oxidation of the ABTS in the presence of H_2O_2.

Results: Colorimetric method for H_2O_2 detection

Optimization of the experimental conditions

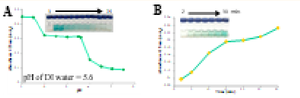

Fig 5 (A) Effect of pH and (B) effects of reaction time for ABTS on the catalytic activity of $Fe^{II}Fe^{III}$ LDHNS.

Steady-state kinetic assay of $Fe^{II}Fe^{III}$ LDHNS

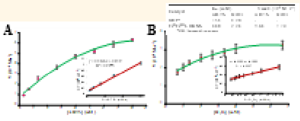

Fig. 6 Michaelis Menten model and Lineweaver Burk model (inset curve): (A) fixed concentration of H_2O_2 (1.0 μM) with varied concentration of peroxidase substrate from 0.3 – 8.0 μM for ABTS. (B) fixed concentration of ABTS (10 mM) with varied concentration of H_2O_2 from 0.5 – 100 μM.

Analytical feature of $Fe^{II}Fe^{III}$ LDHNS for H_2O_2 detection

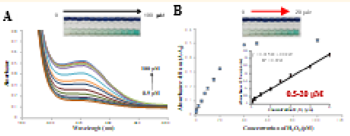

Fig. 7 (A) A dose-response curve for H_2O_2 detection using $Fe^{II}Fe^{III}$ LDHNS with ABTS substrate. (B) The linear calibration plot for H_2O_2 in the range of 0.5-20 μM. The upper insets show the corresponding photographs of different solutions.

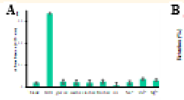

Fig. 8 Selectivity of the colorimetric method of (H_2O_2/$Fe^{II}Fe^{III}$ LDHNS/ABTS systems for H_2O_2 detection

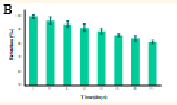

Fig. 9 The stability of $Fe^{II}Fe^{III}$ LDHNS for colorimetric detection of H_2O_2.

Conclusions

In this work, $Fe^{II}Fe^{III}$ layered double hydroxide nanosheets ($Fe^{II}Fe^{III}$ LDHNS) have been successfully prepared by co-precipitation method. The prepared $Fe^{II}Fe^{III}$ LDHNS possesses the superior intrinsic peroxidase-like activity, which can catalyze the oxidation of ABTS chromogenic substrates in the presence of H_2O_2 to produce green colored product of oxidized $ABTS^{\bullet+}$. The colorimetric detection of H_2O_2 experiments were carried out by incubating in deionized water (pH around 5.6) at room temperature contributing the convenient operation. The colorimetric method showed good response towards H_2O_2 detection with a linear range from 0.5 - 20 μM (LOD = 0.2 μM). This selective approach could be applied for H_2O_2 detection in real milk and disinfectant samples. $Fe^{II}Fe^{III}$ as peroxidase mimics exhibited several advantages when compared to natural enzyme for instant; ease of preparation, low-cost, robustness, long-term stability and good biocompatibility. The proposed method is expected to be more potential for exact detection of H_2O_2 in food industry, clinical diagnosis life process and other industries.

Acknowledgment:

The grant from Science Achievement Scholarship of Thailand (SAST) and instrument facilities from the Dept of Chemistry, Fac. of Science, Ubon Ratchathani Univ. are gratefully acknowledged.

Reference:

1. A. Géhin, C. Ruby, M. Abdelmoula, O. Benali, J. Ghanbaja, P. Refait, J.-M. R. Génin, Solid State Sci., 2002, **4**, 61-66.
2. A. S. Pannala, T. S. Chan, P. J. O'Brien, C. A. Rice-Evans, Biochem. Biophys. Res. Commun., 2001, **282**, 1161-1168.
3. H. Wei, E. Wang, Anal. Chem., 2008, **80**, 2250-2254.
4. T. Zhan, J. Kang, X. Li, L. Pan, G. Li, W. Hou, Sens. Actuator B-Chem., 2018, **255**, 2635-2642.

CURRICULUM VITAE

NAME	Miss Kitayanan Ponlakhet
DATE OF BIRTH	20 January 1992, Ubon Ratchathani, Thailand
EDUCATION	Bachelor's Degree of Science, Chemistry, Mahasarakham University, 2010. Master's Degree of Science, Chemistry, Ubon Ratchathani University, 2016.
SCHOLARSHIP	Recipient of the Science Achievement Scholarship of Thailand (SAST) in the Academic Years of 2015-2019